2004

Using Microscopy to Examine Mechanisms of Cell Division

Lily Copenagle

USING MICROSCOPY TO EXAMINE MECHANISMS OF CELL DIVISION

A thesis presented to the faculty of The Rockefeller University in partial fulfillment of the requirements for the degree of doctor of Philosophy

by

Lily Copenagle

Acknowledgements

I would like to thank the Kapoor Lab, past and present, for their support and assistance in helping a physicist become a cell biologist: Jed Gaetz, Sarah Garrett, Mike Lampson, Jeff Kim, Janet Yang, Ben Kwok, Kishore Renduchintala Venkatakrishna, Srinivas Hotha, Joseph Cherian, and Ulf Peters. For endless help and encouragement, I would like to thank my favorite microscopist, Alison North. In addition, I am deeply indebted to my collaborators: Alexey Khodjakov, Duane Compton, and Mike Gordon, with whom it has been an honor to work.

To my family, I would like to express my appreciation for their patience and support.

Finally, I would like to thank my committee, Mike Rout, Hiro Funabiki and Geri Kreitzer for providing their time and expertise. In particular, I would like to express my gratitude to my advisor, Tarun Kapoor for excellent guidance, instruction, and for the opportunity to work in such a fascinating field.

TABLE OF CONTENTS

LIST OF FIGURES

List of Tables

Abbreviations

3D	Three-dimensional
aa	amino acid
APC	Anaphase promoting complex
CCD	Charge-coupled device
DIC	Differential interference contrast
DMEM	Dubelco's modified eagle media
dsRNA	Double stranded RNA
ECL	Enhanced chemiluminescence
EM	Electron microscopy
GFP	Green fluorescent protein
GTP	Guanosine triphosphate
K-fiber	Kinetochore microtubule bundle
MTOC	Microtubule organizing center
MTSB	Microtubule stabilizing buffer
NEB	Nuclear envelope breakdown
NLS	Nuclear localization sequence
NuMA	Nuclear mitotic apparatus protein
PBS	Phosphate buffered solution
RNAi	RNA interference
siRNA	Small interfering RNA
TBS	Tris buffered sulfate
TPX2	Targeting protein for Xklp2
SDS-PAGE	Sodium dodecyl sulfate-polyacrylamide gel electrophoresis

Abstract

The accurate segregation of chromosomes during cell division requires the assembly of a microtubule-based mitotic spindle. In the research presented here, I examined two aspects of mitotic spindle morphogenesis. First, I looked at how chromosomes attach to microtubules in mitosis. The capture of microtubule plus-ends by kinetochores (the site of chromosome-microtubule attachment) has been described previously. However, recent data suggests that another mechanism must also contribute to this essential process. Here, with the aid of real-time confocal microscopy, I present direct evidence for an additional chromosome-spindle attachment mechanism in which the minus-ends of microtubules attached to chromosomes are captured by spindle microtubules and incorporated into the spindle. I also show that this process depends on the microtubule cross-linking MAP (microtubule associated protein), NuMA. Second, I examined the molecular basis of bipolar spindle formation: in particular, the contributions of the non-motor MAP TPX2 to spindle structure and function in mammalian cells. My live cell recordings revealed that in cells depleted of TPX2, multipolar spindles formed by progressive spindle pole fragmentation. Consistent with a structural role for TPX2 in the spindle, I found that while normal bipolar spindles were resistant to collapse to monopolar spindles after inhibition of the mitotic motor Eg5, multipolar spindles that formed in the absence of TPX2 were not. In addition, I found that microtubule nucleation and growth during spindle assembly is not dependent on TPX2, and that cells form robust kinetochore microtubule bundles after TPX2 knockdown. These data do not suggest a direct role of TPX2 in the establishment of chromosome-microtubule attachments. However, my results shed new light on the

spindle defects in cells without TPX2 and confirm an important role for TPX2 in the structural stability of the mitotic spindle.

Chapter 1 - Introduction

The study of mitosis began over one hundred and twenty years ago with the description of the stages of cell division as viewed through a microscope (for a review see Mitchison and Salmon 2001). Using crudely fixed samples and limited staining techniques, the first mitosis biologists were limited to the observation of only the grossest morphologic changes. Since then a series of advances in microscopy have expanded our understanding of mitosis dramatically (for a review see Rieder and Khodjakov 2003). For example, the resolving power of cellular imaging has improved, not only with improvements in visible light optics to show much smaller features in a cell, but in the late 1950's, transmission electron microscopy was first used to image cells, revealing many previously unimagined ultra-structural objects in cells only a few nanometers wide. Several other techniques, such as polarized light, differential interference contrast, phase contrast, and fluorescence microscopy have made it possible to acquire high resolution time-lapse images of dynamic changes in the molecular components of living cells, providing insight into the mechanics of complex processes like protein trafficking, cell motility, and cytoskeletal dynamics. Consequently, today mitosis biologists have a more detailed, although still incomplete, description of spindle dynamics and mechanics at a molecular level.

Developing a comprehensive understanding of cell division is complicated by the rapid dynamics of the multifaceted mitotic machinery: the cytoskeletal network, multiple pairs of chromosomes, and the long list of mitotic proteins that act together throughout the intricate monitoring and self-regulating mechanisms that ensure the accuracy of chromosome segregation in each division. Usually, this machinery works remarkably well, considering that over the course of a lifetime approximately 10^{16} cell divisions occur

in a typical human body (Alberts 2002). In the developing embryo, the number of dividing cells increases exponentially and each division contributes to the development of limbs and organs. In an adult, cells continue to divide (although at a slower rate) in order to adjust metabolic processes and regenerate tissue. Errors in mitosis can lead to mis-segregated chromosomes, resulting in damaged, excess, or missing chromosomes, which are characteristics of many birth defects (reviewed in Nicolaidis and Petersen 1998; Kajii et al. 2001) and cancers (Cahill et al. 1998; Lengauer et al. 1998; Sen 2000). Therefore, it is important to further our understanding of the molecular mechanisms of mitosis and how mitotic accuracy is achieved, as well as possible reasons for its failure.

§ 1.1 The mitotic spindle

Mitosis is the process of cell division in which one copy of each duplicated chromosome (called a sister chromatid) is segregated into each of the two resulting cells (known as daughter cells). The chromosomes contain all of the genetic material that each daughter cell needs to survive; and through evolution, a complex but efficient mechanism to successfully partition these chromosomes has developed. The prokaryotic cell, our evolutionary ancestor, accomplishes cell division by attaching the duplicated chromosomes to the cell wall and pinching itself into two along an axis between the attachment sites (Figure 1.1A). More advanced cells developed a nucleus, which provided many benefits, including separating the chromosomes from the enzymatic and mechanical activity in the rest of the cell and controlling access to the cell's DNA. In yeast, chromosomes are segregated to opposite sides of the nucleus before both the nucleus and the cell wall contract and cleave the cell in two (Figure 1.1B). Animal cells have yet another strategy, wherein the nuclear envelope is broken

down in the early stages of mitosis, allowing the chromosomes to interact with cytosolic proteins, only to form the nuclear envelope again in each new daughter cell (Figure 1.1C).

During vertebrate mitosis, a complex and highly dynamic multi-component structure (collectively termed the mitotic spindle) assembles to provide the mechanical framework for segregating chromosomes (for a review, see Compton 1998). At each end of the spindle, microtubules are focused at the spindle poles. Spindle poles are stable structures which provide the "anchor" to which each set of chromosomes segregate after anaphase. The major force-bearing component of the spindle is the network of microtubules, which can be categorized into three groups: interpolar, astral and kinetochore microtubules (Figure 1.2). The primary sites of microtubule attachment on the chromosomes are the kinetochores, each of which binds approximately 10-40 microtubules in vertebrates, resulting in a bundle of kinetochore-associated microtubules, called a K-fiber (for review, see Compton 2000). The kinetochore is a complex macromolecular assembly of proteins (for review, see Rieder and Salmon 1998) positioned on opposite sides of the primary constriction of the chromosome to facilitate the attachment of each chromosome to microtubules from each pole. During mitosis in animal cells, movement of a kinetochore towards and away from its attached spindle pole is coordinated with the shrinkage and growth of its bound microtubules (Maddox et al. 2003). Several microtubule motors and microtubule associated proteins (MAPs) associated with the kinetochore regulate this dynamic attachment of bundles of microtubules and monitor the tension and attachment of microtubules (reviewed in McIntosh et al. 2002).

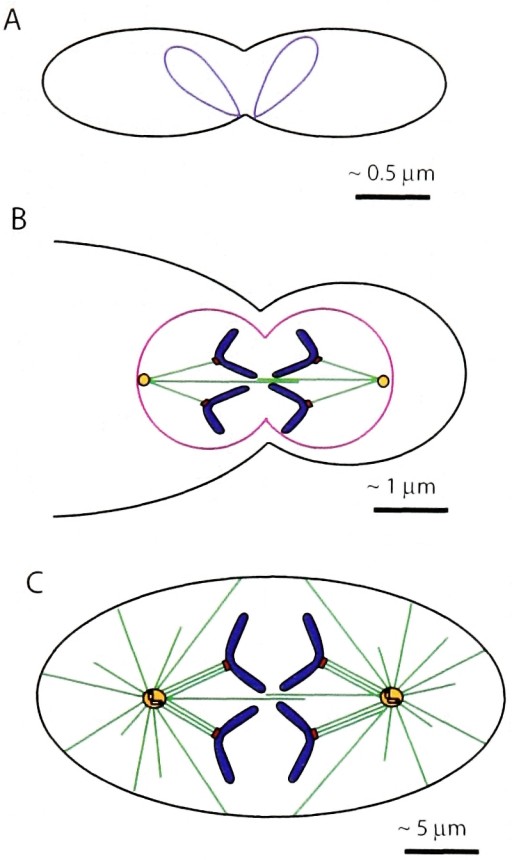

Figure 1.1 A range of mitotic strategies are used by different organisms. Not all organisms use the same mitotic apparatus, although the goal of mitosis is always to equally segregate duplicate copies of chromosomes to each resulting cell. (A) Bacteria attach their chromosomes (blue) to the cell wall (black) and pinch the membrane between the attachment sites. (B) In yeast cells, single microtubules (green) attach kinetochores (red) on chromosomes to the nuclear envelope (pink) at the spindle pole bodies (yellow). (C) In animal cells, the nuclear envelope is broken down in early mitosis and microtubules attach the centrosome (yellow) directly to the cell wall while bundles of microtubules connect the kinetochore to the centrosome. (Diagrams are not to scale, although the relative size of each cell type is shown by the accompanying scale bars.)

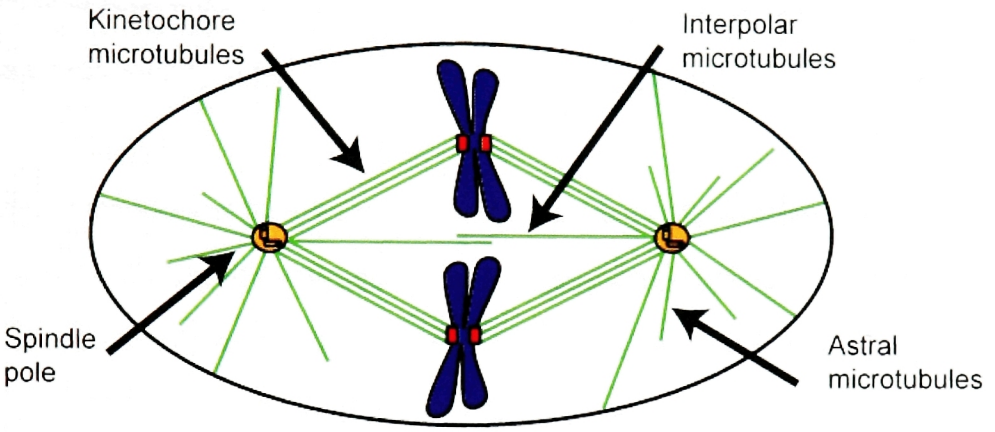

Figure 1.2 The microtubules of the mitotic spindle. In the mitotic spindle, there are three types of microtubules that are classified by the structures with which they interact. The spindle pole describes the focus of microtubules in each half of the spindle. Kinetochore microtubules bind to the kinetochores on chromosomes, which (in vertebrate cells) accumulate to form well-organized bundles that attach the chromosome to the spindle pole. Interpolar microtubules interact with microtubules from the opposite pole and form a region of overlap at the midzone. Astral microtubules radiate outward from the centrosome in an aster, elongating and shortening through the cytoplasm or interacting with the plasma membrane.

In cells as well as *in vitro* (Mitchison and Kirschner 1984b), the dominant nucleation site for microtubules are the centrosomes, which are typically found at the foci of each spindle pole in animal cells. Centrosomes consist of a pair of cylindrical centrioles surrounded by a cloud of proteins collectively called the peri-centriolar material.

One component of the peri-centriolar material is γ-tubulin, a form of tubulin which adorns the outer surface of the γ-tubulin ring complex, a structure that has been shown to provide nucleation sites for microtubule assembly (reviewed in Dammermann et al. 2003). In interphase, a single centrosome is found near the nuclear envelope, at the center of the microtubule-organizing center (MTOC) of the cell, where the minus ends of most microtubules terminate, while the plus ends extend toward the cell periphery. The centrosome duplicates independently but around the same time as the chromosomes, before mitosis initiates (reviewed in Meraldi and Nigg 2002). At the beginning of mitosis, the duplicated centrosomes migrate away from each other along the nuclear envelope; and the interphasic array of microtubules is cleared from the cytoplasm (Rusan et al. 2002). As the nuclear envelope is disassembled, each centrosome becomes the focus of an active aster of microtubules, which will eventually form the microtubule lattice of the mitotic spindle.

Microtubules are essential cytoskeletal polymers that are made of repeating α- and β-tubulin heterodimers and are present in all eukaryotes. Microtubules affect cell shape, cell transport, cell motility, and cell division. All of these functions involve the interaction of microtubules with a large number of microtubule-associated proteins (MAPs), which are important for the regulation and distribution of microtubules in the cell (for a review, see Gadde and Heald 2004).

Tubulin is believed to have evolved from it's bacterial homologue, FtsZ, which has essentially the same three-dimensional structure as tubulin, even though the two proteins exhibit only low sequence identity to each other (10–18% at the amino acid level) (for a review, see Nogales 2000; Addinall and Holland 2002). Both tubulin and FtsZ use GTP to form filamentous polymers. In eukaryotes, microtubules are constructed of 13 linear filaments that assemble from α- and β-tubulin subunits, and arrange to form a hollow tube. In microtubules, the α/β-tubulin heterodimers align end to end and identify the polarity of the two ends of a microtubule (Figure 1.3). Each end of the microtubule has different polymerization rates and has been named accordingly; the faster growing end is referred to as the "plus" end and the slower growing end is called the "minus" end (Allen and Borisy 1974).

The polymerization and depolymerization dynamics of microtubules have been studied extensively in cells as well as *in vitro* (reviewed in Desai and Mitchison 1997). Microtubule dynamics can be described by four parameters: growth rate; shrinkage rate; catastrophe frequency, which is the transition from growth to shrinkage; and rescue frequency, which is the transition from shrinkage to growth (Walker et al. 1988). One of the primary features of microtubule behavior is dynamic instability, which describes the tendency of individual microtubule ends to alternate stochastically between prolonged phases of polymerization and depolymerization (Mitchison and Kirschner 1984a). The polymerization of microtubules is thought to be stabilized by a cap of GTP-bound tubulin at the microtubule tip. Stochastic loss of the "GTP cap," due to hydrolysis or subunit loss, results in a transition to the depolymerizing phase known as catastrophe (see Desai and Mitchison 1997), a transition that can be regulated by interaction with MAPs or even by force applied to the microtubule itself (Janson et al. 2003). In addition to being highly dynamic, microtubules are capable of doing work and can generate both

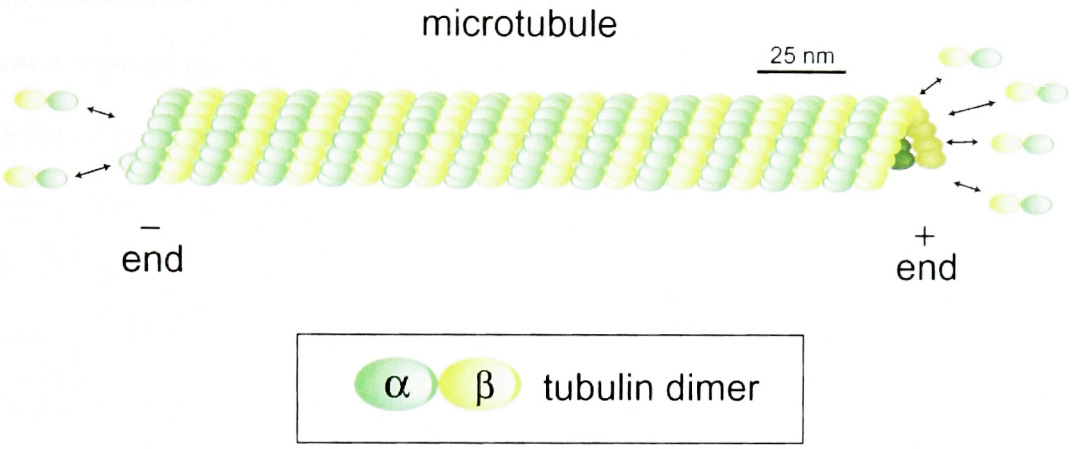

Figure 1.3 Microtubule structure and assembly. Microtubules are composed of tubulin dimers that assemble in staggered helixes to make an asymmetric hollow filament. Net assembly and disassembly of tubulin dimers occurs preferentially at the plus end.

pushing forces by polymerization and pulling forces by depolymerization (Inoue and Salmon 1995).

One of the most striking examples of cellular regulation of microtubule dynamics occurs at the transition from interphase to mitosis. During this transition the microtubule array is dramatically reorganized (Rusan et al. 2002) and the rate of microtubule turnover increases (Salmon et al. 1984; Saxton et al. 1984), which results in a decrease in total microtubule polymer levels at the beginning of mitosis (Zhai et al. 1996). Interphase microtubules are relatively long and have a turnover half time of more than 10 min, however, when cells enter mitosis the rate of catastrophe increases, resulting in a population of microtubules that are relatively short and very unstable with a half time of microtubule turnover of less than 60s (for a review, see Compton 2000). Overall, mitotic microtubules approximately 7 to 10 fold are more dynamic than interphase microtubules, and astral microtubules exhibit an increase in the catastrophe frequency and a decrease in the rescue frequency of microtubules (Rusan et al. 2001). This dramatic change in microtubule stability involves modulation of microtubule dynamics, which is tightly regulated by the opposing activities of several MAPs, which act as microtubule stabilizers, or microtubule destabilizers (for a review, see Desai and Mitchison 1997).

§ 1.2 How do K-fibers form?

For accurate segregation of replicated genetic material into two daughter cells, sister kinetochores on each chromosome must establish stable K-fibers with the opposite poles of the spindle (reviewed in Scholey et al. 2003). The interphasic array of chromosomes and microtubules is dramatically different from the mitotic assembly and the process of building a functional spindle is a subject of active research. In 1986,

Kirschner and Mitchison proposed a model for spindle morphogenesis which suggests that dynamic instability in mitosis allows microtubules to search the three-dimensional space of the cell more effectively than would be possible with equilibrium-dependent polymerization, thereby enabling microtubules to find specific target sites within the cell. In this model, centrosomes nucleate a radial array of dynamic microtubules whose plus-ends are captured and selectively stabilized by kinetochores, resulting in the formation of K-fibers (Figure 1.4).

Several lines of evidence, including direct observations of microtubule capture by kinetochores (Hayden et al. 1990; Rieder and Alexander 1990), provide extensive experimental support for the Kirschner-Mitchison hypothesis (reviewed in Rieder and Salmon 1998). However, the plus-end search-and-capture model implies that all kinetochore microtubules are derived from astral microtubules that were nucleated from centrosomes.

While centrosomes are the dominant site of microtubule nucleation in cells (reviewed in Hyman and Karsenti 1998; Tassin and Bornens 1999), some experimental data are not consistent with the idea that all kinetochore fibers arise from astral microtubules. For example, careful analysis of spindle microtubules by electron microscopy has established that the minus-ends of many spindle microtubules, including some kinetochore microtubules, do not terminate at the centrosome (Rieder 1981; McDonald et al. 1992; Mastronarde et al. 1993). These microtubules are instead focused at the pole and tethered to the centrosome and its associated astral microtubules by the actions of non-centrosomal structural and motor proteins such as NuMA, cytoplasmic dynein, and HSET/Ncd (Gaglio et al. 1995; Gaglio et al. 1996; Merdes et al. 1996; Gaglio et al. 1997; Merdes and Cleveland 1997; Compton 1998). Moreover, even though both ends of microtubules exhibit dynamic instability *in*

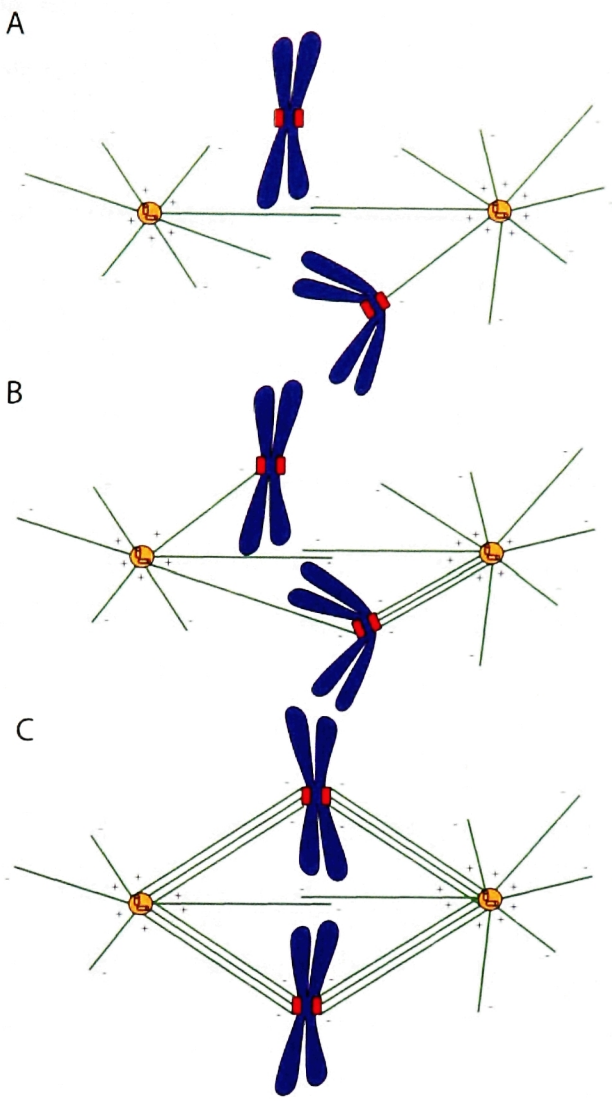

Figure 1.4 The search-and-capture model of spindle morphogenesis. (A) After nuclear envelope breakdown, highly dynamic astral microtubules search the cytoplasm, randomly encountering the kinetochores on chromosomes (lower chromosome). (B) Eventually, all kinetochores are captured by astral microtubules, and attachments accumulate at kinetochores until all kinetochores have a full compliment of kinetochore microtubules. (C) Through coordinated assembly and disassembly in each bundle of kinetochore microtubules, the chromosomes oscillate between the poles until the chromosome is arranged in the mid-zone with a kinetochore microtubule bundle binding each kinetochore to one pole and its sister kinetochore to the other.

vitro (Walker et al. 1988; Erickson and O'Brien 1992), the minus-ends of kinetochore microtubules appear relatively stable *in vivo* even if the centrosome and its astral microtubules are dislocated from the spindle pole (Mitchison and Salmon 1992; Gordon et al. 2001). Finally, a centrosome-independent pathway for mitotic spindle formation has been directly observed in vertebrate cells by ablating centrosomes with a laser during entry into mitosis (Khodjakov et al. 2000). This experiment is particularly revealing, in that it clearly demonstrates that kinetochore fibers do not form through the conventional plus-end search-and-capture mechanism in the absence of centrosomes and their associated astral microtubules. These observations indicate that mechanisms other than plus-end search-and-capture may contribute to spindle assembly in vertebrate cells.

In addition to the centrosomal pathway, another mechanism proposed for mitotic spindle assembly is the local stabilization of microtubules at chromosomes (Nicklas and Gordon 1985; Heald et al. 1996) which is mediated by the small GTPase Ran (reviewed in Heald and Weis 2000). In interphase, Ran in its GTP-bound form (Ran-GTP) is present in high concentrations inside the nucleus, where it releases cargo that has been imported into the nucleus by the nuclear import receptors. In mitosis, when the nuclear envelope breakdown releases the chromatin into the cytoplasm, the chromatin-bound guanine nucleotide exchange factor RCC1 ensures that Ran near the chromatin is in its active GTP-bound form, thereby producing a gradient with a high concentration of Ran-GTP around chromatin (Carazo-Salas et al. 1999; Kalab et al. 2002).

The current model of the mechanism of Ran-dependent microtubule nucleation links the Ran-GTP dependent release of microtubule-stabilizing factors from inhibitory complexes with nuclear import receptors (reviewed in Kahana and Cleveland 2001; Dasso 2002). In *Xenopus* egg extract, addition of a non-hydrolysable Ran-GTP induces

microtubule polymerization, as does the depletion of Ran-GTP binding proteins (Ohba et al. 1999; Zhang et al. 1999). These results suggest that Ran-GTP counteracts the inhibition of aster formation by some other factor. The nuclear import receptors importin α and β inhibit microtubule aster formation and spindle formation around sperm nuclei or chromatin beads in *Xenopus* extract (Gruss et al. 2001; Nachury et al. 2001; Schatz et al. 2003). In mammalian cells, injection of the cargo binding domain of importin β into prometaphase PtK1 cells disrupted spindle formation in mitosis (Nachury et al. 2001). This data supports a model of chromatin-associated microtubule nucleation and polymerization in which the Ran-GTP gradient around chromosomes releases microtubule-nucleating factors from their inhibitory interaction with the import receptors (Gruss et al. 2001; Kahana and Cleveland 2001; Marshall and Kahana 2001; Wiese et al. 2001; Schatz et al. 2003; Trieselmann et al. 2003). Although the specifics of the Ran-GTP pathway of spindle assembly are still being investigated, two MAPs (NuMA and TPX2) have emerged as likely candidates for microtubule stabilizing factors.

Clearly, several mechanisms of mitotic spindle morphogenesis may be acting concurrently in many cell types, and it appears that the strategy used may be at least in part dependent on the model system. For example, the worm *C. elegans* appears to depend primarily on the centrosomal pathway (for example, see Hannak et al. 2002) while in *Xenopus* frog egg extracts the chromosome-mediated pathway may be dominant (Carazo-Salas et al. 1999; Kahana and Cleveland 2001; Kalab et al. 2002). Both mechanisms, however, rely on microtubule-associated proteins to regulate microtubule nucleation, stabilization, dynamicity, and organization. This will be discussed in detail below, but first it is worthwhile to review the role of MAPs in mitosis.

§ 1.3 The role of mitotic MAPs in spindle morphogenesis

All MAPs can be divided into two main categories: microtubule motors and non-motor MAPs. Microtubule motors translocate along microtubules by ATP hydrolysis, and are responsible for force production and transport of cargoes along microtubules. Although the characteristics of MAPs are as diverse as their cellular function, many have been studied in detail (for example, see Maccioni and Cambiazo 1995).

MAPs, microtubules, chromosomes, and other mitotic proteins act in concert to form the highly dynamic mitotic spindle which ultimately must be capable of aligning chromosome pairs at the spindle equator in metaphase and accurately segregating sister chromosomes to opposite poles at anaphase (Sharp et al. 2000; Kapoor and Compton 2002). Microtubule motors use cross-linking and translocation of microtubules to transport spindle microtubules or other mitotic cargoes, creating forces between different points in the spindle (Gaglio et al. 1996; Gaglio et al. 1997; Sharp et al. 2000; Gordon et al. 2001; Howell et al. 2001; Cytrynbaum et al. 2003). In addition, microtubule polymerization dynamics can also produce forces that contribute to spindle morphogenesis (Waters et al. 1996; Janson et al. 2003).

MAPs play a prominent role in the pathology of several diseases and were first identified in brain extract (a good source of microtubules due to the high microtubule concentration in axons and dendrites), in part because of their abundance but also because they provide selective markers for brain development and cell type (reviewed in Mandelkow and Mandelkow 1995).

Although the interaction between MAPs and microtubules is critical, the sequence of the microtubule-binding site is generally not conserved or even predictable. For example, the microtubule binding site of the non-motor MAPs tau and Map2 are in the C-terminus (Butner and Kirschner 1991; Al-Bassam et al. 2002), whereas the related

protein Map1 has the microtubule binding site in the N-terminus (Noble et al. 1989). The microtubule binding sites on each of these proteins are highly basic with many repeating elements. However, another non-motor MAP, NuMA, has a highly acidic microtubule binding site in the C-terminus (Haren and Merdes 2002). In most cases, the microtubule binding site must be determined by generating truncations of the protein to determine which domain(s) is (are) required to bind the negatively charged microtubules.

In addition to sequence diversity, the structures of MAPs are highly variable. Many microtubule motors are dimeric (e.g., the conventional kinesin (Sablin 2000)) while some form tetramers (e.g., Eg5 (Kashina et al. 1996)). Microtubule motors often contain coiled-coil "tail" domains for multimerization or folding, connected to the microtubule binding regions (often called the motor domain) by a "neck" linker. The sizes of MAPs vary from the tiny tau protein of 55 kD to the multi-component dynein complex, weighing in at more than 1000 kD. In addition to forming homodimers, MAPs also bind to each other, forming multi-component complexes like the dynein-NuMA complex (Merdes et al. 1996), which will be discussed later. In addition to binding microtubules and translocating cargoes, MAPs can affect microtubule polymerization dynamics. For example, tau and MAP2 stabilize microtubules during polymerization (reviewed in Mandelkow and Mandelkow 1995); the microtubule motor XKCM1 promotes depolymerization at microtubule minus ends (Kline-Smith and Walczak 2002); and the MAP katanin severs microtubules, promoting disassembly (McNally and Vale 1993).

Microtubule motors can be further divided into two classes, depending on the direction of movement they produce on the microtubule. For example, dynein and Ncd are both minus-end directed motors; while Eg5, CENP-E and classical kinesin are all plus-end directed (reviewed in Sharp et al. 2000). However, the nomenclature is complicated by the fact that all motors except dynein belong to a family of motors called kinesins. In addition, each microtubule motor can be differentiated by their specific set

of cargos (determined by the binding sites at their tail domains), and their translocation velocities (which range from 0.1 μm/second (Ncd) to 1 μm/second (dynein) *in vitro*) (Shimizu et al. 1995).

During mitosis, MAPs perform a range of functions throughout the spindle. For example, the motors MCAK (Maney et al. 1998) and CENP-E (McEwen et al. 2001) link chromosome movement to microtubule dynamics (Hyman and Mitchison 1991), while other non-motor MAPs such as Stu2/XMAP215 act to regulate spindle length by affecting microtubule dynamics (Pearson et al. 2003; Shirasu-Hiza et al. 2003; van Breugel et al. 2003). Some MAPs (both motors and non-motors) focus microtubules at the poles, including the minus-end directed microtubule motor dynein and the microtubule bundling protein, NuMA (Price and Pettijohn 1986; Compton and Cleveland 1994; Gaglio et al. 1995; Merdes et al. 1996; Merdes et al. 2000).

Forces generated by microtubule motors can affect displacement of any of the spindle components whenever there is an imbalance of forces at a specific location. For example, the plus-end directed kinesin, Eg5, is required to establish the bipolarity of the spindle (Sawin et al. 1992), and is believed to act by sliding overlapping microtubules at the spindle mid-zone, creating a force that separates the two spindle poles. Other microtubule motors, such as the chromosome-bound plus-end directed motor Kid, produce a force between the chromosome arms and the astral microtubules, pushing chromosomes toward the spindle equator (Funabiki and Murray 2000). In this way, motors throughout the cell act cooperatively in a dynamic balance of complementary and antagonistic forces to build and maintain the spindle (Gaglio et al. 1996; Mountain et al. 1999; Sharp et al. 1999; Sharp et al. 2000).

Microtubule motors are widely recognized for their roles in transporting mitotic cargoes and arranging microtubules to form a dynamic spindle that is capable of segregating chromosomes (Hyman and Mitchison 1991; Gaglio et al. 1996; Howell et al.

2001). Some non-motor MAPs are also essential for spindle morphogenesis, such as NuMA and TPX2, which are required for bipolarity of the spindle and stabilization of the spindle poles (Compton and Cleveland 1994; Gaglio et al. 1995; Merdes et al. 1996; Merdes et al. 2000; Garrett et al. 2002; Gruss et al. 2002). Interestingly, both NuMA and TPX2 have been identified as candidates for the microtubule nucleating factor (or factors) released from an inhibitory interaction with nuclear import receptors in the Ran pathway of chromosome-associated microtubule nucleation (Nachury et al. 2001; Wiese et al. 2001; Tsai et al. 2003). In the following chapters, I will investigate the roles of both NuMA and TPX2 in the formation of K-fibers in spindle morphogenesis, and so it is worthwhile to introduce these two MAPs in more detail here.

§ 1.4 NuMA is a structural microtubule binding protein involved in focusing poles and anchoring the minus-ends of microtubules in the spindle.

NuMA (Nuclear Mitotic Apparatus protein) is a microtubule associated protein involved in focusing microtubules at mitotic spindle poles (Lydersen and Pettijohn 1980; Gaglio et al. 1995; Merdes and Cleveland 1997). At approximately 236 kD, NuMA is a large MAP and is predicted to contain two globular domains separated by a discontinuous alpha-helix with characteristics for adopting a coiled-coil structure (Compton et al. 1992). NuMA also contains a nuclear localization sequence that ensures nuclear sequestration in interphase (Saredi et al. 1996). However, after nuclear envelope breakdown (NEB), NuMA binds to microtubules and is transported to the minus-end of microtubules, accumulating in a crescent-shaped area of high microtubule density at the poles of mitotic spindles by the dynein/dynactin microtubule motor

complex (Figure 1.5) (Heald et al. 1996; Merdes et al. 1996; Merdes et al. 2000; Haren and Merdes 2002).

NuMA is a soluble protein in mitotic extracts prepared from synchronized cultured cells, but forms insoluble filamentous mesh-works when the extract becomes non-mitotic (Saredi et al. 1996; 1997), indicating a possible structural role at the poles in mitosis. In support of this hypothesis, Merdes et al. (1996) found that microinjection of anti-NuMA into mitotic cultured cells or the removal of NuMA from mitotic extract leads to the disruption of bipolar mitotic spindles (and in extract this can be recovered by adding back purified protein). These results indicate that NuMA is necessary to bundle and organize microtubule minus ends at the spindle poles in mitosis.

The C-terminal tail domain of NuMA, called NuMA tail II, has been shown to bind microtubules, mediate oligomerization and induce the formation of microtubule asters when added to *Xenopus* egg extracts in the absence of chromatin or centrosomes, indicating that NuMA may stabilize microtubules as well (Merdes et al. 1996; Harborth et al. 1999). NuMA tail II also has a nuclear localization sequence, which binds to importin β (a nuclear import receptor) which presumably facilitates the sequestration of TPX2 in the nucleus in interphase. In mitosis, microtubule asters do not form when both NuMA tail II and importin β are added to *Xenopus* extract (Wiese et al. 2001), indicating a possible role for NuMA in the Ran-GTP microtubule nucleation pathway. In fact, when Ran-GTP is added to *Xenopus* extract, importin β no longer binds to the tail domain of NuMA, suggesting that Ran disrupts the interaction between importin β and NuMA (Nachury et al. 2001; Wiese et al. 2001).

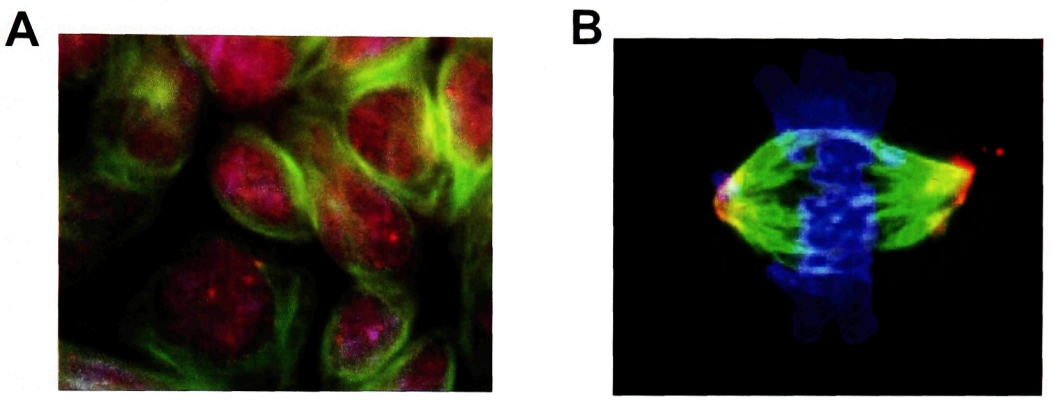

Figure 1.5 NuMA localization in mammalian cells. HeLa cells in culture are stained for chromosomes (blue), microtubules (green) and NuMA (red). Areas where NuMA and chromosomes overlap appear purple. (A) In interphase, NuMA localizes to the nucleus. (B) In mitosis, NuMA binds microtubules and localizes to a crescent shaped region at the poles.

§ 1.5 TPX2 is a non-motor MAP required for bipolar spindle assembly

TPX2 is a 100 kD protein originally identified as the component of purified MAPs required for the recruitment of the kinesin Xklp2 to microtubules (Wittmann et al. 1998) and was subsequently named Tpx2 for Targeting Protein for Xklp2. However, it was later discovered that immunodepletion of TPX2 leads to multipolar spindles while immunodepletion of Xklp2 does not (Wittmann et al. 2000). Although the relationship between TPX2 and Xklp2 is still not well understood, TPX2 has been shown to have other roles in mitosis as well (Gruss et al. 2001; Garrett et al. 2002; Gruss et al. 2002; Kufer et al. 2002; Eyers et al. 2003; Glover 2003; Schatz et al. 2003; Trieselmann et al. 2003; Tsai et al. 2003).

Like NuMA, TPX2 is sequestered in the nucleus in interphase and binds microtubules in all stages of mitosis (Figure 1.6) (see also Wittmann et al. 2000; Schatz et al. 2003). Studies of TPX2 truncation mutants reveal TPX2 contains a nuclear localization sequence and binding domains for both microtubules and the mitotic kinase Aurora-A (also known as Eg2) in the amino terminus as well as a microtubule binding domain in the carboxyl terminus (Figure 1.7) (Kufer et al. 2002; Trieselmann et al. 2003).

In *Xenopus* egg extract, depletion of TPX2 produces aberrant, disorganized spindles with multiple poles, described as "disintegrating poles" although this analysis has been limited to fixed samples (Wittmann et al. 2000). This suggests a role for TPX2 in organizing spindle poles in mitosis. In experiments performed with mammalian cells, TPX2 knockdown by RNAi has shown a variety of results. For example, Gruss et al. (2002) found that TPX2 RNAi led to the formation of two microtubule asters that did not interact and did not form a spindle, although in this study knockdown was shown to be

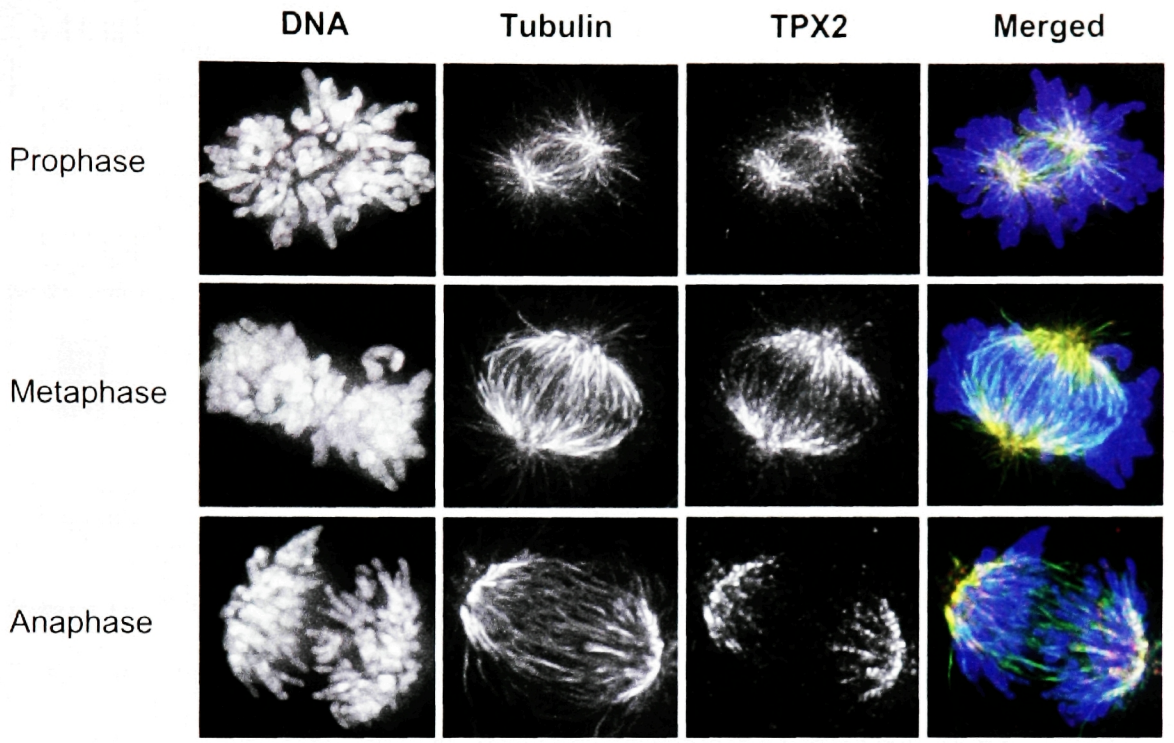

Figure 1.6 TPX2 localizes to microtubules throughout mitosis. HeLa cells fixed in prophase (top), metaphase (middle) and anaphase (bottom) were stained for chromosomes (blue), tubulin (green), and TPX2 (red). Overlaying all three channels (right), shows that TPX2 has strong co-localization with microtubules throughout mitosis.

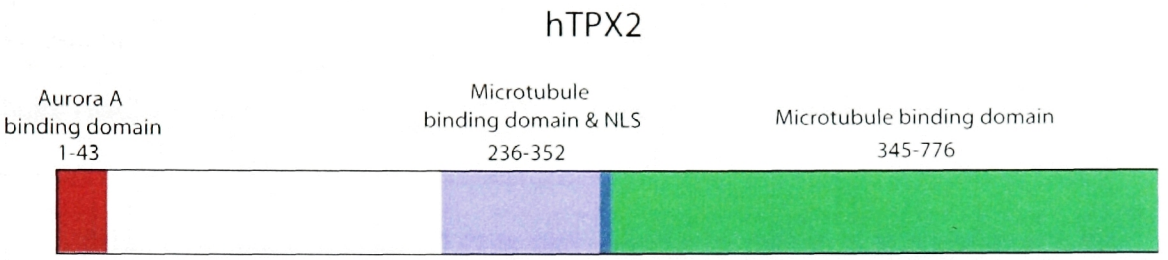

Figure 1.7 The domains of TPX2 as determined by analysis of truncation mutants. TPX2 has a microtubule-binding domain and an NLS in the region between aa 236 and 352, with mutations at aa 284 sufficient to prevent importin-α binding to TPX2. The first 43 amino acids of TPX2 are required for binding and activation of Aurora A. In addition, a second microtubule binding activity has been identified in the carboxyl terminus of TPX2. Adapted from Bayliss et al. (2003), Trieselmann et al. (2003), Schatz et al. (2003), and Kufer et al. (2002).

incomplete by Western blot analysis. In contrast, Garrett et al. (2002) found fragmented spindle poles after TPX2 knockdown (using a different RNAi oligo) which led to a significant increase in the formation of multipolar spindles. Subsequently, Kufer et al. (2002) showed that after TPX2 knockdown in cells in which knockdown was confirmed by immunofluorescence, spindle formation was progressively impaired, and many cells rounded up and arrested in a prometaphase-like stage with fragmented spindle poles. These results suggest that TPX2 has a role in preventing pole fragmentation in human cells.

Other data suggests that TPX2 is also required for microtubule nucleation in the Ran-GTP model of chromatin-induced spindle assembly in the absence of centrosomes (Gruss et al. 2001). Addition of excess TPX2 induces microtubule aster formation in *Xenopus* egg extracts (Wittmann et al. 2000; Gruss et al. 2001) and bundling of microtubules in dilutions of pure tubulin (Schatz et al. 2003). When TPX2 is depleted from *Xenopus* extract, spindle formation around chromatin-coated beads is inhibited, while addition of recombinant TPX2 to depleted extracts rescues microtubule nucleation and spindle assembly (Gruss et al. 2001). These results support a model in which TPX2 is required for microtubule nucleation in acentrosomal *Xenopus* extract.

TPX2 also binds to nuclear import receptors, which is not surprising considering that TPX2 is nuclear in interphase, although recent studies suggest a possible role for the interaction between the nuclear import receptors and TPX2 in mitosis. TPX2 binds importin-α in mitotic *Xenopus* extract while addition of exogenous importin-α prevents TPX2-induced microtubule nucleation (Gruss et al. 2001; Schatz et al. 2003). However, the aster-promoting activity of TPX2 may be independent of microtubule binding, as importin-β does not inhibit the microtubule binding capacity of TPX2 in extracts of human HeLa cells (Trieselmann et al. 2003) and addition of importin-α prevents TPX2-induced microtubule formation but not TPX2-tubulin interaction or microtubule bundling in dilute

solutions of pure tubulin (Schatz et al. 2003). These results have led to a model for chromatin-mediated microtubule assembly where Ran-GTP stimulates the formation of microtubule asters by releasing TPX2 (and/or NuMA) from inhibitory interactions with nuclear import receptors (Figure 1.8) (Carazo-Salas et al. 1999; Zhang et al. 1999; Nachury et al. 2001; Wiese et al. 2001; Tsai et al. 2003).

However, TPX2 may have additional roles in spindle assembly when centrosomes are present. For example, when purified centrosomes are added to TPX2 depleted extract, asters of abnormally long microtubules form in high concentrations of Ran-GTP (Gruss et al. 2002). This suggests that while TPX2 may promote microtubule assembly around chromatin in the Ran-GTP pathway, it may also be required for regulation of microtubule length once microtubules are formed.

Further, it has been proposed that spindle formation in somatic cells requires a population of chromatin-associated microtubules that are dependent on Ran-GTP and TPX2 for assembly, possibly resulting in defects in kinetochore microtubule fibers in the absence of TPX2 (Gruss et al. 2002). However, this has never been directly observed and the role of TPX2 in K-fiber formation and spindle morphogenesis is still unclear.

Another potential clue to understanding the role of TPX2 in mitosis is the interaction between TPX2 and the Aurora-A kinase. Aurora-A is associated with the centrosome and microtubules near the spindle pole, where it recruits γ-tubulin and other MAPs to the centrosome (Giet and Prigent 2000; Hannak et al. 2001; Meraldi et al. 2002; Marumoto et al. 2003; Terada et al. 2003; Tsai et al. 2003). This data suggests that Aurora-A promotes spindle assembly by organizing microtubule nucleating sites at the pole (reviewed in Blagden and Glover 2003). Deletion mutants and ultra-structural analysis show that the amino-terminus of TPX2 binds the carboxyl-terminus of Aurora-A

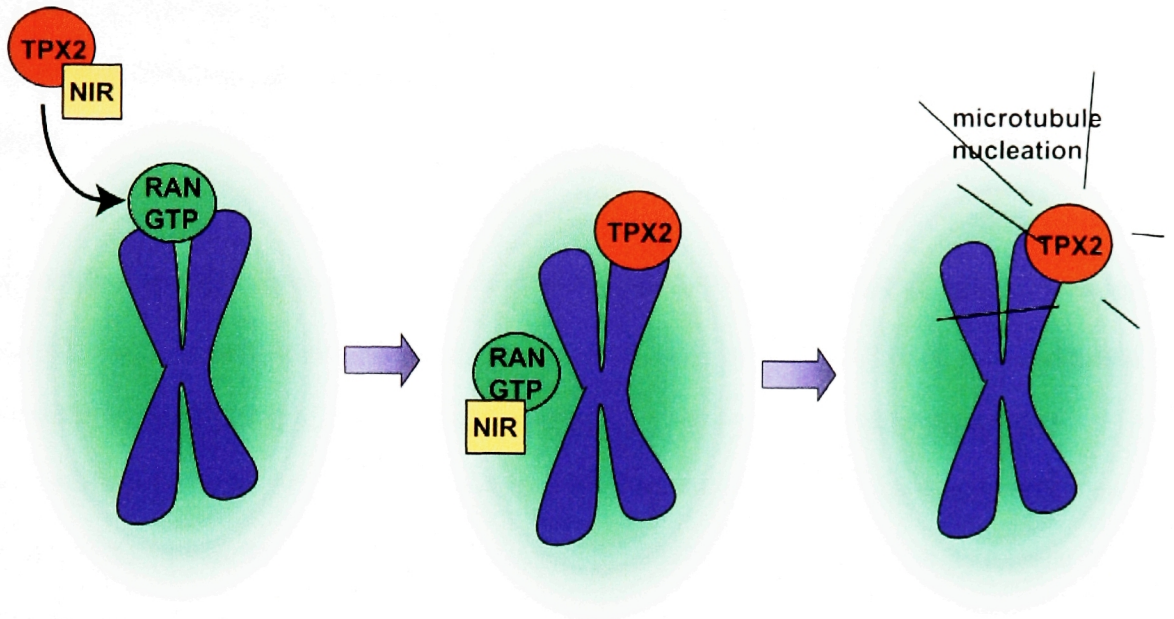

Figure 1.8 A model for how TPX2 may be released from its inhibitory interaction with nuclear import receptors in the presence of Ran-GTP. (Left) TPX2 is normally inactivated by binding to nuclear import receptors (NIR). (Middle) In the presence of Ran-GTP, which is found in high concentrations near chromosomes, TPX2 is displaced from the nuclear import receptors. (Right) It has been proposed that this activated TPX2 is responsible for chromatin-induced microtubule assembly in mitosis. (Adapted from Nanchury et al. (2001) and Gruss et al. (2002).)

(Kufer et al. 2002; Bayliss et al. 2003). Interestingly, inhibition of the interaction between TPX2 and Aurora-A by either TPX2 RNAi or addition of nuclear transport receptors show that in the absence of TPX2, Aurora-A does not target to spindle microtubules (although centrosomal targeting was unaffected) while Aurora-A RNAi does not disrupt TPX2 targeting to the mitotic spindle (Kufer et al. 2002; Trieselmann et al. 2003).

These results suggest that TPX2 produces some effect that allows Aurora-A to target spindle microtubules. Activation of the Aurora-A kinase requires phosphorylation; and although Aurora-A can auto-phosphorylate, the binding of TPX2 to Aurora-A causes a conformational change in Aurora-A, thereby increasing autophosphorylation and protecting Aurora-A from dephosphorylation (Bayliss et al. 2003; Eyers et al. 2003; Tsai et al. 2003). It has also been demonstrated that TPX2 is phosphorylated by Aurora-A (Trieselmann et al. 2003), although the functional significance of this phosphorylation is not yet clear.

In the context of spindle morphogenesis and the origins of spindle microtubules, the interaction between TPX2, Aurora-A, and the nuclear transport receptors is also suggestive. For example, when TPX2 is bound to importin-α, it can still bind microtubules, but not Aurora-A (Trieselmann et al. 2003; Tsai et al. 2003). Together, this may provide insight into the possible mechanism of a TPX2 mediated influence on microtubule nucleation and assembly in the Ran-GTP pathway.

In the following chapters, I will further examine the role of TPX2 and NuMA in mitotic spindle assembly by using three-dimensional microscopy and live cell imaging. Recent advances in microscopy have expanded the capabilities of live cell imaging to provide a new opportunity to elucidate the contributions of MAPs in mitotic spindle assembly.

§ 1.6 Three-dimensional microscopy and live cell imaging

In microscopy, image quality is primarily determined by three factors: spatial resolution, resolution of light intensity, and signal-to-noise ratio. In time-lapse imaging, an additional limitation is the temporal resolution of image acquisition.

Spatial resolution can be affected by many properties (including optical aberrations and background signal), but even under ideal circumstances, spatial resolution is ultimately limited by the diffraction of light by the source (in this case the specimen) (for a review, see Inoue 1990). The minimum radius (r) of the diffraction spot for a self-luminous point of light in the image plane is defined as:

$$r = 0.6 \lambda / NA$$

where λ is the wavelength of light and NA is the numerical aperture of the objective (for a review, see Murphy 2001). This distance (r) is also called the Rayleigh limit – the necessary separation of two self-luminous point sources such that their diffraction patterns show a detectable (≥ 20%) drop in intensity between them. This means that r is the theoretical limit for how close two objects in the image plane can be before they cannot be distinguished optically (see Webb and Dorey in Pawley 1995). The NA is defined by the angle describing the cone of light paths that can be accepted by the objective (2θ), and the refractive index of the medium between the lens and the specimen (η):

$$NA = \eta \sin\theta$$

(Hecht 1998).

While some adjustments can be made to use lower wavelengths of light, in white light microscopy a range of wavelengths are applied at once, and in fluorescence imaging the available fluorescent probes for most applications are limited. The only other option for improving the optical resolution is to use an objective with the highest

possible NA. The NA can be optimized by using objectives designed to maximize light collection from the sample by bridging the gap between the sample and the objective with refractive oils that match the optical qualities of the glass in the objective. A typical high-quality oil immersion objective has an NA of 1.4. In contrast, air has markedly different optical properties than glass or refractive oils, and a typical air objective has an NA of 0.95.

Resolution of light intensity is generally limited by the detector, and is defined as the number of gray levels that are assigned to an image by the detector. While it is always advisable to use a detector with the highest range of grey levels (also called the dynamic range), it is not always possible to utilize the entire range of the detector without harming the sample, which will be discussed later.

The signal-to-noise ratio describes the degree of visibility or clarity of an image and depends directly on three factors: the amplitude of the signal (in numbers of photons) reaching the detector from the object, the amplitude of the signal from the background, and the electronic noise of the imaging system (for a more detailed analysis, see Sheppard et al. in Pawley 1995; Matsumoto 2002). The signal-to-noise ratio is defined by the photon counts from object signal (S) and noise components, including electronic noise and background, (N):

$$\frac{S}{N} = \frac{(S_1 + S_2 + S_3 + \ldots)}{\sqrt{(N_1^2 + N_2^2 + N_3^2 + \ldots)}}$$

(reviewed in Murphy 2001).

Generally, for bright images (when the object signal is high), the background signal usually determines the signal-to-noise ratio, whereas in dim images the electronic noise becomes the limiting factor. One commonly used technique to decrease the electronic noise in an image is to acquire several images and average them. Because

the object signal will be (relatively) constant but the electronic noise is stochastic, the contribution of the electronic noise will decrease.

An additional consideration in imaging is that most cells are inherently transparent and colorless and when viewed by transmitted white light the amplitude differences in the resulting image are generally too small to reach the critical level of contrast required for optical detection. To overcome this limitation, cells are often imaged using contrast-enhancing optics or with fluorescent probes. Both techniques will be used extensively in the following chapters, and so it is worthwhile to examine them in more detail here.

One powerful technique for observing variations in optical density in a sample is called differential interference contrast (DIC) microscopy. DIC transforms local gradients in optical density into optical contrast (for a review, see Murphy 2001). Optical density is related to the time it takes for light to pass through the sample and is therefore a product of the thickness of and the speed of light though the sample (the refractive index) (Hecht 1998). In DIC optics, the amplitude of the signal corresponds to the derivative of the optical density profile and so areas of the sample that show a large gradient in the amount of time it takes for nearby light paths to pass through the sample will show sharp changes in signal intensity (contrast) (Figure 1.9).

In fluorescence imaging, a fluorescent molecule or protein is attached to the protein of interest, which will emit photons of a specific wavelength when it is excited by a different, but also specific, wavelength of light (for review see Miyawaki et al. 2003). In wide field (also called epi-luminescent) fluorescence imaging, the entire volume of the specimen is evenly illuminated while its fluorescence image is recorded. The three-dimensional volume of a cell can be constructed from a series of images taken at sequential focal planes, called a z-series (Figure 1.10 A-G). Often it is more informative to view all focal planes at once using a maximum projection. A maximum projection is

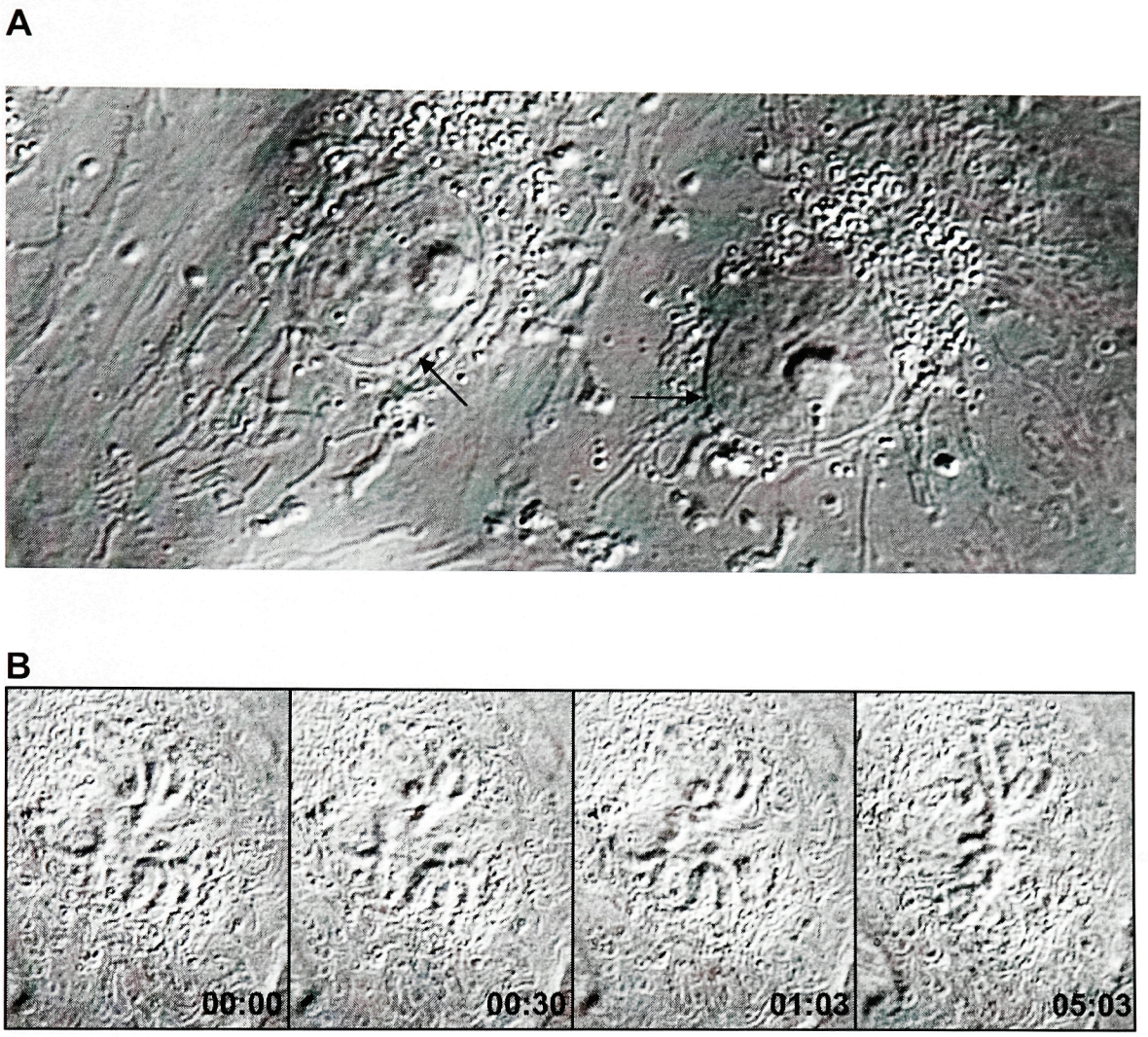

Figure 1.9 Examples of DIC microscopy. Using transmitted white light, DIC optics transforms gradients in optical density in the sample to gradients of signal amplitude at the detector. (A) Two PtK2 cells in interphase as viewed by DIC optics clearly show the nuclear envelope (arrows) and the surrounding organelles. (B) Selected frames from a time-lapse movie showing the optically dense, condensed chromosomes during congression in mitosis.

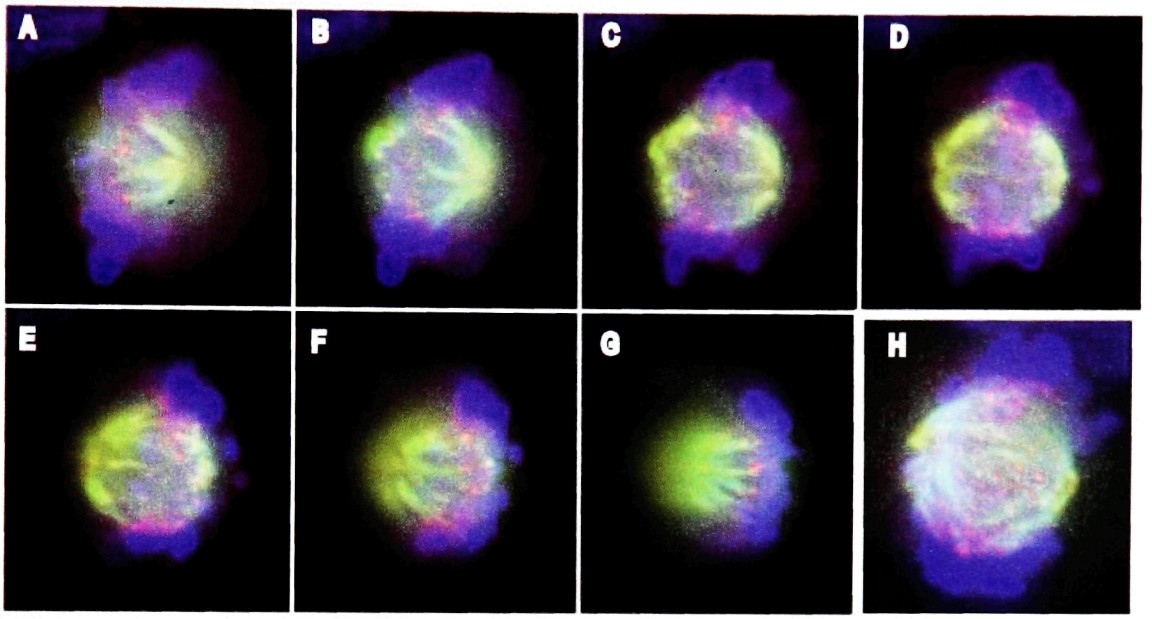

Figure 1.10 Optical sections of a three-dimensional sample can be viewed as a Z-series or a maximum value projection. (A-G) Images of a mitotic HeLa cell acquired at 1.5 µm steps can be viewed as a series of sequential images to show individual optical sections. (H) To display all optical sections in the same image, a maximum value projection can be constructed and displayed as a single image. This cell was stained for DNA (blue), microtubules (green) and kinetochores (red).

constructed by compressing a z-series of images into a single image based on the maximum brightness for each pixel through all the planes in the stack (Figure 1.10 H).

Often, cells are imaged after being preserved by treatment with a fixative. These preserved cells can then be stained with antibody-based fluorescent markers. However, for the dynamics of proteins in living cells to be observed using fluorescence microscopy, either fluorescently labeled proteins must be injected into individual cells or the cells must be induced to produce the protein of interest with a fluorescent marker on it (this is achieved by transfection or by engineering stable clones).

One of the difficulties with imaging three-dimensional objects like cells where fluorescent probes are present at different focal planes is the problem of out-of-focus light. In wide-field fluorescence optics, bright fluorescent signals from objects outside the focal plane increase the background and give low-contrast images. Recent advances in fluorescence microscopy have improved the resolution of three-dimensional imaging and the viability of time-lapse imaging of cellular processes in living cells. Prominent among these advances are deconvolution and spinning disk confocal microscopy. Both techniques greatly improve the image quality by removing out-of-focus light (for a review see Pawley 1995).

Deconvolution is a process by which out-of focus light is mathematically re-assigned to the correct focal plane by comparing the acquired image to the predicted distribution of photons from sources above or below the plane of interest (Figure 1.11) (for a review see Swedlow 2003). This algorithm is based on the acquired series of images and a detailed knowledge of the optical degradation introduced by the imaging process.

In confocal microscopy, out-of-focus light is prevented from reaching the detector in two ways. First, the illuminating beam is focused at the sample to produce a very high light intensity at the center of the focal spot and rapidly decreasing intensity over a broad

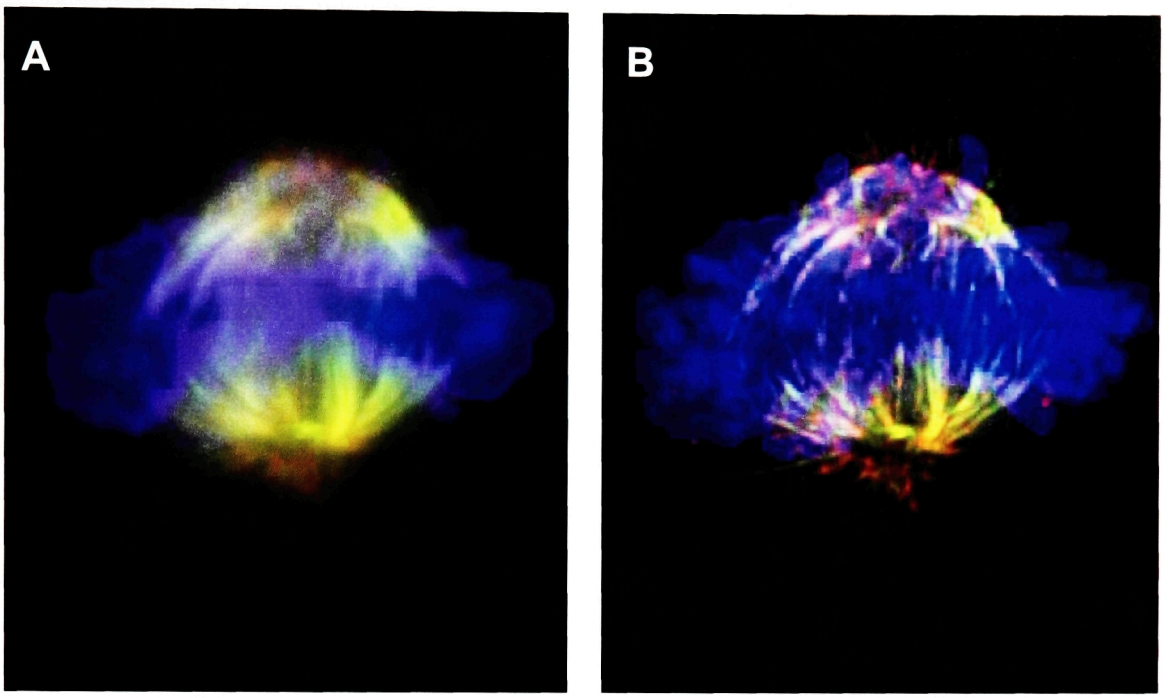

Figure 1.11 Deconvolution improves image quality by mathematically re-assigning out-of-focus light in a three-dimensional series of images. Based on the predicted spread of out-of-focus light from the plane of origin into other focal planes (the point-spread function), a three-dimensional stack of images can be analyzed to predict the origin of each photon detected by the camera. In this way, the image quality of a wide-field image like the projection shown in A can be improved by reassigning out of focus light like the projection of the same z-series after deconvolution shown in B.

region above and below this spot, thereby preventing excess excitation light from reaching the sample. In addition, a pinhole or small aperture is placed in front of the detector at a location that blocks light from other focal planes from reaching the detector (Figure 1.12). By using a pinhole with a diameter one-quarter the size of the diffraction spot diameter, the effective spot diameter of a point-source signal is reduced by a factor of 1.4 from the wide-field limit. Therefore, the minimum radius (r) of the diffraction spot for a self-luminous point of light in the image plane in a confocal microscope is:

$$r = 0.4 \lambda / NA$$

In confocal microscopy, taking images at sequential focal planes produces a z-series of "optical sections," the thickness of which are determined by the numerical aperture of the objective used, the wavelength of light and the size of the pinhole. Using the minimum pinhole size as defined above, the theoretical limit of resolution in the z-axis (z) is described by:

$$z = 1.4 \eta \lambda / NA^2$$

(for a review see Oldenbourg et al. 1993; Pawley 1995). Modern confocal microscopes are also usually equipped with an adjustable pinhole to allow the user to control the thickness of the optical sections acquired. In a scanning confocal microscope, the focused beam of a laser is scanned across the sample to produce a complete image of the sample at each focal plane (Matsumoto 2002).

One of the consequences of scanning confocal microscopy is that the very high light intensity can saturate the fluorophores at the center of the focal spot, limiting the excitation intensity that can be used effectively (Pawley 1995). When the laser intensity is reduced enough to avoid saturation, it often becomes necessary to scan the sample several times, integrating the signal intensity to acquire an image with an acceptable signal to noise ratio. In addition, since not all photons from the light source reaching the sample result in the excitation and emission of a fluorophore, the sample is exposed to

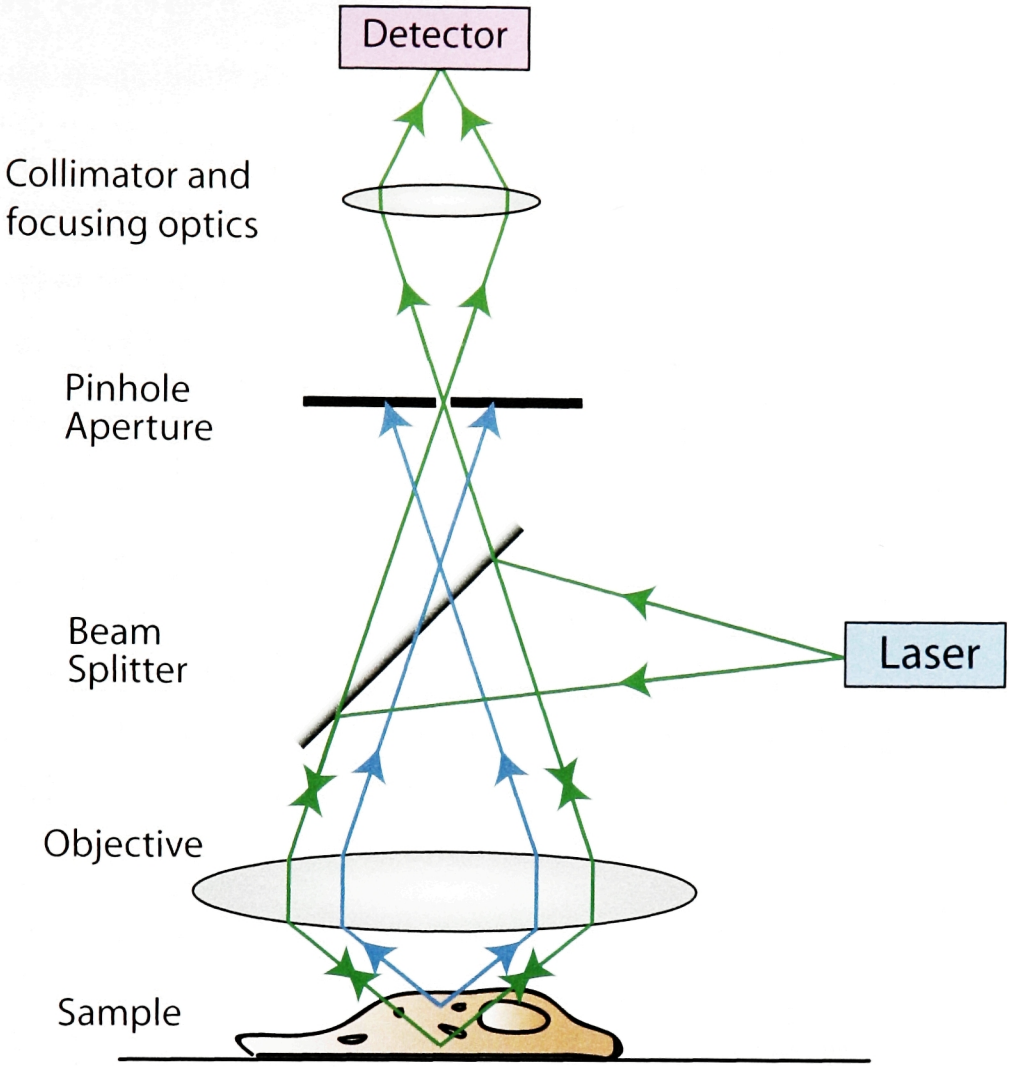

Figure 1.12 A simplified light path diagram for confocal microscopy. In a confocal microscope, the excitation light is focused to a well-defined spot in the sample, reducing excess radiation at the sample. In addition, the placement of a pinhole at a focal point between the sample and the detector allows only photons from a limited section of the sample to reach the detector (green), while out of focus photons do not (blue). (Not to scale.)

damaging levels of electromagnetic energy, where the energy of each photon (E) is related to the wavelength (λ):

$$E=hc/\lambda$$

where h is Plank's constant and c is the speed of light (for a review, see Hecht 1998).

In live cell imaging, cells can be damaged or even killed by the imaging process. This effect is called photo-toxicity. Two main sources of photo-toxicity exist in the live cell imaging techniques described here. First, absorption of excess radiation can cause damage to the ultra-structural components of the cell or result in disruptively high temperatures inside the cell. Second, in fluorescence imaging, cells can be damaged by the products of the fluorescence conversion (for a review see Matsumoto 2002).

Photo-bleaching is an additional problem that exists for time-lapse imaging where several fluorescence images are required in succession. Photo-bleaching describes the tendency of a fluorescent protein to lose its ability to fluoresce. During time-lapse imaging, photo-bleaching can cause the ratio of the signal intensity to decrease in relation to the background noise (for a review see Murphy 2001).

One technique that reduces the effects of photo-bleaching and photo-toxicity is spinning disk confocal microscopy (for a detailed review, see Inoue and Inoue in Matsumoto 2002). A spinning disk confocal microscope uses a series of co-aligned disks (sometimes called a Nipkow disks), one with pinholes and another with micro-lenses, spinning rapidly to scan the sample, simultaneously exciting the fluorescent markers in the sample and collecting emitted light (Figure 1.13) (Inoue and Inoue 2002; Nakano 2002; Rawlings and Byatt 2002; Adams et al. 2003). The thousands of pinholes in the Nipkow disk perform the same function as the pinhole in a single-point scanning system and the micro-lens disk improves the light-gathering efficiency and transmission. Using the two disks in tandem greatly reduces the radiation to which the cell is exposed and assures efficient photon detection (Adams et al. 2003; Maddox et al. 2003). The

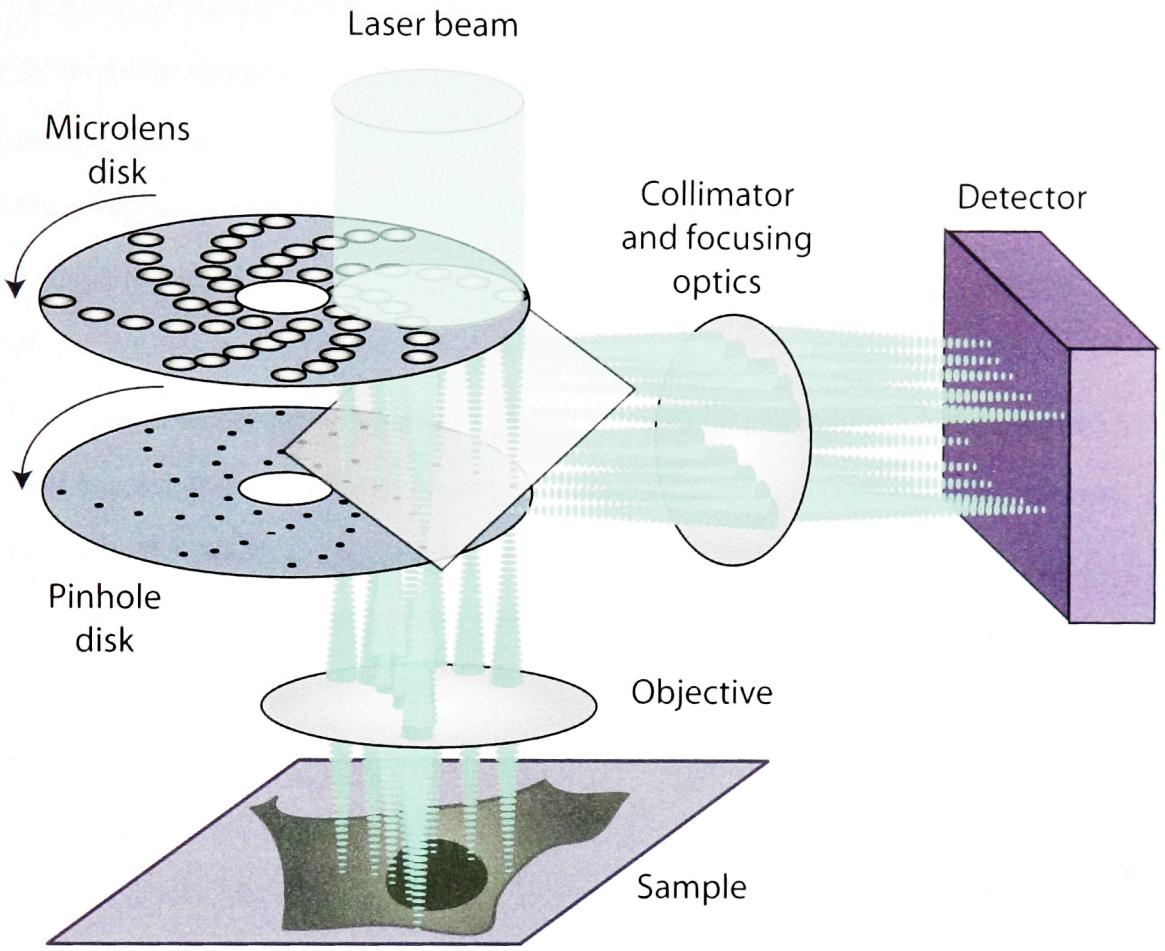

Figure 1.13 A simplified schematic of the spinning disk confocal microscope. In the spinning disk confocal microscope, light is projected on to a disk of micro-lenses with a matching disk of pinholes immediately below. The focused mini-beams of light that reach the sample are focused to the same plane and trace out concentric and slightly overlapping arcs, illuminating a single plane in the sample. When the fluorescent molecules in the sample emit photons, only those that pass through the pinholes are allowed to reach the detector, producing an image of the desired focal plane in the sample at the detector. (Diagram is not to scale.) (Adapted from Inoue and Inoue in Matsumoto 2002)

real-time, full-field scanning allows the use of a low-noise, fast, and quantum-efficient cooled charge-coupled device (CCD) with a high dynamic range as a detector as opposed to the noisier photomultiplier tubes (PMTs) used in laser-scanning confocal systems. The spinning disk microscope also combines the exclusion of out-of-focus light of the confocal system while addressing the rapid acquisition rates required of many live-cell imaging experiments. By acquiring images at sequential focal planes at regular intervals, a three-dimensional time-lapse movie can be compiled of the sample (Figure 1.14). One of the disadvantages of the spinning disk confocal microscope is that the size of the pinholes is fixed, and so optical section thickness is not adjustable; however, projections of z-stacks can be constructed to show the whole cell at once.

In recent years, spinning disk confocal microscopy has facilitated a new era in high-resolution low-noise time-lapse imaging. Highly dynamic cellular processes of organelles and molecular assemblies (such as the cytoskeleton) have been revealed in fine detail for the first time through acquisition of a series of fluorescence images over time in living cells that allow quantitative analysis of movement (for example, see Waterman-Storer et al. 1998; Cimini et al. 2001; Grego et al. 2001; Maddox et al. 2002; 2003a; 2003b). In the following chapters, I will present new techniques and applications for spinning disk confocal microscopy in examining live cell dynamics in mitotic spindle morphogenesis.

§ 1.7 Studying protein function by using small molecule inhibitors and RNAi

In cell biology, it is often advantageous to perturb the cellular machinery by inhibiting or depleting a protein. To inhibit the activity of a protein in the cell, one

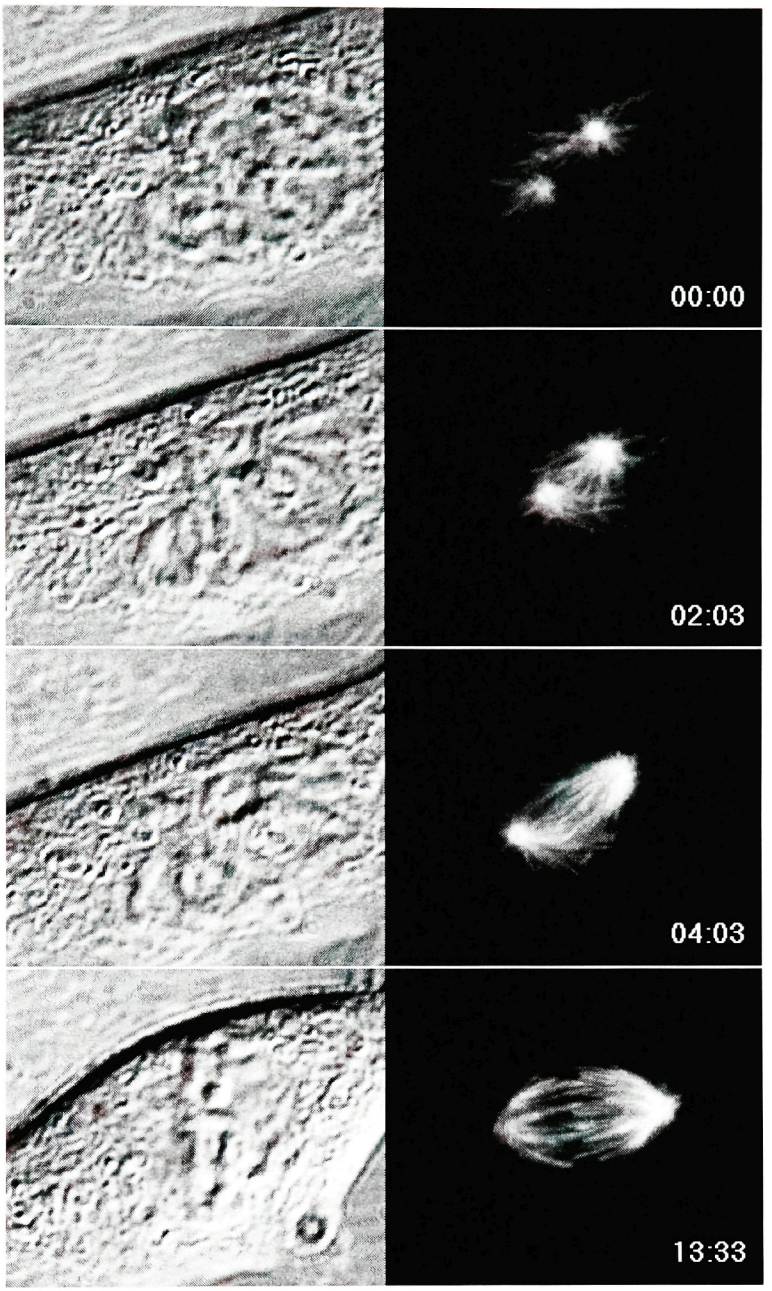

Figure 1.14 Live cell imaging using near-simultaneous DIC and spinning disk confocal microscopy. By alternating between DIC (left) and spinning disk confocal fluorescence (right) microscopy of PtK2 cells stably expressing GFP-tubulin, both chromosomes and microtubules can be observed in the same cell over time.

powerful technique, known as microinjection, involves the injection of inhibitory antibodies into individual cells (for review see Wadsworth 1999). Microinjection is particularly useful when precise temporal control of the inhibition is required (for example, see Howell et al. 2000). However, this technique is not always appropriate, as microinjection can be laborious and antibody effects can be unpredictable. Another approach is to use small molecule inhibitors, chemical compounds that bind to and disrupt the activity of the target protein (Fry et al. 1994; Sakowicz et al. 1998; Mayer et al. 1999; Blake et al. 2000; Hauf et al. 2003). Cell-permeable small molecule inhibitors can be very powerful tools because they can be added to the media surrounding the cells and cross the cell membrane, providing highly desirable temporal control over the inactivation. One such small molecule is monastrol, which inhibits the mitotic kinesin Eg5, thereby inducing monopolar spindle formation in mitotic cells (Mayer et al. 1999; Kapoor et al. 2000; DeBonis et al. 2003). Unlike other known small molecule inhibitors of mitotic proteins, monastrol does not perturb microtubule dynamics (Mayer et al., 1999). Further, Eg5 inhibition is rapidly reversed by removing the monastrol-containing media, allowing precise temporal control over the transition of monopolar arrays to bipolar spindles (discussed in chapter 3).

In cell-free systems involving cell lysate, proteins can be depleted by passing the lysate over beads coated with antibodies to the protein; however, this cannot be accomplished in intact live cells. Recently, the process of RNA interference (or RNAi) was developed for use in mammalian cells and is now widely used for degrading the RNA that encodes the protein of interest. Since proteins in the cell are regularly degraded and replaced by newly translated proteins, the absence of RNA for a particular protein results in the net depletion of the protein in the cell (for reviews see Nishikura 2001; Sharp 2001). RNAi is triggered by introducing small double stranded RNA (dsRNA) which is homologous to the gene targeted for silencing. Once in the cell, the

dsRNA is cleaved into smaller (21-25 nucleotide) bits of RNA called small interfering RNA (siRNA), which signals the destruction of RNA with similar sequences. Although RNAi is a very effective technique for affecting the depletion of some proteins, it is limited to organisms for which the sequence of the gene of interest is known and is most effective in organisms for which the genome has been sequenced. In addition, RNAi has been shown to have possible unpredicted effects and must be used and interpreted with caution (Chi et al. 2003; Jackson et al. 2003; Semizarov et al. 2003).

Considering the potential of the recent technological advances in microscopy, small molecule inhibitors, and RNAi, this is a very exciting time in experimental cell biology. Each of these techniques has proved to be quite powerful; but possibly even more exciting is the potential for advancement when they are combined to provide molecular and structural insight into the dynamic processes in living cells.

Chapter 2 – Materials and Methods

§ 2.1 Cell Culture

Stable clones, constitutively expressing α-tubulin/GFP (Clontech), were isolated from the PtK2 and CV-1 parental cell lines (both purchased from ATCC, MD) by G-418 (geneticin) (Clonetech) selection and limited-dilution cloning. These clones express growth characteristics very similar to their parental cell lines. LLC-PK cells constitutively expressing α-tubulin/GFP (LLC-PK-αT) were kindly provided by Dr. Patricia Wadsworth (University of Massachusetts, Amherst, MA). PtK-αT cells were maintained in Ham's F12 or DMEM (GIBCO) media supplemented with 10% fetal bovine serum (Sigma) at 37°C in humidified atmosphere with 5% CO2. HeLa cells constitutively expressing α-tubulin/GFP (kindly provided by Tim Yen, Fox Chase Cancer Center, Philadelphia, PA) were maintained in DMEM media supplemented with 10% FBS and pen/strep, and kept under constant selection with 400 µg/ml geneticin (GIBCO). CV-αT and LLC-PK-αT cells were maintained in DMEM media also supplemented with 10% fetal bovine serum. HeLa and DLD-1 cells were maintained in DMEM media supplemented with 10% FBS and pen/strep (GIBCO). All cell cultures were maintained at 5% CO_2 in a humidified 37° incubator.

§ 2.2 Live Cell Imaging

Cells for live imaging experiments were plated on poly-lysine coated 22x22-mm #1.5 coverslips (Fisher) except for relocation experiments, which used photo-etched alphanumeric glass coverslips (Bellco Glass Co.). Before imaging, the cultures were

mounted in Rose chambers (Rose et al. 1958) in phenol-free L15 media (GIBCO), supplemented with 5% fetal bovine serum and pen/strep. During live cell imaging cells were kept at 34-37° by a microscope incubator (Solent Scientific) or by using an air-curtain (Grego et al. 2001).

Confocal GFP fluorescence time-lapse images were acquired on a Carl Zeiss MicroImaging, Inc. Axiovert 200M, using either a 63x or 100x, 1.4 NA, Plan Apochromat objective with 2x2 binning. Confocal sections were imaged with a PerkinElmer Wallac UltraView confocal head with 488nm excitation filter and argon ion laser (Melles Griot 643R), and an Orca ER cooled CCD camera (Hamamatsu). Sequential z-planes were imaged using a Carl Zeiss MicroImaging, Inc. z-motor. Timelapse sequences and were acquired and z-projections were performed by the software (MetaMorph; Universal Imaging Corp.). At each time point, 10 z-planes were acquired at 0.5 or 1 µm steps. For DIC image acquisition a fixed analyzer in the motorized reflector was rotated into position by the software (MetaMorph, Universal Imaging Corporation).

§ 2.3 Treatments and RNAi

For nocodazole experiments cells on coverslips were transferred to either DMEM or L-15 media with 5% FBS and pen/strep supplemented with 33µM nocodazole 1 hour before imaging, fixation, and/or washout. Nocodazole washout was accomplished by transferring treated coverslips to culture dishes with 10ml warm media without nocodazole and this was repeated twice before imaging or fixation. For monastrol experiments, three hours before imaging or fixation, cells on coverslips were transferred into either DMEM or L-15 media with 5% FBS and pen/strep supplemented with 100 µM monastrol and 10 µM MG132 to prevent mitotic exit. Live wash-in or wash-out of monastrol was accomplished by exchanging the media in the imaging chamber as

described before (Khodjakov et al. 2003) with monastrol-free L-15 media with 10 μM MG132 to prevent mitotic exit.

Cells were plated for RNAi in 6-well plates (Fisher) at least six hours before transfection using 2 ml tissue culture medium supplemented with 10% FBS but without antibiotics. For each well transfected, 200 pmol siRNA oligo in buffer salt solution (Dharmacon) was gently diluted in 175 μl of Opti-MEM Reduced Serum Medium without serum or antibiotics (Invitrogen). At the same time, 3μl Oligofectamine (Invitrogen) was gently diluted in 12μl Opti-MEM Reduced Serum Medium without serum or antibiotics in a separate tube. After 5 to 10 minutes incubation at room temperature, both the siRNA and Oligofectamine dilutions were combined and incubated for an additional 15 to 20 minutes at room temperature. Meanwhile, cells were rinsed gently with Opti-MEM Reduced Serum Medium without serum or antibiotics. Finally, the siRNA-Oligofectamine mix was added to cells to a final volume of 1 ml with Opti-MEM Reduced Serum Medium without serum or antibiotics. Cells were transfected at 10 to 30% confluency with either siRNA or with sterile ddH_2O 36 (TPX2) or 48 (Aurora-A) hours prior to imaging or fixation.

The following TPX2 targeted oligos were used: functional oligo #1 sequence: AAGGAGAUACUCAAAACAUAG, corresponding to bases 74–94 of TPX2 (Garrett et al. 2002), functional oligo #2 sequence: AACUUGCUCUGGCUGGAAU, corresponding to bases 710-728 of TPX2, non-functional oligo sequence: AACAUAGAUUCAUGGUUUGAG, corresponding to bases 88-108 of TPX2. The Aurora-A oligo sequence, AUGCCCUGUCUUACUGUC, was targeted to bases 725-743 of Aurora-A. All oligos were prepared by Dharmacon Laboratories.

§ 2.4 Immunofluorescence and deconvolution

For PtK2 cells fixed after monastrol wash-out without time-lapse imaging in Chapter 3, 10 minutes of fixation and permeablization in pre-warmed 4% formaldehyde solution (100 mM PIPES, 10 mM EGTA, 1mM MgCl2, 0.2% TritonX-100, 4% formaldehyde, pH 6.8) at 37 °C was followed by three washes in TBSTx (0.15 M NaCl 0.02 M Tris-Cl, 0.1% Triton X-100, pH 7.4) at room temp before blocking with Abdil (0.15 M NaCl, 0.02 M Tris-Cl, pH 7.4, 0.1% Trinon-X, 2% BSA) at room temperature for at least 30 minutes before incubation with antibodies (discussed below). However, the PtK2 cell immunofluorescence figure contributed by Alexy Khodjakov was permeabilized with 1% Triton X-100 in PEM buffer (100 mM PIPES, 1 mM EGTA, 5 mM Mg^{2+}, pH 6.9) for 1 min and fixed with 1% glutaraldehyde in PEM.

For immunofluorescence analysis of HeLa cells previously followed by time-lapse microscopy in Chapter 4, cells were fixed by immersion in -20° methanol for 20min, and then permeabilized with Abdil block (0.15 M NaCl, 0.02 M Tris-Cl, pH 7.4, 0.1% Trinon-X, 2% BSA) at room temperature for at least 30 minutes before incubation with antibodies (discussed below).

All other cells were fixed by first rinsing with PHEM buffer (60 mM Pipes, 25 mM Hepes, pH 6.9, 10 mM EGTA, 4 mM $MgSO_4$) at 37 °C and then lysed for 5 minutes in 0.5% Triton-X in PHEM, also at 37 °C. Next, cells were fixed for 20 minutes in pre-warmed 4% formaldehyde in PHEM at 37 °C, then rinsed in PBST (PBS with 0.05% Tween-20) and subsequently blocked in 2% BSA in PHEM for 1 hour at room temperature.

For kinetochore labeling with CENP-E, cells were treated with a high-calcium buffer (100mM PIPES, 1mM $MgCl_2$, 0.1 mM $CaCl_2$, 0.1% Triton X-100, pH 6.8) before fixation in 4% formaldehyde as above (see also Kapoor et al. 2000).

After at least 30 minutes of blocking at room temperature, cells were treated with primary antibodies diluted in the same solution used for blocking for one to four hours. This was followed by 3 washes of 5 minutes each in blocking solution before 30 minutes of incubation with secondary antibody, also diluted in the same solution used for blocking. Finally, cells were treated with a final wash in Hoechst 33342 (Sigma). Coverslips were then mounted on glass slides with mounting media (0.5% phenylenediamine in 20 mM Tris, pH 8.8 in 90% glycerol) and sealed with clear nail polish (Sally Hanson).

Deconvolved immunofluorescence images were collected as 3-D volumes on a DeltaVision system on an Olympus IX70 microscope using a 100x PlanApo N.A. 1.35 objective (Applied Precision Instruments) with refractive index 1.518 LaserLiquid immersion oil (Cargille). Image stacks were subsequently deconvolved using iterative constrained decovolution and z-projections were calculated by maximum intensity with the software (SoftWorks, Applied Precision Instruments).

§ 2.5 Antibodies

The following primary antibodies were used: polyclonal rabbit anti-TPX2 (Garrett et al. 2002), monoclonal mouse anti-α-tubulin (Sigma), monoclonal mouse FITC-labeled anti-α-tubulin (Sigma), polyclonal rabbit anti-NuMA (Gaglio et al. 1995), polyclonal rabbit anti-γ-tubulin (Sigma), polyclonal rabbit anti-Eg5 (gift of Duane Compton, Dartmouth Medical School, Hanover, NH), polyclonal rabbit anti-CENP-E (gift of Tim Yen, Fox Chase Cancer Center, Philadelphia, PA), and monoclonal mouse anti-Aurora-A (Pharmingen).

The following secondary antibodies were used: donkey Texas-Red-labeled anti-rabbit (Jackson Laboratories), donkey horseradish peroxidase (HRP) labeled anti-rabbit

(Jackson Laboratories), and donkey horseradish peroxidase labeled anti-mouse (Jackson Laboratories). DNA was stained with Hoescht 33342 (Sigma).

§ 2.6 Cell lysates and Western blotting

Cell lysates were prepared by gently scraping the culture dish with a rubber policeman, transferring the suspended cells into a 1.5 ml Eppindorf tube, pelleting at 2000 RPM in a desktop Microfuge 18 centrofuge (Beckman Coulter), aspirating the remaining media and adding 50 µl lysis buffer (25 mM Hepes, 150 mM NaCl, 0.1% Triton-X, 1 mM EDTA, pH 7.4 and 2 mM PMSF) or quick frozen in liquid nitrogen and stored at -80 °C if lysis buffer was to be added later. After lysis buffer was added, 2µl of the vortexed sample is removed for total protein concentration analysis by spectrophotometry for optical density at 595 nm in Bradford Protein Assay (BioRad). SDS loading buffer was then added to the cell lysate and boiled for 5 to 10 minutes.

Samples were loaded at 10 µg/well and separated in 7.5% polyacrylamide gels at 200 mA in running buffer (25 mM Tris, 192 mM glycine, 0.1% SDS, pH 8.3) at room temperature for 50 minutes. Gels were transferred at 350 mA for 60 minutes in transfer buffer (50 mM Tris, 380 mM glycine, 0.1% SDS, 20% MeOH, pH 8.3) at 4° C to nitrocellulose membrane (Schleicher and Schuell). All subsequent manipulations were in Tris-buffered saline with 0.1% Tween (TBST). Blots were blocked in 5% nonfat dry milk TBST (TBST-milk) and incubated in primary antibody in TBST-milk either for 1 hour at room temperature or overnight at 4 °C. Blots were washed at least 5 times over 60 minutes, incubated with secondary antibody for 1 hour at room temperature, washed again as before and visualized by enhanced chemiluminescence (ECL) (Amersham Biosciences) on Hyperfilm Chemiluminescence film (Amersham Biosciences). Films were developed with a Kodak X-omat developer.

§ 2.7 Microinjections (provided by D. Compton and M. Gordon)

For antibody microinjection, CFPAC-1 cells were maintained in Iscove's Modified Dulbecco's Medium containing 10% FBS at 37° C in a humidified 5% CO2 atmosphere. CFPAC-1 cells were grown on photo-etched alphanumeric glass coverslips (Bellco Glass Co.) and were microinjected as previously described (Gordon et al. 2001). The antibodies used for microinjection were raised against full-length recombinant NuMA (Gaglio et al. 1995) and the central rod domain of Eg5 (Mountain et al. 1999). IgG was affinity purified from whole serum using protein A-agarose (Roche Molecular Biochemicals), exchanged into microinjection buffer (100 mM KCl, 10 mM KPO4, pH 7.0) using PD-10 Sephadex G-25 columns (Amersham Pharmacia Biotech), and injected at concentrations of 5 mg/mL (Eg5) and 20 mg/mL (NuMA).

For immunofluorescence analysis of microinjected cells, coverslips were first immersed in microtubule stabilizing buffer (MTSB: 4 M glycerol, 100 mM PIPES, pH 6.8, 1 mM EGTA, 5 mM MgCl2) for 1 minute, followed by a 2-minute extraction in MTSB/0.5 % Triton X-100. Cells were then rinsed in MTSB for 2 minutes and fixed in 1% glutaraldehyde. The glutaraldehyde was quenched with two 10-minute rinses in 0.5 mg/mL NaBH4 and the cells were rinsed in TBS (10 mM Tris, pH 7.5, 150 mM NaCl) containing 1% BSA (TBS-BSA) for 5 minutes. α-Tubulin was stained for using the mouse monoclonal antibody DM1α (Sigma) and centrosomes were detected with a human α-centrosome antibody provided by J.B. Rattner (University of Calgary, Calgary, Alberta). DNA was stained with DAPI (Sigma-Aldrich).

§ 2.8 Electron Microscopy (provided by A. Khodjakov)

Cells previously followed *in vitro* were fixed and prepared for electron microscopy according to standard protocols (Khodjakov et al. 1997; Rieder and Cassels 1999). After flat-embedding they were relocated using phase-contrast microscopy and serially thick-sectioned (0.25 μm). The sections were then imaged and photographed in a Zeiss 910 microscope operated at 100 kV.

Contours of chromosomes, kinetochores, and adjacent microtubules were traced manually using the Sterecon software package developed at Wadsworth Center (Marko and Leith 1996). Surface-rendered 3-D models of chromosomes were assembled from the Sterecon tracings in Open Inventor (SGI) software package.

Chapter 3 - Minus-end capture of pre-formed kinetochore fibers contributes to spindle morphogenesis

Abstract

Near-simultaneous three-dimensional fluorescence/differential interference contrast microscopy was used to follow the behavior of microtubules and chromosomes in living α -tubulin/GFP-expressing cells after inhibition of the mitotic kinesin Eg5 with monastrol. Kinetochore fibers (K-fibers) were frequently observed forming in association with chromosomes both during monastrol treatment and after monastrol removal. Surprisingly, some of these K-fibers were oriented away from, and not directly connected to, centrosomes and incorporated into the spindle by the sliding of their distal ends toward centrosomes via a NuMA-dependent mechanism. Similar preformed K-fibers were also observed during spindle formation in untreated cells. In addition, upon monastrol removal, centrosomes established a transient chromosome-free bipolar array whose orientation specified the axis along which chromosomes segregated. We propose that the capture and incorporation of preformed K-fibers complements the microtubule plus-end capture mechanism and contributes to spindle formation in vertebrates.

(The following chapter was accomplished in collaboration with Drs. Alexey Khodjakov, Duane Compton and Mike Gordon and published in The Journal of Cell Biology (Khodjakov et al. 2003).)

§ 3.1 Mono-oriented chromosomes provide a unique opportunity to observe kinetochore microtubule dynamics.

For accurate segregation of replicated genetic material into two daughter cells, sister kinetochores on each chromosome must establish stable connections with the opposite poles of the spindle. Kirschner and Mitchison (1986) proposed a model that provides powerful explanations for how spindle formation occurs in vertebrate somatic cells. In this model, centrosomes nucleate a radial array of dynamic microtubules whose plus ends are captured and selectively stabilized by kinetochores. Over time, these initial microtubule attachments mature to form kinetochore fibers (K-fibers). Several lines of evidence, including direct observations of microtubule capture by kinetochores (Rieder and Alexander 1990), provide extensive experimental support for this hypothesis (for review see Rieder and Salmon 1998).

In its original form, the plus-end search-and-capture model implies that all kinetochore microtubules are derived from astral microtubules nucleated from centrosomes. However, spindle assembly has been shown to occur efficiently in the absence of centrosomes in extracts prepared from frog eggs through a mechanism that relies on microtubule nucleation and organization in the vicinity of chromosomes (Heald et al. 1996; Walczak et al. 1998; for review see Karsenti and Vernos 2001). Recent studies reveal that this chromosome-directed mechanism for spindle assembly is operative in cell types that normally form a typical "astral" spindle, as shown by eliminating centrosome activity by laser micro-ablation (Khodjakov et al. 2000) or genetic mutations (Bonaccorsi et al. 1998; Megraw et al. 2001), which did not prevent formation of functional bipolar spindles. Moreover, recent experiments suggest that proteins acting downstream of Aurora A kinase and Ran GTPase to promote chromosome-directed spindle organization in frog egg extracts may be playing similar roles in vertebrate

somatic cells (Gruss et al. 2002; Kufer et al. 2002); however, direct evidence for this is currently limited. These observations indicate that mechanisms other than plus-end search and capture contribute to spindle assembly in vertebrate cells and cast doubt that all K-fibers arise from captured astral microtubules.

One of the problems in determining whether K-fibers can form by mechanisms not involving centrosomes is that in bipolar spindles, chromosomes typically have each of their two kinetochores oriented toward one of the two separated centrosomes. Under these conditions, forming K-fibers become submerged in a mass of astral and interpolar microtubules that obscure direct visualization of individual K-fiber behavior. This limitation can be overcome by following the behavior of microtubules associated with the kinetochores distal to centrosomes in monopolar spindles.

Formation of monopolar spindles in vertebrates occurs when the centrosomes fail to separate before nuclear envelope breakdown (NEB) (Roos 1976; Cassimeris et al. 1994) or when they separate too far from one another (anaphase-like prometaphase) (Bajer 1982; Rieder and Hard 1990). In both cases, the monopolar configurations are transient, and over time, these structures transform into functional bipolar spindles as centrosomes separate or come closer together (in the case of anaphase-like prometaphase). Although naturally occurring monopolar spindles have proven to be a valuable model for studying mechanisms of mitosis, their rarity and the unpredictable time before they transform into bipolar arrays limit their usefulness. Monastrol, a small molecule inhibitor of the mitotic kinesin Eg5, provides a convenient tool by which monopolar spindles can be induced (Mayer et al. 1999; Kapoor et al. 2000). Unlike other known small molecule inhibitors of mitotic proteins, monastrol does not perturb microtubule dynamics (Mayer et al. 1999). Thus, monastrol-induced monopolar spindles present a unique opportunity to examine the behavior of K-fibers in vertebrate mitoses. Further, the rapid reversibility of the monastrol arrest allows precise temporal control

over the transition of monopolar arrays to bipolar spindles. Combining the use of monastrol and high-resolution multidimensional microscopy, we have obtained direct evidence for a mechanism other than plus-end search and capture that contributes to spindle morphogenesis in vertebrate cells. Our data also reveal how centrosomes contribute to the organization of bipolar spindles before chromosome segregation.

§ 3.2 Capture and incorporation of preformed microtubule bundles into the monopolar spindle in monastrol-treated cells

We used near-simultaneous three-dimensional (3-D) GFP fluorescence/two-dimensional (2-D) differential interference contrast (DIC) multimode microscopy to follow the behavior of both the microtubules and chromosomes in live monastrol-treated PtK2 cells that express α-tubulin/GFP (PtK-αT). Typically, we began observation immediately after NEB and then followed the cell for 2 h, recording one DIC image and a corresponding 3-D fluorescence stack every minute. In some experiments (e.g., Figure 3.1), we followed cells over shorter periods (10–30 min) but at higher temporal resolution (10–30-s intervals).

Our 2-h time-lapse recordings of 20 cells revealed that within 5–10 min after NEB, all chromosomes in monastrol-treated cells became mono-oriented and assumed a star-like configuration, with their centromere regions oriented toward the centrosomes and the arms pointing outwards (see Video 1, available at http://www.jcb.org/cgi/content/full/jcb.200208143/DC1). At the moment of NEB in the presence of monastrol, the centrosomes were often already spatially separated (Figure 3.1). This has also been observed in untreated PtK cells (Roos 1976). In the presence of monastrol, centrosomes generated two radial microtubule arrays that coalesce within

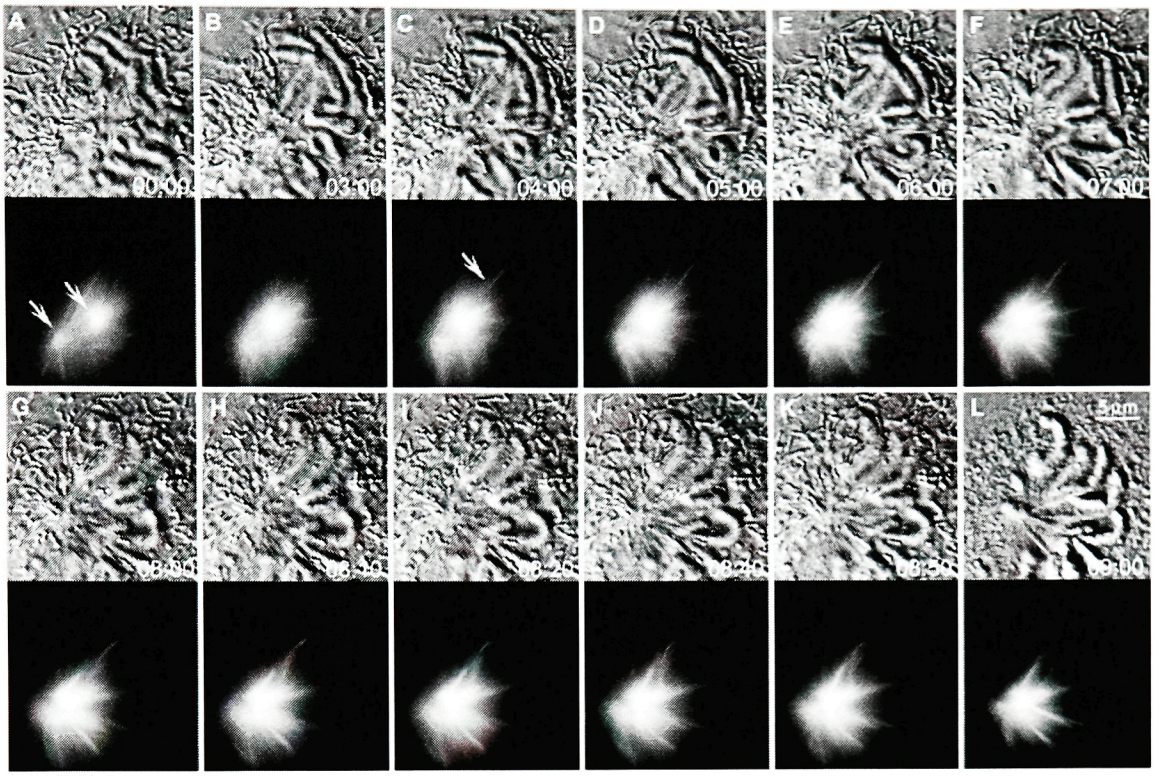

A. Khodjakov, Wadsworth Center

Figure 3.1 Formation, looping, and incorporation of microtubule bundles in monastrol-induced monopolar spindles in PtK-αT cells. Selected frames are shown from a near-simultaneous 3-D fluorescence/DIC time-lapse microscopy experiment. The top half of each image represents a DIC slice through the central part of the cell, whereas the bottom half is a maximal intensity projection of a 3-D fluorescence volume recorded at 0.5-μm z-steps. After NEB, both centrosomes come together (A, arrows) and form a common pole. The chromosomes orient toward the unseparated centrosomes and surround the pole (B and C). A new microtubule bundle (C, arrow), not associated with the centrosomes, forms and rapidly grows outwards (compare C–E), reaching 10-μm length in 3 min (E). This bundle begins to bend (G) and its distal tip moves toward the pole (H–J). As a result, the bundle forms a loop with both ends embedded into the central part of the spindle (K). At this point, the cell was fixed and permeabilized for immunofluorescence analysis (L; see also Figure 3.2). Time is in minutes:seconds.

a few minutes after NEB (Figure 3.1). Initially, the chromosomes may be positioned only on one side of the centrosomes, but, over time, they gradually rearranged into a spherical array encircling the centrosomes. These aspects of monopolar spindle formation were largely expected from previous fixed cell analyses of monastrol-treated cultures (Mayer et al. 1999; Kapoor et al. 2000).

One unexpected feature conspicuous in our time-lapse recordings was that in all cells imaged, we observed prominent bundles of microtubules extending from the chromosomes toward the cell periphery. These bundles appeared in the vicinity of the centromere regions of chromosomes and then rapidly grew outwards (Figure 3.1). Temporal resolution in most of our time-lapse records was not sufficient to determine precise elongation rates of the bundles that can often reach up to 10–12 μm within 3 min. To document these events in greater detail, we used a spinning-disk confocal microscope, which acquired images at a higher temporal resolution, sampling the cellular volume every 15 s (Figure 3.2). Under these conditions, I observed elongation rates of ~3–4 μm/min (Figure 3.3).

After reaching ~10 μm in length, the bundles usually underwent a rapid bending, and their ends distal to the chromosome moved back toward the center of the spindle (Figures 3.1, 3.2). As a result, the bundle formed a transient microtubule "loop" as its distal end moved inwards to the pole while the proximal end remained relatively stationary. This configuration was transient, and in ~2–5 min, the bundle made a complete 180° turn so that its distal end incorporated into the spindle. Overall, this behavior is suggestive of the distal end of the microtubule bundle being suddenly captured and experiencing a force directed toward the center of the spindle.

The phenomenon of formation, capture, and incorporation of microtubule bundles was very common in monastrol-induced monopolar mitoses. On average, we observed ~10–12 such events in a cell during a 2-h observation period (range 8–20; 19 events in

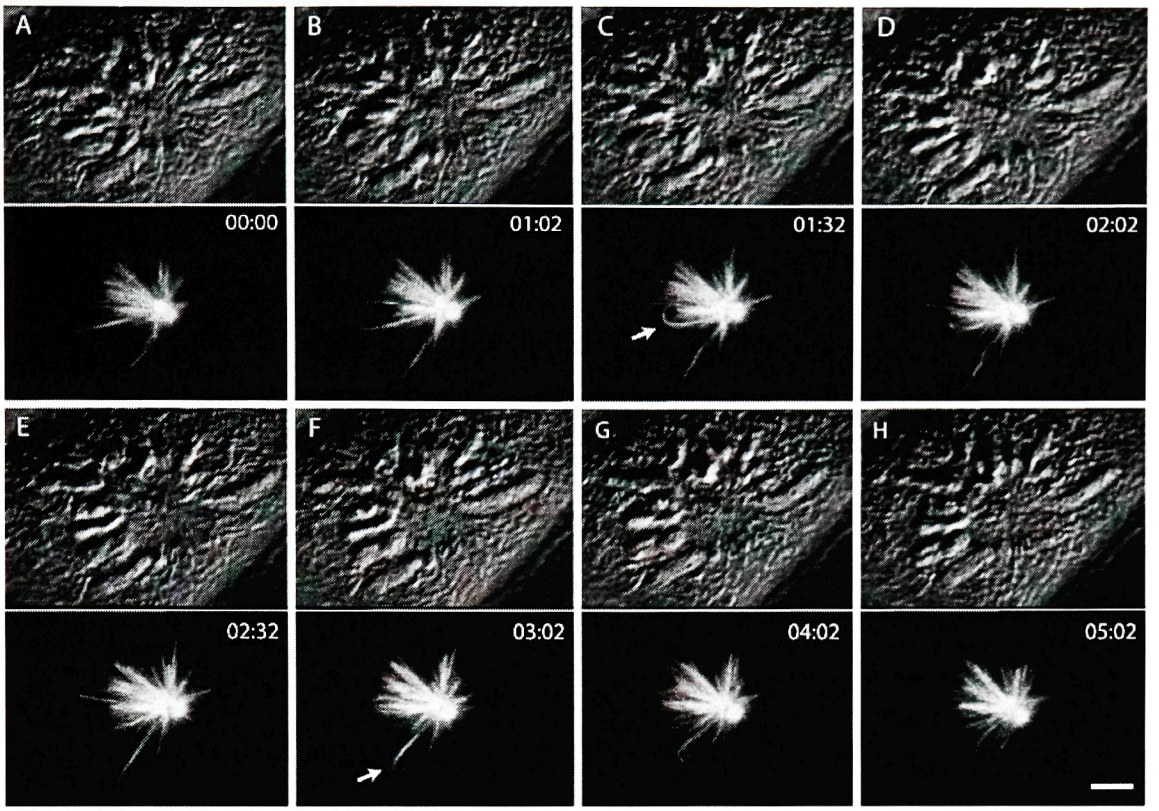

Figure 3.2 Live imaging of the formation, looping and incorporation of microtubule bundles with spinning disk confocal microscopy. Selected frames from a near-simultaneous 3D spinning disk confocal fluorescence/ 2D DIC microscopy movie. The top half of each image depicts a DIC slice though the central part of the cell, while the bottom half shows a maximum intensity projection of a 3D fluorescence volume recorded at 0.5μm z-steps. In the presence of 100 μM monastrol, a spindle is monoastral, with a single pole surrounded by chromosomes and associated kinetochore microtubule bundles (A). A new microtubule bundle grows outwards, eventually bending back towards the poles, resulting in a loop with both ends at the poles (arrows, C and F). Scale bar is 5 μm. Time is in minutes:seconds.

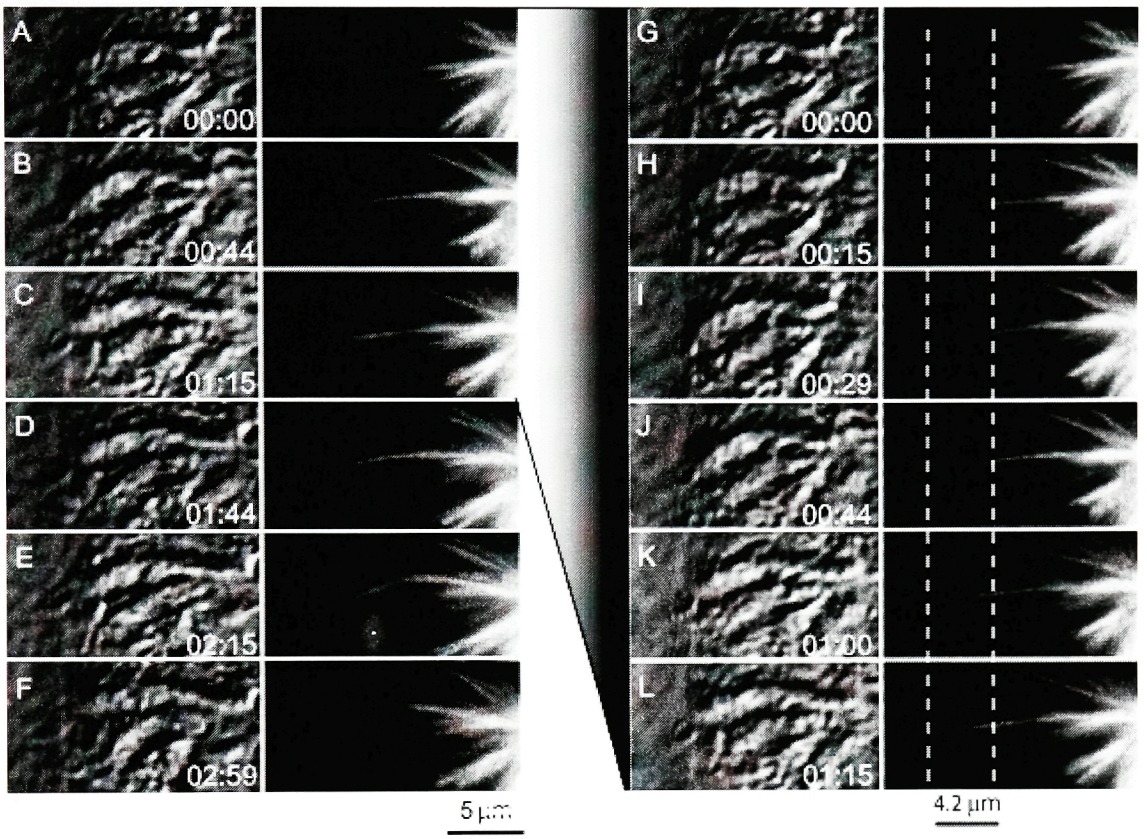

Figure 3.3 Chromosome-associated looping microtubules are observed during spindle morphogenesis. (A-F) Microtubule bundles that are associated with the kinetochore region of a mono-oriented chromosome elongate away from the spindle pole (A). In this cell, the microtubule bundle extends approximately 4 µm (C), at which point the bundle undergoes rapid bending (D-F). This forms a transient microtubule loop, while the end of the microtubule is translocated in toward the centrosome. (G-L) During the growing stage, the microtubules elongate approximately 4.2 µm in 75 seconds. Time is in minutes:seconds.

Video 1). Once a bundle of microtubules formed (reached ~10-μm length), it was typically captured within 5 min. Infrequently, some bundles remained extended for up to 15–20 min before incorporating into spindles.

This microtubule formation, capture, and incorporation phenomenon is not limited to the PtK-αT cells. We also observed similar behavior of microtubule bundles in other cell types, including LLC-PK and CV-1 (both constitutively expressing α-tubulin/GFP; data not shown).

§ 3.3 Microtubule loops result in the formation of syntelic-oriented chromosomes in monastrol-treated cells

To determine the structural organization of microtubule loops, we followed a cell by 3-D fluorescence/ 2-D DIC microscopy and then fixed it during a microtubule looping event. The fixed cells were subsequently processed for immunofluorescence analysis. This analysis revealed that the proximal end of the microtubule bundle (one that remains stationary during looping) was always associated with the primary constriction of a chromosome (Figure 3.4). As a result, upon incorporation of the distal end of the looping microtubule bundle into the spindle, the chromosome becomes syntelic, i.e., its primary constriction connected to the spindle pole by two bundles of microtubules (Figure 3.4). This configuration implies that before the distal microtubule bundle was captured and looped toward the spindle pole, it extended from the primary constriction toward the cell periphery. To confirm this, we analyzed a population of monastrol (100 μM)-induced monopolar mitoses in PtK-αT cells after fixation and immunostaining for microtubules, kinetochores, and chromosomes. Our analysis revealed that ~10% of monopolar mitoses contain conspicuous bundles of microtubules that emanate directly from distal

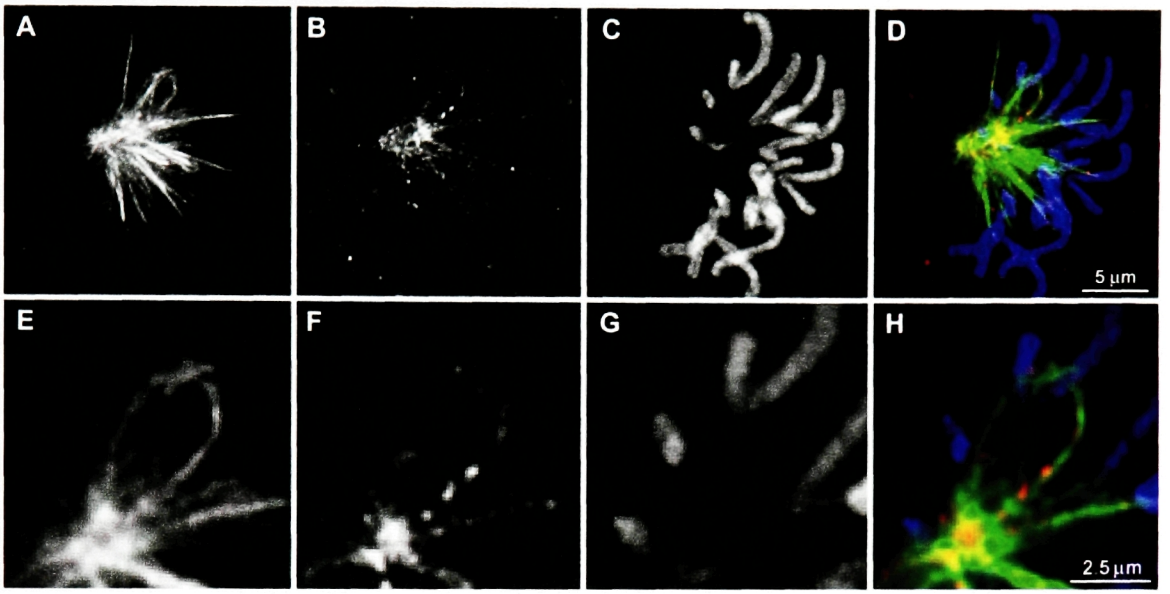

A. Khodjakov, Wadsworth Center

Figure 3.4 Small aggregates of NuMA are associated with the parts of the microtubule loop that move poleward. Same cell as in Figure 3.1. (A–D) Maximal projections of 3-D fluorescence volumes representing microtubules (anti–α-tubulin; A), NuMA (rabbit polyclonal; B), chromosomes (Hoechst 33342; C), and a pseudo colored overlay of these three channels (D). (E–H) Individual slices of the 3-D volumes presented in A–D, at higher magnification. Note that NuMA is present along the microtubule bundles that extend toward the periphery of the spindle and on the leading half of the loop (B and F, arrow).

kinetochores and extend for several micrometers away from the spindle pole and toward the cell's periphery (Figure 3.5, A–D).

To investigate the structural organization of these distal K-fibers at a greater resolution, we analyzed two monopolar mitoses in a population of PtK cells treated with 100 μM monastrol by serial section EM. The cells were selected without bias, and spindle structures were not evaluated by immunofluorescence before processing for EM. Nevertheless, in these two cells, we found three unambiguous cases of well-developed K-fibers emanating from distal kinetochores toward the cell periphery (Figure 3.5, E–K). Each individual kinetochore plate was associated with several microtubules (up to 12). It is important to emphasize that in all three cases, the distal kinetochore faced directly away from the spindle pole and was shielded from the astral microtubules by the chromosome mass (Figure 3.5, E–K). Thus, our serial section EM data confirmed the existence of K-fibers not directly oriented to the spindle pole.

§ 3.4 Inhibition of NuMA prevents microtubule fiber looping

Thus far, our data revealed that microtubule loops form when the free ends of preformed K-fibers are captured and actively transported toward the spindle pole. To examine the molecular mechanism of this poleward sliding of spindle microtubules, we examined the localization of NuMA, a protein responsible for maintaining microtubule ends focused at spindle poles (Gaglio et al. 1995; Merdes et al. 1996; Gordon et al. 2001). We found NuMA to be present at the leading end of the looping microtubule bundle in all cells analyzed (n = 4) (Figure 3.4 F, arrow). Because NuMA has been shown to interact with the dynein/dynactin complex (Merdes et al. 1996), this observation is consistent with the capture and incorporation of microtubule bundles being driven by dynein motility.

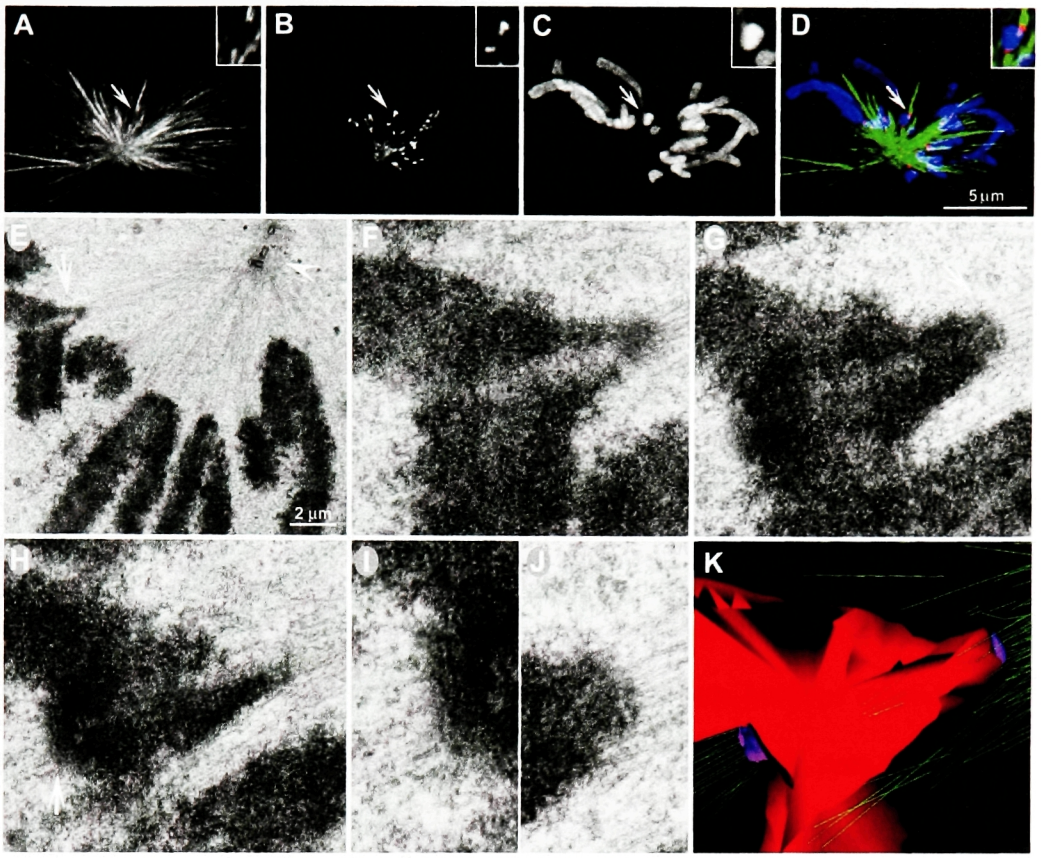

A. Khodjakov, Wadsworth Center

Figure 3.5 Some of the distal kinetochores in monastrol-induced monopolar spindles are associated with well-developed bundles of microtubules (K-fibers). (A–D) A PtK-α T cell stained for microtubules (anti-α-tubulin; A), kinetochores (anti-CENP-E; B), and chromosomes (Hoechst 33342; C). Note a prominent bundle of microtubules (A, arrow) emanating from the distal kinetochore (B, arrow) of one of the mono-oriented chromosomes (C, arrow) and extending toward the cell's periphery. (D) A composite of all three channels. Insets in each panel are at 2x. (E–K) A PtK-αT cell analyzed by serial section EM. (E) Lower magnification overview of the cell. Both centrosomes remain unseparated (three centrioles are present within this section [E, arrowhead] and the fourth one is in the adjacent section). (F and G) Serial 0.25-µm sections through the primary constriction of one of the chromosomes (E, G, and H, arrows). Well-developed bundles of microtubules emanate from both the proximal (G) and the distal (H) kinetochores. (I and J) Higher magnification of G and H. (K) Surface-rendered model based on serial section reconstruction of the chromosome presented in F–H. Note that both the proximal and the distal kinetochores are associated with similar numbers of microtubules.

To test whether NuMA activity is required for microtubule looping, we microinjected cells with a NuMA-specific antibody (Gaglio et al. 1996). It has previously been demonstrated that injection of this antibody into cultured cells aggregates NuMA and prevents it from interacting appropriately with spindle microtubules (Gaglio et al. 1996; Gordon et al. 2001). For these experiments, we used human CFPAC-1 cells, as available anti-NuMA antibodies do not react sufficiently with marsupial NuMA to inhibit its function in PtK cells. Inhibition of Eg5 function in human CFPAC-1 cells through either injection of Eg5-specific antibodies (unpublished data) or monastrol treatment prevented centrosome separation and led to the formation of monopolar spindles (Figure 3.6 A). The microtubule distribution in these monopolar spindles was indistinguishable from that observed in PtK-αT cells, with only a few microtubule bundles extending toward the cell periphery (on average one bundle in every other cell; data from 16 cells analyzed by 3-D microscopy). In contrast, upon simultaneous perturbation of Eg5 (by either treatment with monastrol [unpublished data] or injection of Eg5-specific antibodies) and NuMA (by antibody injection), numerous straight microtubule bundles were seen to extend from the chromosomes in an orientation opposite that of the pole defined by the two unseparated centrosomes (Figure 3.6 B; on average five to six bundles per cell; data from 17 cells analyzed by 3-D microscopy). If monastrol was removed from cells injected with NuMA antibodies and treated with monastrol, then we observed centrosome separation, but K-fibers failed to recruit appropriately toward the centrosomes (unpublished data), resulting in disorganized spindles with splayed spindle poles analogous to those observed after perturbation of NuMA alone (Gaglio et al. 1996; Gordon et al. 2001). These changes in microtubule distribution are consistent with the idea that NuMA is functionally responsible for the capture and incorporation of preformed K-fibers. Upon inhibition of NuMA, the fibers that would normally loop back to the single pole remained extended and accumulated over time.

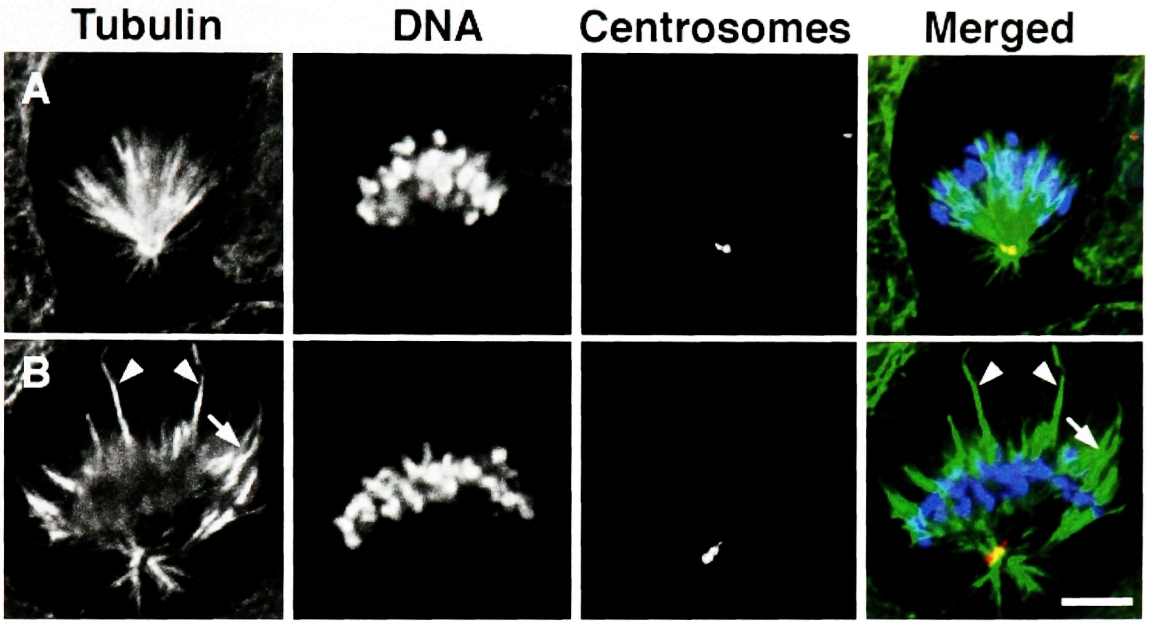

D. Compton and M. Gordon, Dartmouth Medical School

Figure 3.6 NuMA is required for K-fiber orientation in monopolar spindles formed in cells lacking Eg5 activity. Human CFPAC-1 cells treated with 100 μM monastrol (A) or injected with both Eg5- and NuMA-specific antibodies (B) were fixed in mitosis. Mitotic spindle morphology was visualized in these cells by staining for microtubules using the tubulin-specific monoclonal antibody DM1α, for centrosomes using a human centrosome-specific autoimmune serum, and for DNA using DAPI. Arrowheads highlight K-fibers, and the arrow points to a group of K-fibers that appear to be focused into a small spindle pole. Bar, 20 μm.

§ 3.5 Capture of preformed microtubule bundles occurs during spindle bipolarization after monastrol washout

The mitotic arrest due to monastrol is completely reversible, and monopolar spindles rapidly rearrange into normal bipolar mitoses upon monastrol washout (Kapoor et al. 2000). To investigate whether the capture and looping of preformed microtubule bundles occurs during the transformation of monopolar structures into bipolar spindles, we examined microtubule behavior in cells released from monastrol arrest. Our initial attempts to follow these transformations revealed that the redistribution of microtubules could often be too complex to be followed by wide-field fluorescence microscopy. Therefore, we employed near-simultaneous 3-D confocal fluorescence/2-D DIC time-lapse microscopy for these experiments. The use of a spinning-disk confocal microscope allowed us to track individual microtubule bundles within complex arrays with greater precision than conventional wide-field fluorescence microscopy. Scanning depth was set to match the parameters of our wide-field time-lapse recordings used to examine cells in the presence of monastrol. Images sampling the cell volume were acquired at 30-s intervals.

Our recordings revealed that bipolarization of the spindle began immediately upon monastrol removal, and cells consistently initiated anaphase ~75 min after washout. The bipolarization began with the separation of centrosomes, which often detached from the rest of the spindle (Figures 3.7 and 3.8).

However, in contrast to monopolar spindles where K-fibers looped around chromosomes and became incorporated into the single spindle pole, during bipolarization of the spindle, each bundle exhibited one of two types of motion. First, those K-fibers that emanated from chromosomes toward the cell's periphery behaved

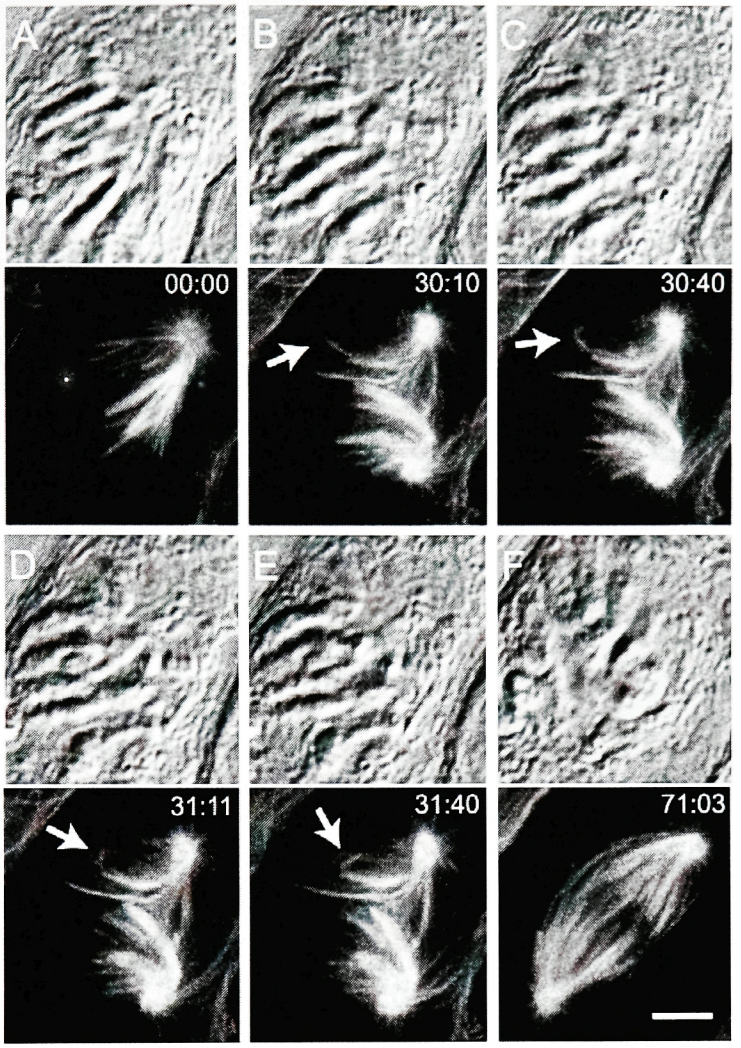

Figure 3.7 Looping and capture of microtubules contributes to spindle morphogenesis in PtKαT cells released from a monastrol arrest. PtKαT cells with monopolar spindles formed in the presence of 100 μM monastrol were placed in monastrol-free medium, and the first image (time = 0:00) of the near-simultaneous 3-D confocal fluorescence/DIC time-lapse microscopy experiment was acquired within 60 s. Each time point shows a DIC image from a focal plane in the center of the cell (above) and a maximum intensity projection of confocal fluorescence Z-sections of a 6-μm-thick Z-series acquired at 1.5-μm steps (below). (A) Microtubules in a mono-astral array are shown in a PtKαT cell immediately after the removal of monastrol. (B–E) The formation and looping of a microtubule bundle from the distal end of an existing K-fiber (arrow) is shown. This microtubule bundle is captured (E) to form a connection to the spindle pole proximal to the minus end of the microtubule bundle from which this fiber emerged. Time is shown in minutes:seconds. Bar, 5 μm.

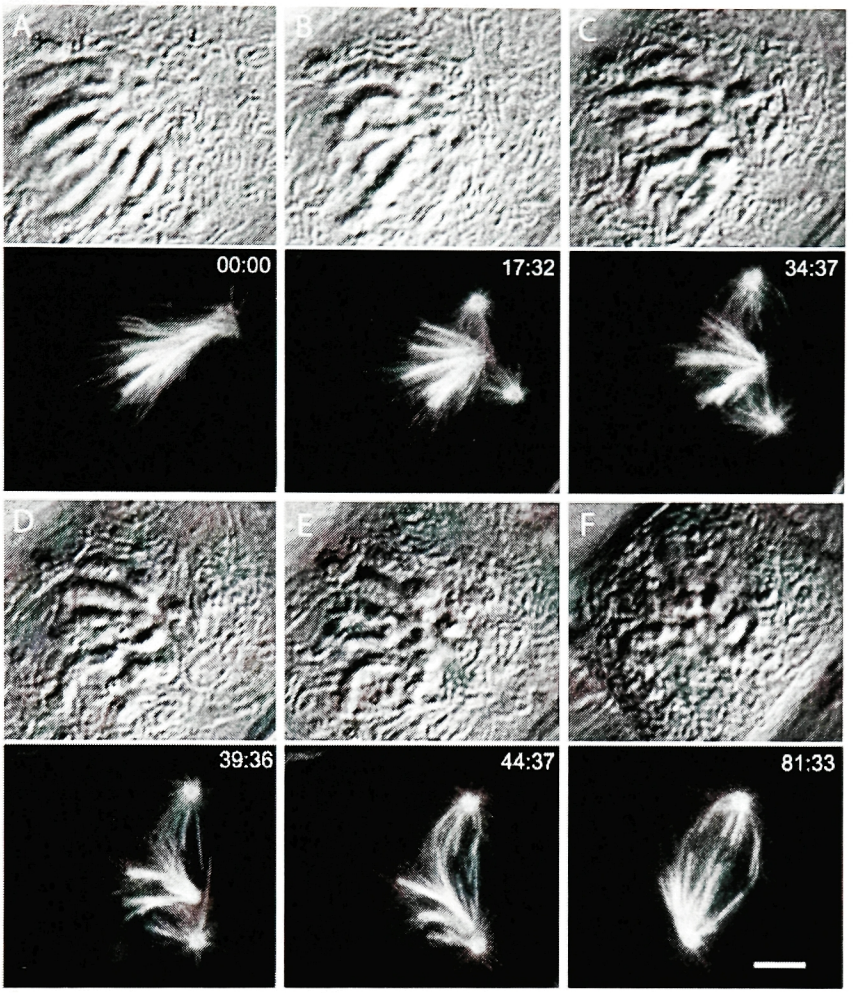

Figure 3.8 The "capture" of stable K-fiber minus ends contributes to bipolar spindle formation and chromosome alignment in PtKαT cells released from a monastrol arrest. Selected frames from a near-simultaneous 3-D confocal fluorescence/2-D DIC time-lapse microscopy experiment are shown. At each time point, a DIC image from a focal plane in the center of the cell is presented with the maximum intensity projection of confocal fluorescence sections of a 6-μm-thick Z-series acquired in 1.5-μm steps. (A) A monopolar spindle within 60 s after removal of monastrol from the cell medium. (B) At early time points, a small bipolar array of microtubules forms at the center of the mono-aster. (C) Several K-fibers maintain their astral arrangement while the bipolar array increases in length and establishes the dominant spindle axis. K-fibers not associated with the poles of the emerging bipolar spindle support robust chromosome oscillations. (D–F) Stable minus ends of these K-fibers are eventually drawn toward the poles of the bipolar microtubule array and chromosomes align. Time is shown in minutes:seconds. Bar, 5 μm.

exactly as the distal K-fibers in monopolar spindles. The K-fibers bent and looped around chromosomes, with their minus ends sliding toward one of the two separating centrosomes (Figure 3.7). Second, those K-fibers that emanated from the side of chromosomes that faced the centrosomes exhibited direct translocations toward one of the two separating centrosomes. As a result, each chromosome became either syntelic (when minus ends of both K-fibers were captured by the same centrosome) or properly bioriented (Figure 3.8).

Intriguingly, the orientation of the axis of centrosome separation was not related to the original orientation of the K-fibers within the monopolar spindle, and the centrosomes often separated in a direction perpendicular to the majority of the K-fibers (Figure 3.8). As the centrosomes separated, they remained associated with prominent arrays of astral microtubules. These microtubules overlap and appear to interact, forming a structure very similar to the "chromosome-free spindles" described by Faruki et al. (2002) in PtK-αT polykaryons. Detachment of centrosomes did not immediately affect the organization of the monopolar spindle. K-fibers remained focused at a single spindle pole that now lacked astral microtubules (Figure 3.8 B). These K-fibers exhibited rapid changes in length corresponding to oscillations of attached chromosomes (data not shown). Importantly, during bipolarization of the spindle, the K-fibers continued to exhibit capture and incorporation of their minus ends into the spindle.

Capture and incorporation of K-fiber minus ends was a common phenomenon we observed in every cell released from a monastrol arrest. Looping of K-fibers distal to the centrosome was often seen during the initial stages of spindle bipolarization with an average frequency of seven loops per cell (range 1–24; n = 15). The high density of microtubules on the side proximal to the centrosomes precluded accurate quantification of direct translocations of K-fiber minus ends toward the separated centrosomes.

However, this phenomenon was at least as common as the "looping" of distal K-fibers during the initial stages of spindle bipolarization and predominant during later stages.

Our observations reveal that spindle morphogenesis in vertebrates does not only depend on the microtubule plus-end search and capture mechanism but also includes the capture and incorporation of preformed K-fibers at their minus ends.

§ 3.6 NuMA is consistently associated with the minus ends of K-fibers during spindle bipolarization

Our data have shown that minus ends of distal K-fibers incorporating into monopolar spindles were always associated with NuMA (see above). To determine if this was the case for the persistent K-fibers that faced centrosomes and exhibited more direct translocation toward a centrosome, we examined the distribution of NuMA in cells released from a monastrol arrest (Figure 3.9, A–E). In all cells examined, NuMA was distributed in numerous small patches spread over the region between the separating centrosomes. The strongest NuMA staining corresponded to the ends of K-fibers (Figure 3.9 E; 2.5x magnification of three-color overlay and line scan). This is consistent with our data that NuMA function is required for the capture and incorporation of the preformed K-fibers into the mitotic spindle.

The fact that NuMA was consistently spread over a large area between the separating centrosomes raised a formal possibility that centrosomal material was similarly fragmented in cells released from monastrol. To evaluate this, we examined localization of γ-tubulin, a protein that has been shown to delineate the boundaries of centrosomes (Khodjakov and Rieder 1999). This analysis revealed that in contrast to the NuMA distribution, the centrosomal material remained focused at the spindle poles, and thus the centrosomes were not fragmented under these conditions (Figure 3.9, F–I).

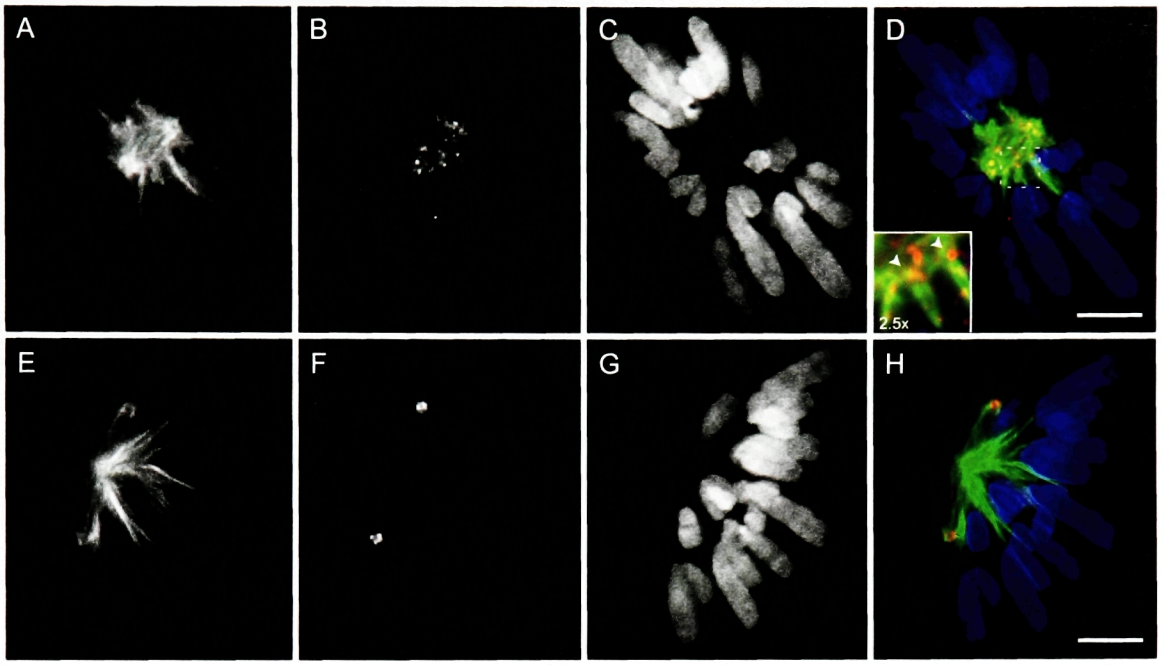

Figure 3.9 In cells establishing bipolar spindles after release from a monastrol arrest, kinetochore microtubule minus ends are associated with interpolar microtubules and NuMA but not centrosomes. (A–D) PtK2 cells arrested in the presence of monastrol (100 μM) for 3 h were transferred to monastrol-free media and fixed after 26 min. The distribution of α-tubulin (A), NuMA (B), and DNA (C) in a cell is shown. (E) An enlarged view shows NuMA localized to discrete points along the spindle, which are brightest at the intersections of kinetochore microtubule minus ends and microtubules (arrowheads) in an emerging bipolar array. A line scan along the K-fiber indicated by the black arrowhead compares NuMA and tubulin distribution (NuMA, red; tubulin, green). (F–I) In an independent experiment, a PtK2 cell released from a monastrol arrest was fixed after 10 min and processed for immunofluorescence. The organization of α-tubulin (F), γ-tubulin (G), and DNA (H) in the cell is shown. Note that γ-tubulin is concentrated at the spindle poles separated by an interpolar network of microtubules. Intersections between kinetochore microtubule bundles and the interpolar microtubules are observed at almost right angles. Three-color overlays are shown in D and I. Images are maximum intensity projections of deconvolved fluorescence image volumes. Bars, 5 μm.

Overall, these observations suggest that common mechanisms contribute to the capture and incorporation of K-fiber minus ends in monopolar spindles and during spindle bipolarization.

§ 3.7 Capture of preformed microtubule bundles occurs during mitotic spindle formation in control cells

Thus far, our data revealed that capture and incorporation of preformed K-fibers contributes to spindle morphogenesis in cells treated with monastrol. The question remained whether this phenomenon also occurs during normal bipolar spindle formation in unperturbed cells. We reviewed a library of time-lapse recordings of spindle formation in control PtK-αT cells (~20 cells) and found two examples of clear incorporation of preformed K-fibers into the forming spindle. Figure 3.10 illustrates one such event. In both cases, the fibers were incorporated into the correct half spindle, resulting in accurate bi-orientation of the chromosome.

§ 3.8 Three key insights into the morphogenesis of the mitotic spindle

3.8.1 Kinetochore microtubule fibers can form without direct connections to centrosomes.

We consistently observed prominent microtubule bundles that were not connected to the centrosomes but emanated from primary constrictions of chromosomes (kinetochores). Serial section EM analysis of monopolar mitoses confirmed the existence of well-developed bundles of parallel microtubules that terminated within

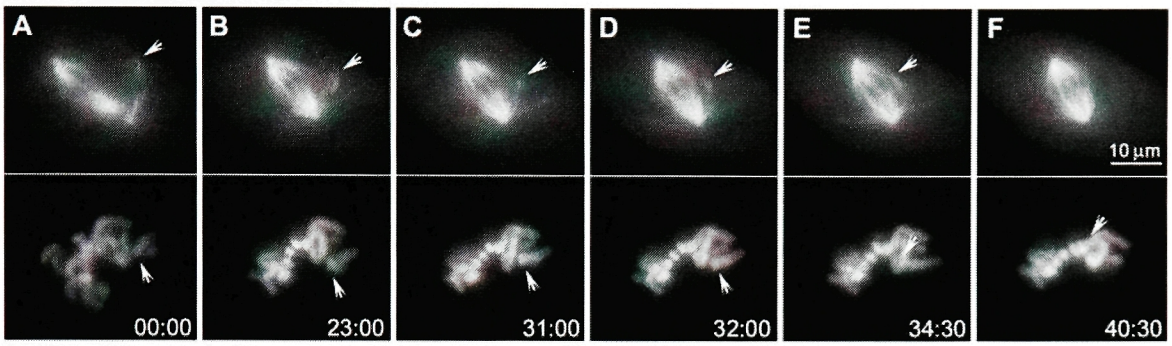

A. Khodjakov, Wadsworth Center

Figure 3.10 Capture and incorporation of preformed K-fibers into the spindle occurs during spindle formation in control PtK cells. Selected frames from a fluorescence time-lapse recording of a PtK-αT cell also stained with Hoechst 33342 to visualize chromosomes. The top half of each image represents the green channel (α-tubulin/GFP), and the bottom half represents the blue (Hoechst 33342) channel. Arrows in A–E point at a bundle of microtubules that initially forms in association with one of the chromosomes (A–E, arrowheads). This bundle persists for ~30 min until it begins to slide toward the distal spindle pole (D–E) and eventually incorporates into the spindle (F). Time is in minutes:seconds.

trilaminar plates of distal kinetochores. These bundles were seen to extend from kinetochores that were often completely shielded from the centrosomes by chromosome masses surrounding the kinetochore. Such a configuration excluded centrosomal microtubules from participating directly in the formation of these distal K-fibers.

There are three mechanisms that may contribute to the formation of these distal K-fibers. One possibility is that distal kinetochores capture microtubules that are spontaneously nucleated in the cytoplasm (Rusan et al. 2002). Our observations of several distal K-fiber formation, looping, and capture events showed no single event consistent with this mechanism, and in all cases, the microtubules emerged rapidly from the vicinity of the chromosome (Figures 3.1, 3.2). Another possibility is that two microtubule bundles nucleated by a centrosome or two unseparated centrosomes may capture each of the two sister kinetochores on a chromosome (syntelic orientation), and the distal K-fiber results from the release of one of these two microtubule fibers. This would be consistent with these distal K-fibers resulting from events correcting syntelic mal-orientations. However, our live cell recordings do not provide any examples of microtubule loops that emerge from monoasters and unravel to form the distal K-fibers, i.e., looping followed by microtubule release. Indeed, recent studies on the correction of syntelic mal-orientations have revealed that corrections are achieved through selective disassembly of kinetochore-microtubule fibers, rather than by alternative mechanisms involving initial release of microtubules from either kinetochores or spindle poles (Lampson et al. 2004).

The mechanism that we favor is that these distal K-fibers emerge directly from the kinetochore. Unfortunately, the temporal and spatial resolution of our microscopy does not allow us to determine whether these fibers are directly nucleated by kinetochores (Witt et al. 1980) or emerge from small remnants of previous microtubule attachments. Given that neither NuMA nor γ-tubulin show detectable localization to the

minus ends of these growing K-fibers, the identities of the molecules responsible for both this proposed nucleation of kinetochore microtubules and the bundling of kinetochore microtubules into stable K-fibers remain unknown.

Regardless of how distal K-fibers are formed, the fact that they interact with the kinetochore plate in a typical end-on fashion implies that these K-fibers have a polarity such that the plus ends of microtubules are embedded into the kinetochore (Mitchison et al. 1986; Inoue and Salmon 1995). This means that the free ends of the distal K-fibers corresponded to the minus ends of microtubules. Even though the minus ends of these K-fibers were not associated with centrosomes, the fibers remained stable for many minutes and often exhibited growth (Figure 3.3). This observed stability of free K-fiber minus ends is not unexpected. Evidence from EM has established that the minus ends of many spindle microtubules, including some kinetochore microtubules, do not terminate at the centrosome (Rieder 1981; McDonald et al. 1992; Mastronarde et al. 1993). These microtubules are focused at the pole and tethered to the centrosome and its associated astral microtubules by the actions of non-centrosomal structural and motor proteins, such as NuMA, cytoplasmic dynein, and HSET/ncd (Gaglio et al. 1995; Gaglio et al. 1996; Merdes et al. 1996; Gaglio et al. 1997; Merdes and Cleveland 1997; Compton 1998). Furthermore, minus ends of kinetochore microtubules appear relatively stable even if the centrosome and its astral microtubules are dislocated from the spindle pole (Mitchison and Salmon 1992; Gordon et al. 2001) or when K-fibers are severed at half length using UV microbeams (Spurck et al. 1990).

The growth of these K-fibers may result from addition of tubulin subunits proximal to the kinetochore. This would be consistent with previous studies where kinetochore-nucleated microtubule growth has been documented (Mitchison et al. 1986; Geuens et al. 1989). The polewards flux of K-fibers observed in mitotic spindles requires that tubulin subunits be constantly incorporated at microtubule plus ends proximal to the

kinetochores (Mitchison 1989). It is likely that similar mechanisms may contribute to the growth of the distal K-fibers. Further experiments and technological improvements will be needed to clarify the mechanisms of growth and formation of these distal K-fibers.

3.8.2 Incorporation of preformed K-fibers into the spindle.

Our second key observation was that over time, the minus ends of preformed K-fibers inevitably exhibited rapid sliding toward the spindle pole and became incorporated into the polar region of the spindle. Specific patterns of the incorporation of the preformed K-fibers depended upon where the minus end of the fiber was located with respect to the pole. Because distal K-fibers were always pointing away from the centrosome in monopolar spindles, their incorporation always involved formation of a transient loop, resulting in syntelic mono-orientation (both K-fibers on one chromosome connected to the same pole). It is noteworthy that this mechanism offers a straightforward explanation for the high frequency of syntelic chromosomes described previously in monastrol-arrested cells (Kapoor et al. 2000).

During spindle bipolarization upon monastrol washout, the geometry of minus-end incorporation was more complex. Those K-fibers that extended away from the separating centrosomes continued to form transient loops, whereas the minus ends of the K-fibers that pointed at the center of the original monopolar spindle exhibited more direct translocations, in both cases toward one of the two separating centrosomes. Importantly, incorporation of preformed K-fibers into the forming spindle was also detected in untreated PtK-αT cells, albeit with lower frequency (Figure 3.10). Together, these data reveal that astral arrays of microtubules associated with the centrosomes constantly search for, capture, and incorporate the minus ends of preformed K-fibers.

A question that remains is, how common is the formation and incorporation of K-fibers not connected to centrosomes during normal mitosis? During unperturbed

mitosis, such events have not been reported previously. One explanation for this is that these events are difficult to observe. In control mitosis, most chromosomes become amphitelic (properly bioriented) within just a few minutes after NEB. Furthermore, during this time, most chromosomes are in close spatial proximity to one another, and microtubule distribution is too complex for individual K-fibers to be visualized even by modern microscopy. Due to this complexity, most observations on the K-fiber formation were made on individual chromosomes that were incorporated into the spindle at later stages of spindle assembly (for example see Rieder and Alexander 1990). To circumvent these problems, the formation of K-fibers was studied under special conditions, such as microtubule re-polymerization after C-mitosis (Witt et al. 1980; Rieder and Borisy 1981) or by inhibiting individual components of the spindle using antibody microinjections (Gordon et al. 2001).

Our data reveal that formation and incorporation of K-fibers by the kinetochores is very common in monopolar mitosis. We observed continuous looping over 2 hour observation periods with up to 20 events per cell. Further, the frequency of these events did not decrease with time, suggesting that syntelic mal-orientations resulting from these events are not stable and are constantly being corrected. If syntelic chromosomes were stable, then the frequency of looping would gradually decrease as more and more chromosomes would lock in this configuration. We propose that this high frequency of formation and incorporation of K-fibers correlates with the number of chromosomes with kinetochores oriented such that their chromosome bodies sterically shield them from interacting with astral microtubules nucleated from either unseparated centrosome. Therefore, in mono-astral mitoses, the frequent correction of syntelic orientation results in chromosomes with such orientations. In untreated cells, this event is observed at a lower frequency, as only a few chromosomes stochastically orient such that they cannot interact with microtubules from both centrosomes (Figure 3.11).

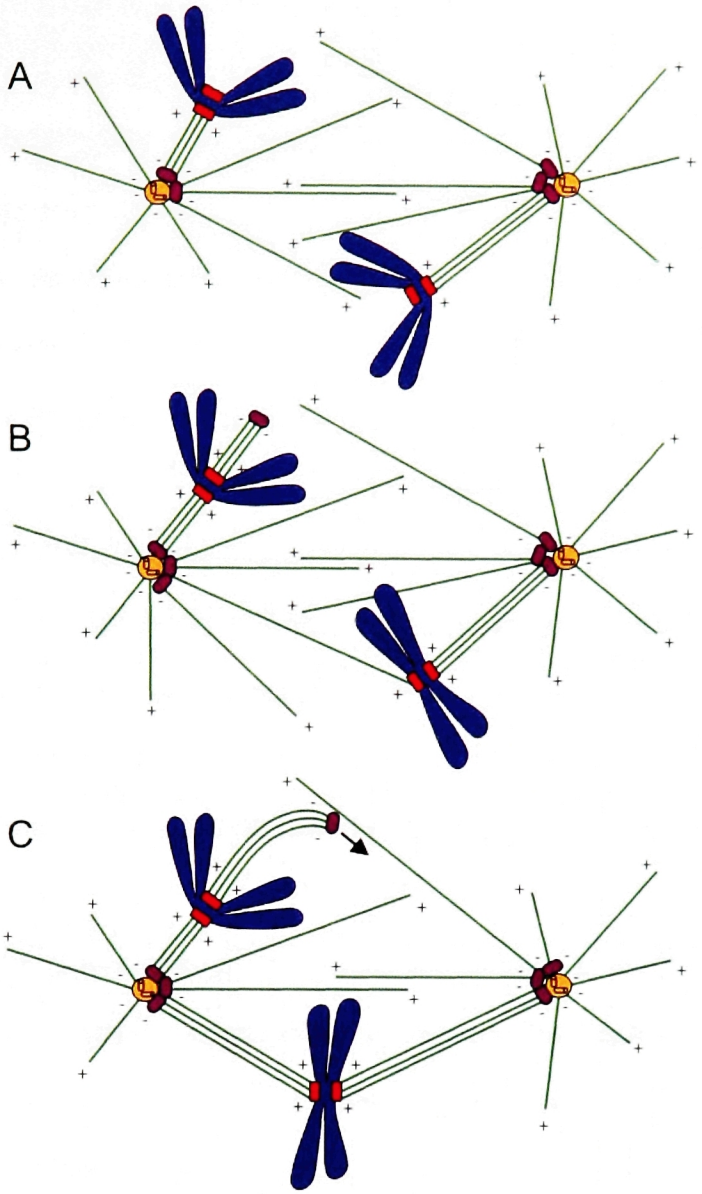

Figure 3.11 Two mechanisms contribute to the attachment of chromosomes to spindle poles. Microtubules (green) grow from centrosomes (yellow, circle) and interact with kinetochores (red) oriented toward the centrosomes. If a sister kinetochore on the mono-oriented chromosome (blue) is oriented toward the distal centrosome (A, right chromosome), its interaction with plus ends of microtubules from the opposite pole is highly probable (B). If the sister kinetochore is shielded from the dense array of microtubules between the two separated centrosomes (A, left chromosome), a K-fiber emanates from the kinetochore and interacts at its minus ends with microtubules connected to centrosomes. NuMA (purple) and associated proteins contribute to the sliding and incorporation of K-fiber minus ends into the spindle (B and C).

Cassimeris et al. (1994) did not observe any microtubule bundles associated with distal kinetochores in naturally occurring monopolar mitoses in fixed newt lung cells (four serial section EM reconstructions). It is likely that this apparent discrepancy reflects differences between cell types (newt pneumocytes vs. mammalian cells). This may also indicate that the frequency of distal K-fiber formation is somehow increased by monastrol. Consistent with the former proposition, well developed distal K-fibers have been documented in PtK cells recovering from cold treatment (Rieder and Borisy 1981). Our observations of distal K-fiber formation in untreated PtK-αT cells (Figure 3.10) further suggest that the mechanism of K-fiber formation we observed contributes to normal spindle morphogenesis and is not limited to monastrol-treated cells.

3.8.3 Microtubule minus ends are recruited to centrosomes to determine spindle orientation.

Finally, another unexpected phenomenon, conspicuous in our time-lapse recordings, is that during spindle bipolarization upon monastrol washout, the centrosomes transiently detach from the original monopolar spindle and separate independently of the K-fibers, which remain stable and focused. The axis of centrosome separation is unrelated to the original orientation of the focused K-fibers. During separation, the centrosomes remain connected by an array of overlapping interpolar microtubules, forming a spindle-like structure reminiscent of "chromosome-free spindles" (Faruki et al. 2002). Stable K-fibers are gradually recruited by the chromosome-free spindle via capture and incorporation of their minus ends. During this process, the K-fibers bend and reorient to align with the axis of the spindle defined by the separating centrosomes. Thus, the centrosomes appear to be responsible for spindle rotations and

for establishing the ultimate orientation of the spindle and the direction of chromosome segregation (O'Connell and Wang 2000; Khodjakov and Rieder 2001).

We propose that during vertebrate mitosis, in addition to providing sites of microtubule nucleation, the centrosomes also establish proper spindle orientation via searching, capturing, and focusing different components of the spindle, i.e., unattached kinetochores, and preformed microtubule bundles, including preformed K-fibers. Formation of K-fibers and bipolar spindles can occur via centrosome-independent mechanisms (for review see Karsenti and Vernos 2001). However, in the absence of centrosomes, the spindle is inherently bipolar and incapable of proper orientation, which in turn affects cytokinesis (Khodjakov and Rieder 2001). By providing astral arrays of microtubules, centrosomes define the number of spindle poles and link the spindle to the cell cortex, providing for proper orientation of the spindle. In this regard, cells of higher plants that are encased in a rigid cell wall, and thus do not need to adjust orientation of the spindle during the course of mitosis, do not possess centrosomes and never form multipolar mitotic spindles (Smirnova and Bajer 1992).

§ 3.9 The search and capture of microtubule plus ends and minus ends during mitosis

The search and capture mechanism proposed by Kirschner and Mitchison (1986) applied only to the capture of plus ends of astral microtubules by kinetochores. Accumulation of new data, including our observations reported here, now allows us to extend this principle onto preformed microtubules (Rusan et al. 2002) and to the minus ends of preformed K-fibers. We propose that the minus-end capture of K-fibers that we have directly observed in vertebrate cells provides a mechanism for a chromosome with such an orientation that its kinetochore cannot encounter dynamic plus ends of

microtubules emanating from either centrosomal aster in a bipolar spindle (Figure 3.11). A microtubule bundle can grow from the unattached kinetochore and extend beyond the region shielded by the chromosome body. NuMA contributes to the capture of this growing microtubule end by spindle microtubules and, through a motor-dependent activity, facilitates the transport of the K-fiber minus end toward the spindle pole. The polewards transport of NuMA and its interaction with dynein/dynactin have been previously reported and may directly account for this mechanism (Merdes et al. 2000). Together, the plus-end and the minus-end capture of microtubules should account for the attachment of all chromosomes to the spindle during mitosis.

Chapter 4 – Progress towards determining the function of TPX2 in mitosis

Abstract

Recent observations have demonstrated that the non-motor MAP, TPX2, plays a key role in mitotic spindle assembly. Specifically, TPX has been shown to be a component of the Ran/RCC1 centrosome-independent microtubule nucleation pathway (Gruss et al. 2001; 2002; Kufer et al. 2002; Schatz et al. 2003; Trieselmann et al. 2003; Tsai et al. 2003) and to be required for the proper assembly of a bipolar mitotic spindle (Garrett et al. 2002; Gruss et al. 2002). However, the precise contribution of TPX2 activity to spindle morphogenesis is still unclear. In human cells, TPX2 RNAi leads to defects in spindle microtubules, which has lead to a hypothesis that TPX2 is required for chromosome-microtubule attachments in animal cells (Gruss et al. 2002). To directly test this possibility I proposed using real-time high resolution microscopy assays in cells depleted of TPX2 using RNAi to examine the possible role of TPX2 in kinetochore fiber formation and its incorporation into spindles during mitosis (Khodjakov et al. 2003). Unfortunately, I found that an accurate analysis of microtubule dynamics in HeLa cells after TPX2 RNAi was limited by the resolution and photo-toxicity of the microscopy experiments.

TPX2 knockdown by RNAi in human cells has also been shown to result in a significant increase in multipolarity (Garrett et al. 2002). However, previous analysis of this phenotype has been limited to fixed samples. To better understand the basis of

multipolar spindle formation after loss of TPX2 function, I have used confocal microscopy to examine the origin of multipolarity as well as the role of TPX2 in spindle structure and function in response to spindle perturbations. My time-lapse video recordings of cells treated with TPX2 RNAi revealed that multipolarity is a result of progressive pole fragmentation. In addition, using the small molecule monastrol to inhibit the activity of the mitotic kinesin Eg5 after TPX2 knockdown, I have shown that in contrast to control pre-formed spindles that remain bipolar after addition of monastrol, multipolar spindles resulting from TPX2 knockdown collapse to monopolar spindles and resume a multipolar structure when Eg5 activity is restored. My studies do not suggest a role for TPX2 in the formation of all kinetochore microtubules, and find that microtubule nucleation and growth in spindle morphogenesis is not dependent on TPX2. My studies suggest that TPX2 may play a more important role in spindle pole organization than in chromosome-microtubule attachment. Consistent with this proposal, I have found that the loss of Aurora-A, a kinase believed to be involved in centrosome maturation which is activated by TPX2 (Kufer et al. 2002), also results in a multipolar spindle phenotype, similar to that observed after TPX2 knockdown.

§ 4.1 Using microscopy to examine TPX2 in the human mitotic spindle

Previous studies of TPX2 in spindle morphogenesis have relied on fixed cell analysis to examine the role of this non-motor MAP in spindle morphogenesis. In this chapter, I have used RNAi and live cell imaging to examine the implications of several recent studies on TPX2 in human cells. First, since TPX2 is a component of the Ran-GTP/RCC1 pathway (Gruss et al. 2001; Gruss et al. 2002; Schatz et al. 2003;

Trieselmann et al. 2003), I wanted to test whether TPX2 played a role in microtubule minus-end capture during spindle morphogenesis (Khodjakov et al. 2003). Next, Garrett et al. (2002) showed by analysis of fixed samples that siRNA of TPX2 in human cells results in multipolar spindles. My goal was to use live cell imaging to observe spindle morphogenesis in individual TPX2 knockdown cells to understand how these multipolar spindles form. In addition, Gruss et al. (2002) have implicated TPX2 in K-fiber formation in mitosis. I proposed that live cell imaging of TPX2 knockdown cells provided an opportunity to examine the possibility that K-fiber formation is inhibited after TPX2 knockdown. Further, Kufer et al. (2002) have shown that TPX2 is an activator of Aurora-A. I wanted to use microscopic techniques and RNAi to understand the implications of such an interaction in spindle morphogenesis.

§ 4.2 TPX2 and minus-end capture of microtubules

In the previous chapter, I have provided evidence that microtubules form in close proximity to chromosomes, possibly through nucleation at kinetochores. Unfortunately, I found that the GFP-tubulin HeLa cell line available showed a low threshold for photo-toxicity compared with the GFP-tubulin PtK2 cells used in the previous chapter. Even with the use of spinning disk confocal microscopy to minimize damage to the cells, the optical and temporal resolution required for observation of microtubule looping events at distal kinetochores was not possible (data not shown). However, by developing a technique to combine live cell spinning disk confocal microscopy and RNAi I was able to examine other aspects of the role of TPX2 in spindle morphogenesis.

§ 4.3 Spindle multipolarity after TPX2 knockdown is due to progressive spindle pole fragmentation

In fixed cell analysis, knockdown of TPX2 by RNAi has been shown to result in multipolar spindles (Garrett et al. 2002). RNAi is a new and exciting technique in cell biology, and recent studies have shown that some caution must be exercised in interpreting results from RNAi knockdown due to the fact that RNAi oligos have been shown to have off-target effects (Chi et al. 2003; Jackson et al. 2003; Semizarov et al. 2003). To test the previous observations of TPX2 RNAi, I used a second RNA oligo that was designed to target a different region of TPX2. By Western blot and immunofluorescence analysis this oligo produced efficient knockdown of TPX2 protein after 36 hours and generated the same multipolar spindle phenotype (Table 4.1). In addition, a third oligo that was designed to target TPX2 but did not produce knockdown (as evaluated by Western blot analysis) showed no effect on mitotic spindles (data not shown). Furthermore, to confirm that the multipolar spindle phenotype I observed after TPX2 knockdown was not dependent on the cell type used previously (HeLa), I depleted TPX2 from DLD1 (human colorectal adenocarcinoma) cells using both functional oligos (Figure 4.1). In these cells I observed a similar multipolar spindle phenotype (Table 4.1).

Analysis of fixed samples is useful to determine the spindle morphologies that develop as a result of TPX2 RNAi. However, to understand the process that produced this phenotype, the sequence of events that precedes it can be observed with live cell imaging. In the context of TPX2 RNAi, live cell imaging can elucidate the origin of the extra poles in multipolar spindles and distinguish between poles that form through fragmentation of existing poles or de novo formation, away from poles already associated with the spindle. In addition, live cell imaging offers an opportunity to examine the behavior of microtubules in spindle morphogenesis after TPX2 knockdown.

	Percent of mitotic cells with multipolar spindles			
	DLD-1		HeLa	
	Oligo #1	Oligo #2	Oligo #1	Oligo #2
TPX2 RNAi	56 (±15)	36 (±13)	98 (±2)	82 (±6)
Mock Transfected	2 (±3)	0 (±0)	9 (±5)	10 (±1)

Table 4.1 TPX2 knockdown with either of two unique oligos in two human cell lines results in an increase in multipolar spindles compared to mock transfection. Cells were fixed 36 hours after transfection with either TPX2 siRNA or mock transfected with ddH_2O. Both TPX2 oligos show a much larger percentage of cells with multipolar spindles when compared to mock transfected cells. Table values are the average of three experiments for DLD1 cells and two experiments for HeLa cells, showing percentage of mitotic cells with multipolar spindles, calculated from 1000 cells counted in each condition. Standard deviation is shown in parentheses.

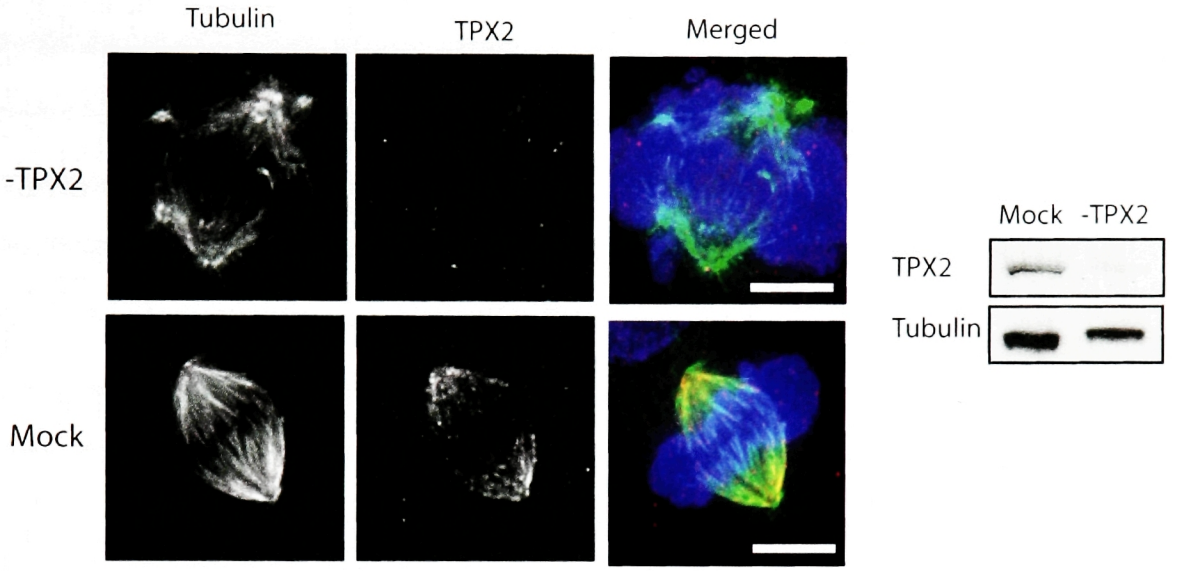

Figure 4.1 TPX2 knockdown results in multipolar spindles in DLD1 cells. (Left) In addition to HeLa cells, DLD-1 cells exhibit multipolar spindles after knockdown of TPX2 (above). For comparison, mock transfected cells show strong TPX2 staining on spindles (below). Scale bars are 5μm. (Right) Western blot of cell lysate made from cells scraped from similarly transfected cells immediately after fixation shows that TPX2 is successfully depleted (-TPX2) compared to mock transfected cells (Mock). Tubulin is shown as a loading control.

The efficiency of knockdown in a cell population can be determined by Western blot of cell lysate from a pool of cells. However, after knockdown by RNAi, a population of cells exhibited a statistical distribution of knockdown efficiencies. To examine the origin of multipolarity after TPX2 knockdown, I used live spinning disk confocal microscopy of individual HeLa cells expressing GFP-tubulin (HeLa-GFP-tub), combined with TPX2 RNAi and immunofluorescence (Figure 4.2). To verify that the particular cell imaged had been knocked down effectively, the coverslip was fixed and stained for TPX2 after observing a cell in mitosis by live imaging.

Direct observation of the progression of mitosis after knockdown of TPX2 by RNAi revealed that TPX2 knockdown cells become multipolar due to dynamic pole fragmentation (Figure 4.3). During imaging, the spindle structure changed dramatically, often rotating and changing shape. Notably, additional poles were only observed to originate from fragmentation, and de novo formation was not observed.

Instead, I observed that the poles of multipolar mitotic spindles split into several additional poles (a process referred to here as "fragmentation"), which then moved away from each other with microtubule arrays between them after TPX2 knockdown (Figure 4.3 A). Of the multipolar cells that were imaged after TPX2 RNAi treatment alone (n=4), all of the spindles exhibited fragmentation, increasing the number of poles by an average of 4.5 (range 2 to 5 poles) over the duration of imaging (average duration = 91 minutes, range 66 to 110 minutes). These recordings also demonstrated that, after TPX2 knockdown, pole fragmentation is progressive, and poles continue to fragment over time. To verify knockdown in each cell imaged, I relocated the same cell after fixation and compared TPX2 levels with mock transfected cells, which were fixed, stained, and imaged under the same conditions (Figure 4.3 B).

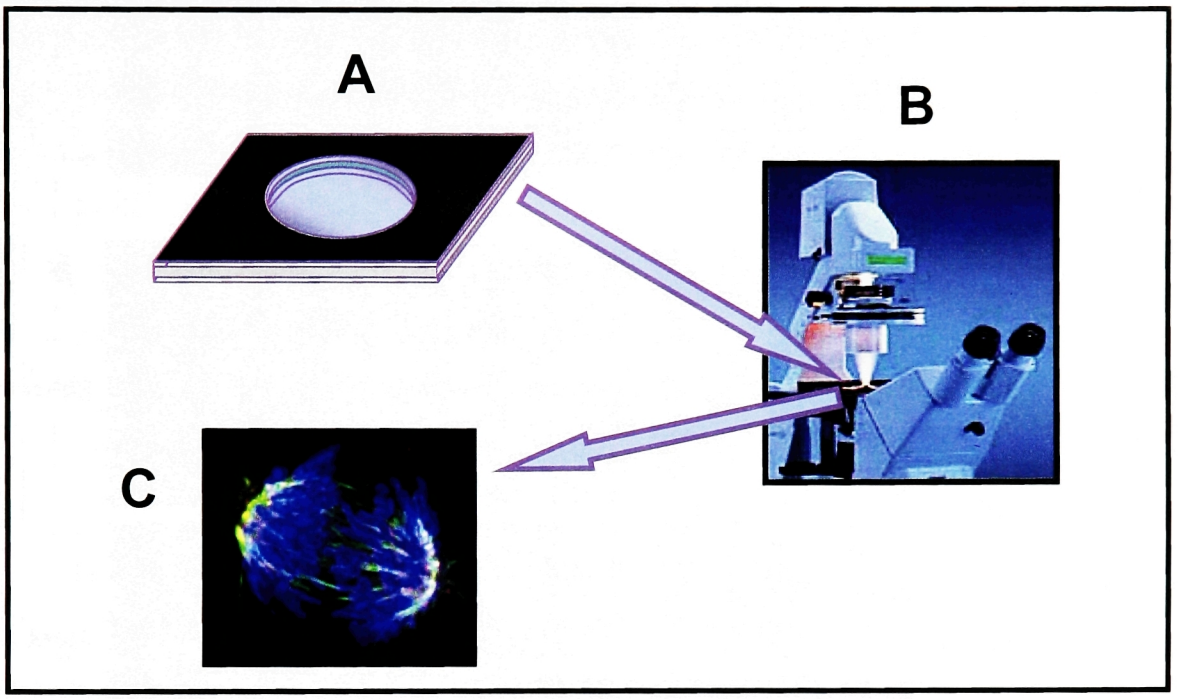

Figure 4.2 Live cell imaging of cells treated with RNAi is followed by immunofluorescence and analysis after relocation. (A) Cells are plated on alphanumeric gridded coverslips before transfection with RNAi oligos. Thirty-six hours after transfection with RNAi oligos, the coverslip is mounted in a closed perfusion chamber filled with imaging media. (B) Using a spinning disk confocal microscope enclosed in a temperature-controlled chamber, a cell is imaged by fluorescence and/or DIC microscopy. (C) Cells were then fixed and treated for immunofluorescence. Using the grid location to relocate the same cell imaged by live video microscopy, the cell is imaged again for analysis after image deconvolution.

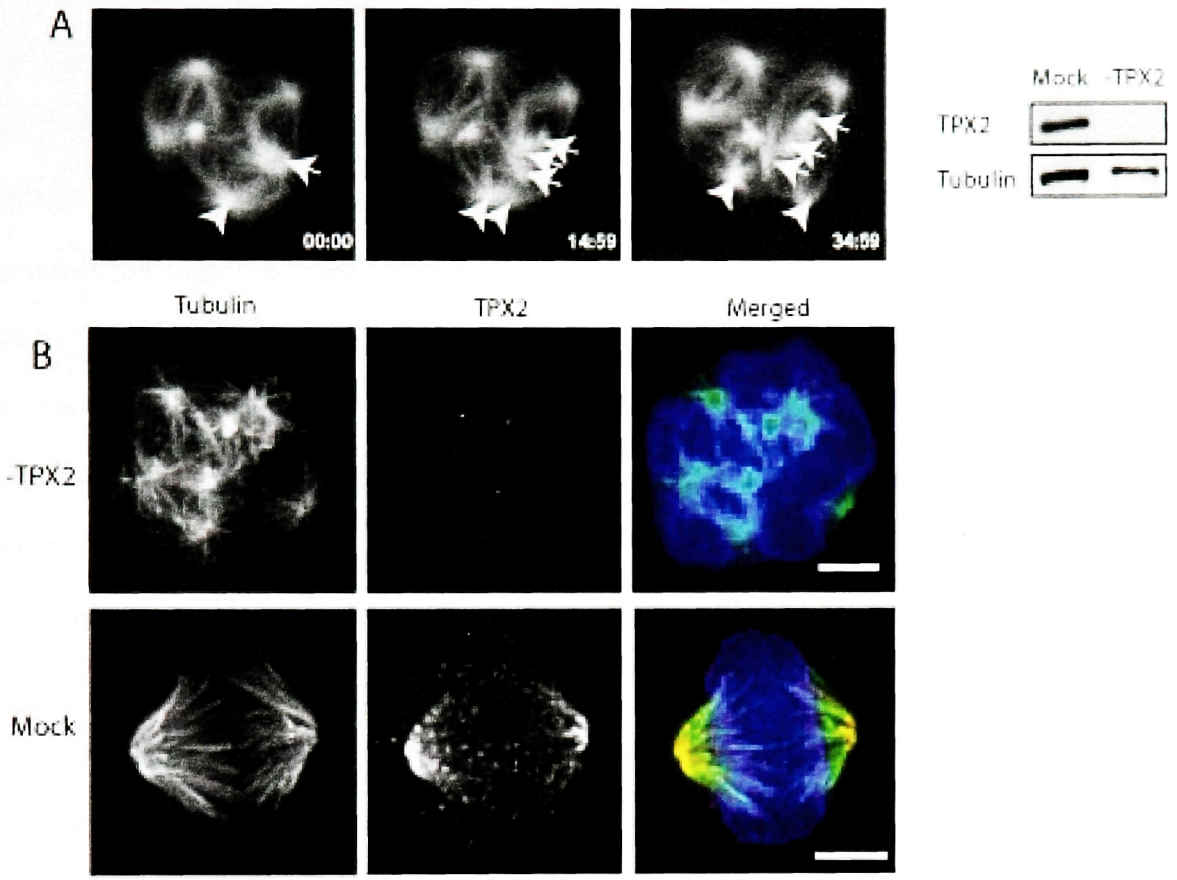

Figure 4.3 Multipolar spindle pole fragmentation after TPX2 knockdown is progressive. (A) A multipolar mitotic HeLa cell expressing GFP-tubulin is observed by time-lapse spinning disk confocal fluorescence imaging 36 hours after TPX2 RNAi. Initially, six poles are present; and over time, two of these poles (arrow, arrowhead) are observed to fragment into two and three poles, respectively. Time is in minutes:seconds. (B, Top) After fixation, the same cell imaged in A is relocated and imaged by immunofluorescence for tubulin, TPX2 and DNA, showing effective TPX2 knockdown in this cell. (B, Bottom) For comparison, a mock transfected cell is also imaged by immunofluorescence for tubulin, TPX2 and DNA, showing strong TPX2 staining at the poles and along spindle microtubules, typical of bipolar spindles. Scale bars are 5μm. (Right) Western blot of cell lysate made from cells scraped from similarly transfected cells immediately after fixation shows that TPX2 is successfully depleted (-TPX2) compared to mock transfected cells (Mock). Tubulin is shown as a loading control.

To determine whether the cells that initially formed bipolar spindles after TPX2 knockdown would eventually exhibit typical pole fragmentation, I accumulated cells in prophase with a nocodazole arrest. After TPX2 knockdown, cells on coverslips were treated with 33 μM nocodazole for one hour before being transferred into non-nocodazole containing media, allowing microtubule polymerization and release from mitotic block. Immediately after the nocodazole washout, I performed time-lapse microscopy on individual cells at lower time resolution to avoid photo-toxicity (Figure 4.4). After imaging mitotic TPX2 knockdown cells for 45 minutes or longer after nocodazole washout, 33% of cells that had two distinguishable poles exhibited an increase in pole number during imaging (n = 6) (Figure 4.4 A), and 66% of cells that started with multiple poles exhibited an increase in pole number (n=6) (as shown in Figure 4.3 A). It follows from these observations that the cells that directly formed multipolar spindles after nocodazole washout are likely to have been in mitosis, with already fragmented poles, before the introduction of nocodazole.

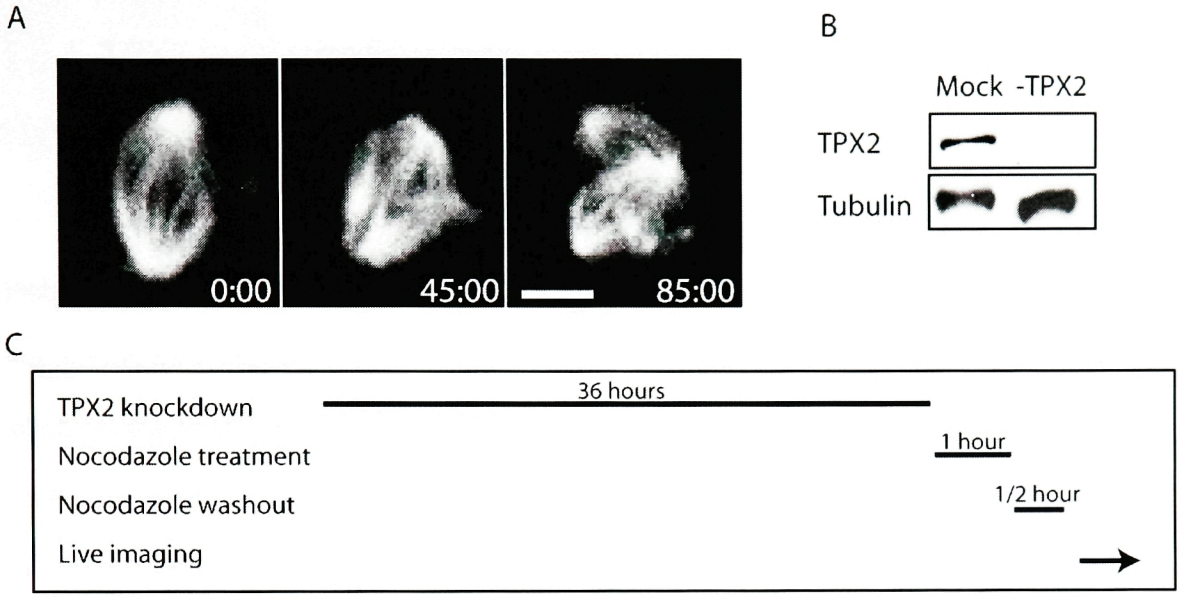

Figure 4.4 Bipolar spindle poles fragment over time in the absence of TPX2. A mitotic HeLa cell expressing GFP-tubulin is observed by time-lapse spinning disk confocal fluorescence imaging 36 hours after TPX2 RNAi. (A) After TPX2 knockdown and release from mitotic arrest by nocodazole treatment, some cells formed bipolar spindles that were observed to fragment when imaged over time. Time is shown in minutes:seconds. Scale bar is 5μm. (B) Western blot of cell lysate made from cells scraped from similarly transfected cells immediately after fixation shows that TPX2 is successfully depleted (-TPX2) compared to mock transfected cells (Mock). Tubulin is shown as a loading control. The experimental time course is shown in C.

§ 4.4 TPX2 is required for mitotic spindle stability after inhibition of Eg5

To examine whether TPX2 knockdown spindles could be observed to collapse instead of fragment, I used two reversible, cell permeable small molecule inhibitors of the microtubule motor Eg5: monastrol and HR22C16 (Mayer et al. 1999; DeBonis et al. 2003; Hotha et al. 2003). Eg5 inhibition in mitotic cells through treatment with monastrol, immunodepletion from a cell free extract, or antibody microinjection causes the interpolar separation between centrosomes to decrease, which eventually results in monopolar spindles (Gaglio et al. 1996; Mountain et al. 1999; Kapoor et al. 2000; Faruki et al. 2002; Khodjakov et al. 2003).

To observe the effects of inhibition of Eg5 on individual cells, monastrol-containing media was perfused over HeLa-GFP-tubulin cells through an imaging chamber during live fluorescence video microscopy. To maintain a mitotic arrest, all cells were kept in the presence of MG132, a proteasome inhibitor that prevents entry into anaphase. After TPX2 knockdown, spindles imaged by live time-lapse microscopy (n = 8) collapsed from a variety of pole numbers (range 2 to 7) to monoasters after addition of monastrol in an average of 44 min (range 25 to 102) (Figure 4.5 A). This effect was reversible; after the removal of monastrol from the media surrounding the cells by perfusion of media without monastrol, the cells re-formed multipolar spindles. Interestingly, I observed that only a partial knockdown of TPX2 is required to cause a pre-formed spindle to collapse to a monoaster after introduction of monastrol (Figure 4.5 B). In contrast, pre-formed spindles in mock transfected cells showed no collapse to monoasters after perfusion with monastrol-containing media. These cells were also

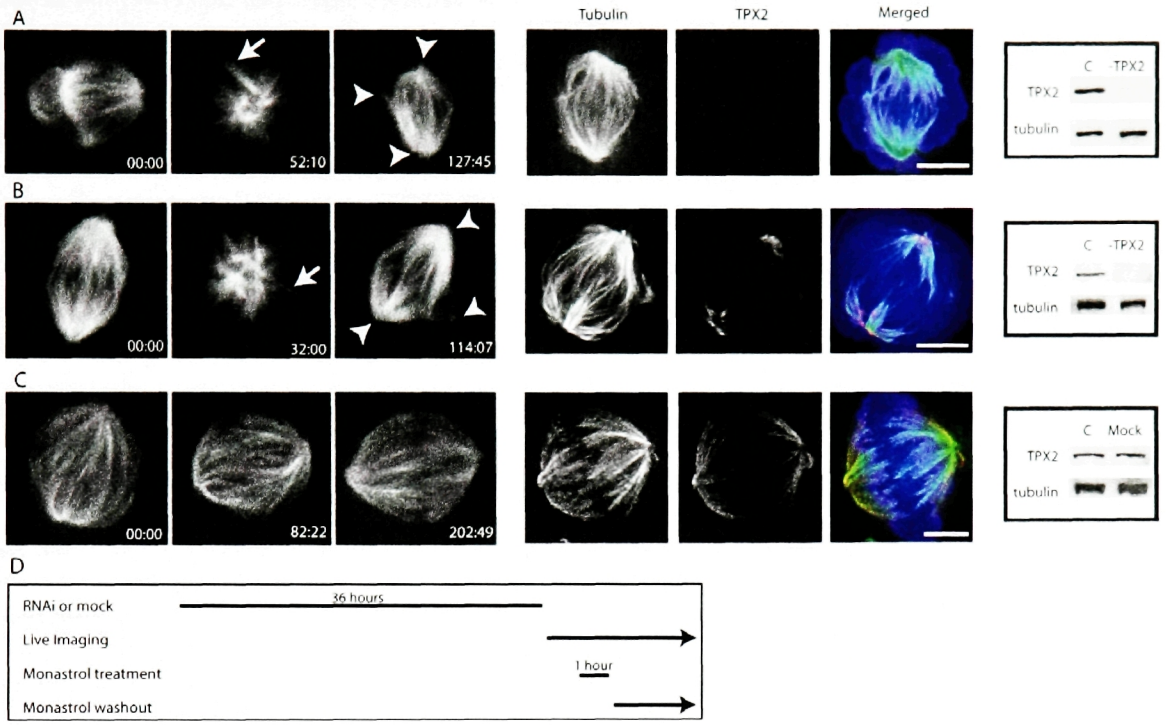

Figure 4.5 TPX2 is required for spindle stability against forces acting inward on the poles. Multipolar HeLa-GFP-tubulin spindles were observed to collapse reversibly to monoasters after inhibition of Eg5 and depletion or even reduction of TPX2. (A-C, left) Immediately after the first image at t=0, media containing monastrol was perfused into the imaging chamber during live video microscopy. (A and B) After TPX2 knockdown, the poles collapsed to a single monoaster with prominent microtubule bundles (arrow). Following the removal of the monastrol containing media in the imaging chamber by perfusion, the poles again separated and a multipolar spindle re-formed with three poles (arrowheads). (C) A mock transfected cell was observed to remain bipolar after the introduction of monastrol. (A-C, right) Following imaging, the same cells were stained for TPX2 and DNA; and Western blots of cell lysates prepared from the remaining cells, which were transfected with the cells that were imaged, were blotted against TPX2 to detect knockdown of the cell population. The time course for these experiments is depicted in D. Tubulin is shown as a loading control. Time is in minutes:seconds.

treated with MG132 to prevent mitotic exit; and the spindles remained bipolar in the presence of monastrol for over three hours (n = 4, range 1.75 to 3.3 hours) (Figure 4.5 C).

The susceptibility of spindles to collapse after TPX2 knockdown and Eg5 inhibition was also observed in populations of cells that were treated with either monastrol or HR22C16 (Table 4.2). After mitotic arrest by treatment with MG132, TPX2 RNAi and mock transfected cells were either fixed (0 hour time point) or transferred to media with MG132 and either monastrol or HR22C16 to induce Eg5 inhibition. Cells that were fixed at regular timepoints after Eg5 inhibition exhibited the same spindle weakness toward inward directed forces after addition of monastrol or HR22C16, just as was observed in our live cell imaging. Cells that were mock transfected showed the same predominance of bipolar spindles in the presence of MG132 or in the presence of MG132 and monastrol or HR22C16. In contrast, after TPX2 knockdown, the same fraction of mitotic cells that were multipolar in MG132 alone were found to be monopolar within 30 minutes after addition of monastrol or HR22C16. Importantly, these phenotypes persisted for 3 hours after the addition of monastrol or HR22C16 for both TPX2 knockdown and mock transfected cells (data not shown).

§ 4.5 Microtubule nucleation and growth in spindle morphogenesis is not dependent upon TPX2 function

The involvement of TPX2 in both spindle assembly and in the Ran-GTP/RCC1 pathway has led to a model for chromatin-mediated microtubule assembly wherein Ran-GTP stimulates the formation of microtubule asters by releasing TPX2 from inhibitory

	Percent of mitotic cells					
	Before Eg5 inhibition			0.5 h after Eg5 inhibition		
	bipolar	multipolar	monopolar	bipolar	multipolar	monopolar
TPX2 RNAi	11 (±13)	83 (±13)	3 (±4)	2 (±0)	3 (±1)	95 (±0)
Mock Transfected	85 (±7)	14 (±5)	1 (±2)	88 (±9)	6 (±4)	6 (±5)

Table 4.2 After inhibition of Eg5, TPX2 RNAi cells show an increase in monopolar spindles, while mock transfected cells do not. After either transfection with TPX2 RNAi oligo or mock transfected with ddH_2O for 36 hours, cells were either fixed or treated with monastrol or HR22C16 to inhibit Eg5 for ½ hour and were then fixed. Both TPX2 oligos showed a dramatic increase in multipolar spindles over mock transfected cells. Table values are the average of two experiments for DLD1 cells and two experiments for HeLa cells, showing percentage of mitotic cells with multipolar spindles, calculated from 1000 cells counted in each condition. Standard deviation is shown in parentheses.

interactions with nuclear import receptors (Carazo-Salas et al. 1999; Zhang et al. 1999; Nachury et al. 2001; Tsai et al. 2003). Further, it has been proposed that spindle formation in somatic cells requires a population of chromatin-associated microtubules that are dependent on Ran-GTP and TPX2 at the chromosomes for assembly, possibly resulting in defects in kinetochore microtubule fibers in the absence of TPX2 (Gruss et al. 2002).

Live imaging of HeLa-GFP-tubulin cells after TPX2 knockdown provides a unique opportunity to observe directly the role of TPX2 in microtubule nucleation and growth in mitosis. To examine the hypothesis that TPX2 is required for microtubule nucleation around chromosomes, I arrested cells in mitosis with nocodazole for one hour and observed the formation of spindles after nocodazole was removed and microtubules were allowed to re-polymerize. This technique has been utilized previously in the analysis of spindle morphogenesis in CHO cells (Terada et al. 2003) and PtKαT cells (Cimini et al. 2003); and here it was used to observe microtubule re-growth in HeLa-GFP-tubulin cells by live imaging and in HeLa cells for analysis of fixed populations of cells. In these experiments, both control and TPX2 knockdown cells quickly formed spindles after nocodazole washout (Figure 4.6). The time-course of this recovery were observed both by live imaging of single cells and by analysis of populations of cells fixed at regular intervals. Analysis of spindle morphogenesis revealed that the formation of spindle microtubules was not substantially inhibited by the absence of TPX2.

Mock transfected cells formed spindles an average of 13 minutes after nocodazole washout (n = 13, range = 8 to 25 minutes) (Figure 4.6 A). Following TPX2 knockdown, cells imaged after nocodazole washout showed spindle formation after an average of 17 minutes (n = 13, range = 9 to 19 minutes) (Figure 4.6 B), demonstrating

that the absence of TPX2 does not substantially delay spindle morphogenesis after nocodazole washout.

While live cell imaging can examine the morphology of spindle assembly, it cannot reveal the time-course of microtubule polymer recovery after nocodazole washout, due to the background signal from soluble tubulin in the cell. To analyze the process of microtubule polymerization after nocodazole washout in TPX2 RNAi and mock transfected cells, I examined fixed populations of cells which have had the soluble tubulin removed (Figure 4.6 C). After nocodazole washout, cells were extracted to remove soluble tubulin dimers before fixation at regular time intervals. Microtubules were stained with FITC-labeled α-tubulin antibody and TPX2 was stained with Texas Red labeled TPX2 antibody. Quantization of tubulin polymer was calculated as the integrated intensity of FITC fluorescence over equivalent sized regions of interest (n = over 700 mitotic cells quantified over two separate experiments); and polymer levels were found to be similar between TPX2 RNAi and mock transfected cells. Although the resolution of this experiment cannot elucidate the nucleation or polymerization dynamics of individual microtubules, this result reveals that rates of microtubule polymerization are also not substantially affected by the absence of TPX2.

§ 4.6 Robust kinetochore microtubule fibers form in the absence of TPX2

To test the possibility that the multipolar phenotype observed in TPX2-depleted cells could be a result of defects in kinetochore microtubules (Gruss et al. 2002), TPX2 RNAi and mock transfected HeLa cells were stained for the kinetochore-associated protein CENP-E and examined by deconvolution of three-dimensional fluorescence images. In this way, I was able to examine single kinetochores for the presence or

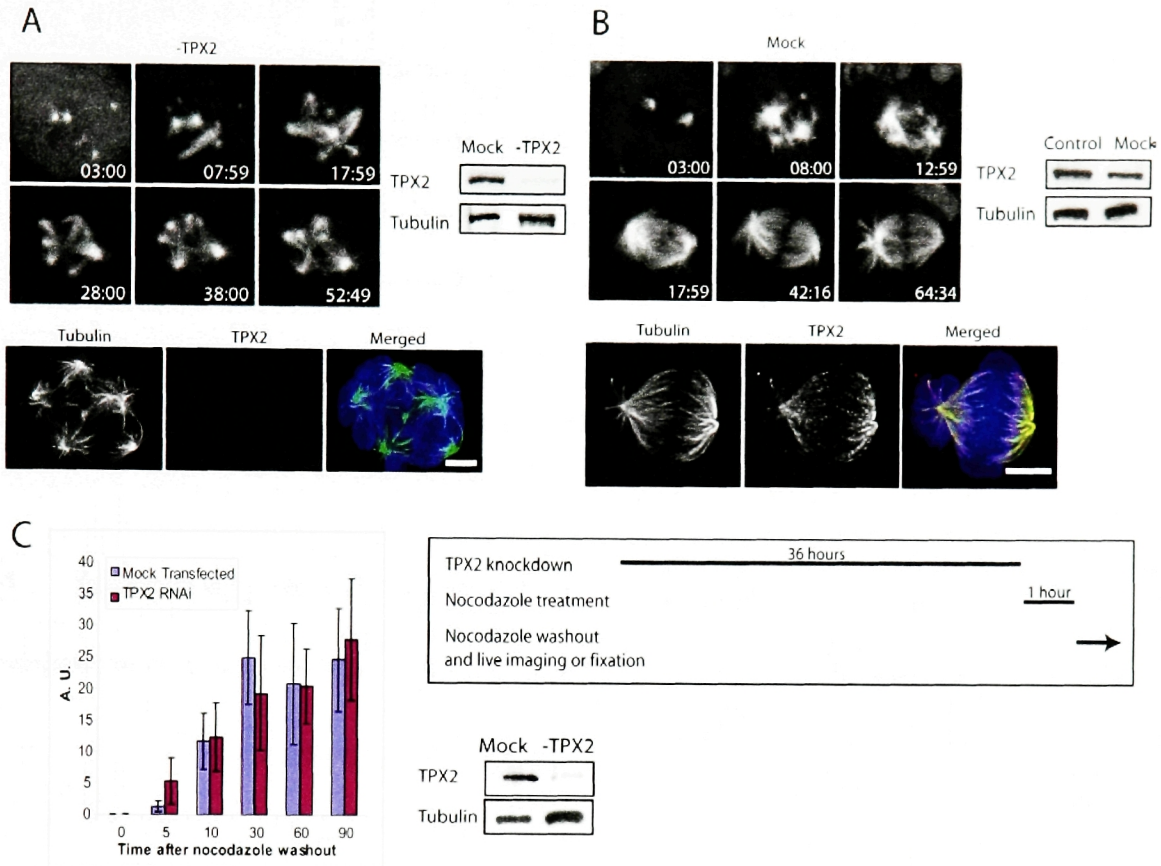

Figure 4.6 Microtubule nucleation in spindle morphogenesis is not dependent upon TPX2. (A, B) Microtubule recovery was observed by live video microscopy in HeLa-tub-GFP cells after release from one hour of nocodazole treatment. Cells were either transfected with TPX2 siRNA (A) or mock transfected (B) 36 hours before nocodazole was added to the media surrounding the cells. (A, B, Top) Selected frames from live video microscopy show comparable levels of spindle morphogenesis in both TPX2 RNAi (A) and mock transfected (B) cells. (A, B, Bottom) Relocation of the cells imaged in A and B (Top), and analysis by immunofluorescence revealed that knockdown of TPX2 after RNAi is complete (A). TPX2 levels in the mock transfected cell are shown for comparison (B). (C) Nocodazole washout was observed in HeLa cells by fixed timepoints for cells transfected with TPX2 RNAi and for mock transfected cells. Cells were stained for DNA, tubulin and TPX2. Error bars show standard deviations. (A, B, C, Right) Western blots for cell lysate prepared from the surrounding cells show that TPX2 is effectively knocked down (A and C) (-TPX2) compared to control (B) and mock transfected cells. Scale bars are 5 μm. Tubulin is shown as a loading control.

absence of kinetochore microtubules. I found that kinetochore microtubule bundles are readily observed in multipolar spindles after TPX2 knockdown (Figure 4.7). The presence of kinetochore microtubules in multipolar cells after TPX2 knockdown illustrates that TPX2 is not an absolute requirement for the formation of kinetochore microtubule bundles. However, the presence of microtubules at the kinetochore does not necessarily indicate that all kinetochores are occupied by a full compliment of microtubule fibers in the absence of TPX2.

§ 4.7 Preliminary results suggest that loss of Aurora-A function by knockdown or inhibition results in weak multipolar spindles

Aurora-A contributes to centrosomal maturation and microtubule organization at the pole (reviewed in Blagden and Glover 2003) and is activated by TPX2 in the presence of Ran-GTP (Eyers et al. 2003; Tsai et al. 2003). To investigate the possibility that the multipolar spindle phenotype observed after TPX2 RNAi was due to its interaction with Aurora-A, I used RNAi of Aurora-A to compare with the results for TPX2.

Using a previously published oligo (Kufer et al. 2002) Western blot analysis of Aurora-A RNAi showed knockdown of Aurora-A protein levels 48 hours after transfection. Examination of spindles after Aurora-A knockdown by immunofluorescence revealed that 61% of mitotic cells treated with Aurora-A RNAi exhibited multipolar spindles, compared to 6% of mock transfected cells (n=2, 1000 cells counted in each treatment condition) (Figure 4.8). To confirm this phenotype, it will be important to confirm knockdown in individual cells by immunofluorescence in addition to Western blot and to test Aurora-A knockdown with other oligos and additional cell lines as I have shown in my analysis of TPX2 RNAi.

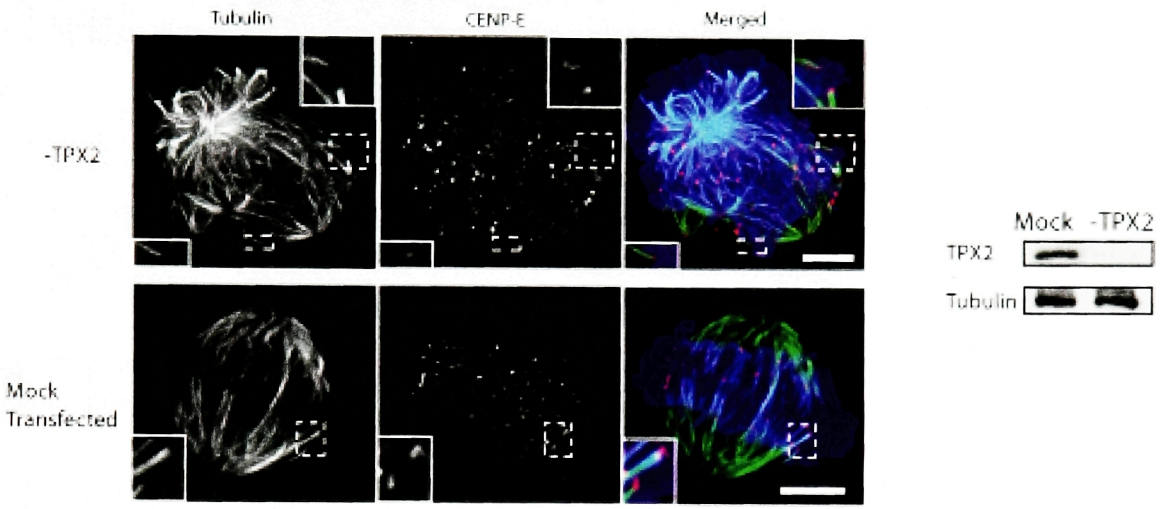

Figure 4.7 Kinetochore microtubule formation in spindle morphogenesis is not dependent on TPX2. (Top) Mitotic HeLa cells were fixed in a high calcium buffer to remove non-kinetochore microtubules 36 hours after TPX2 siRNA transfection and were stained for tubulin and CENP-E. Multipolar spindles were found to have strong kinetochore microtubule attachments at centromeres. (Bottom) Mock-transfected HeLa cells exhibited similar kinetochore microtubule attachments at centromeres in a bipolar spindle. Insets show 2x magnifications of chromosomes with kinetochore microtubule attachments. (Right) Western blot of cell lysate made from cells scraped from the remaining transfected cells immediately after fixation (-TPX2) shows that TPX2 was successfully depleted compared to mock transfected cells (Mock). Tubulin is shown as a loading control. Scale bars are 5μm.

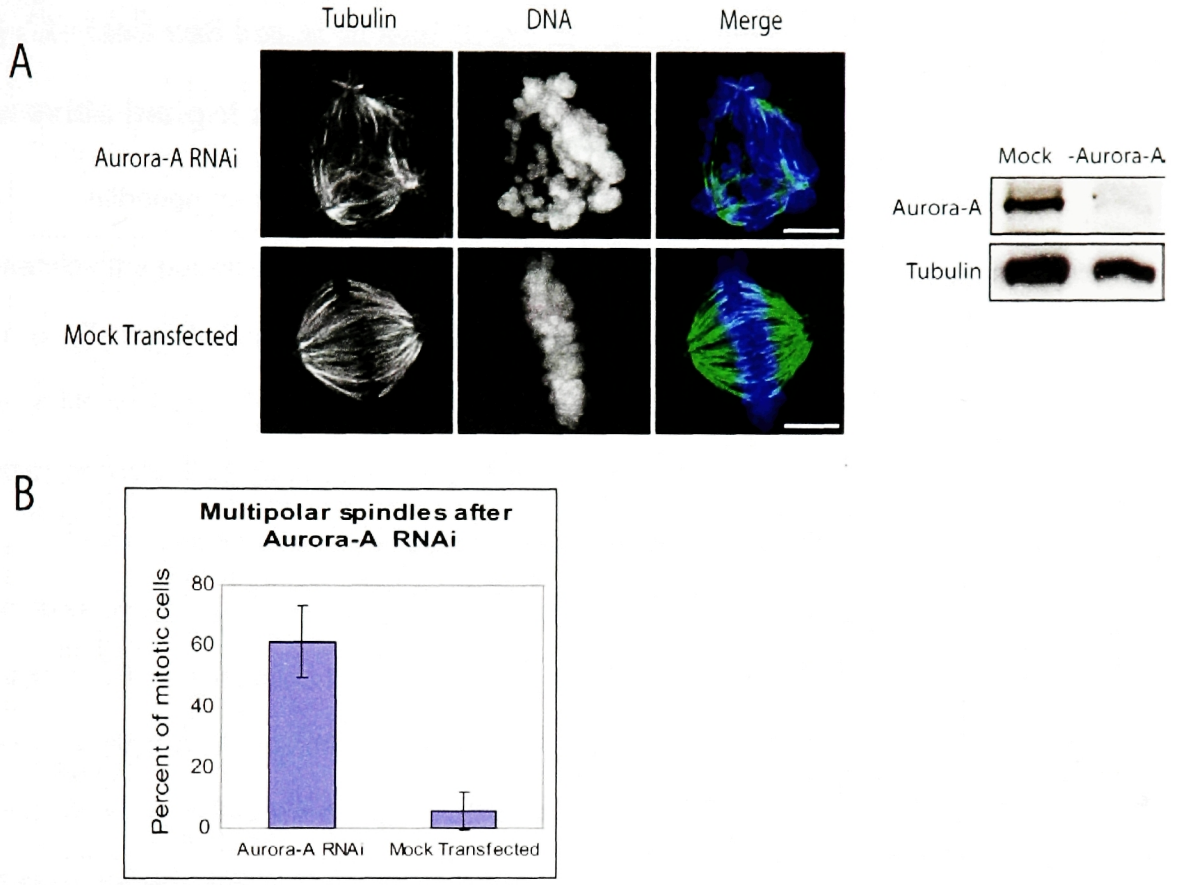

Figure 4.8 Depletion of Aurora-A activity by RNAi knockdown produces multipolar spindles. (A) Knockdown of Aurora-A in HeLa cells was evident by Western blot (right) 48 hours after siRNA transfection; while cells fixed at the same time exhibited a strong multipolar phenotype compared to mock transfected cells (left). (B) Quantification of this phenotype (n=2) showed that approximately 61% of all mitotic cells were multipolar after Aurora-A knockdown. Cell counts are for 1000 cells in each condition and error bars show standard deviation. Scale bars are 5 μm.

§ 4.8 Live cell imaging and RNAi of human cells are combined to provide insight into the role of TPX2 in mitosis

Although my original interest in using live video microscopy and RNAi was to examine the possible roles of the TPX2/Ran pathway in microtubule minus-end capture in spindle morphogenesis, this turned out to be beyond the photo-toxicity threshold of the cells available. However, I found that this technique is still quite useful for examining other aspects of TPX2 in spindle morphogenesis.

First, I directly observed the progression of multipolarity in TPX2 knockdown spindles, which are characterized by dynamic arrays of microtubules and progressive fragmentation, illustrating that multipolarity after TPX2 knockdown is a result progressive pole fragmentation. In addition, my live cell imaging revealed that, after TPX2 knockdown, spindles are unable to maintain inter-polar separation and collapse to monoastral spindles after inhibition of Eg5. This is a marked difference from the response of mock transfected cells to Eg5 inhibition after the spindle has formed; in this case bipolar spindles were observed to remain bipolar and not collapse to monoasters (see also Kapoor et al. 2000).

The data presented here also clarified several points about the role of TPX2 in the Ran/RCC1 pathway and microtubule nucleation and polymerization in spindle morphogenesis. Although I was unable to address the role of TPX2/Ran pathway in microtubule minus-end capture, I used spinning disk confocal microscopy and RNAi to examine the role of TPX2 in K-fiber formation and microtubule nucleation. Recent experiments suggest that TPX2 activity is required to promote chromosome-directed spindle organization in frog egg extracts in the absence of centrosomes, and that defects

in spindle morphology in the absence of TPX2 are due to a lack of TPX2-mediated microtubule nucleation (Gruss et al. 2002). However, I have shown here that in human cells TPX2 is not required for the polymerization of spindle microtubules after nocodazole washout or for the formation of robust kinetochore microtubule bundles.

Other studies on the role of TPX2 in mitosis have focused on the activation of the Aurora-A kinase by TPX2 (Trieselmann et al. 2003), although the role of Aurora-A in spindle morphogenesis is still unclear. TPX2 binds to Aurora-A and has been shown to regulate Aurora-A activity and microtubule targeting in mitosis (Eyers et al. 2003; Tsai et al. 2003). Aurora-A has been shown to contribute to centrosome maturation and separation in spindle morphogenesis (reviewed in Blagden and Glover 2003); although the contribution of Aurora-A to the structural stability of spindles has never been examined in this context. After either knockdown by Aurora-A RNAi, my preliminary results indicate that the same weak spindle phenotype I observed after TPX2 knockdown was exhibited by spindles without Aurora-A activity. In addition, spindles lacking Aurora-A had a much higher incidence of multipolarity and were susceptible to spindle collapse after inhibition of Eg5.

Chapter 5 - Conclusion

§ 5.1 Summary

Mitotic spindle morphogenesis requires the orchestration of a complex assembly of microtubules, chromosomes, MAPs, and other mitotic proteins. As described in the previous chapters, I combined four-dimensional (volumetric and temporal) confocal imaging of single cells with analysis of the same cells by immunofluorescence. I found that this combination of techniques greatly improves the usefulness of other tools of cell biology (e.g. RNAi) and allows analysis of both the functional and the molecular components of mitotic proteins in spindle morphogenesis. In particular, my results shed light on the origin of kinetochore microtubules and the role of two non-motor MAPs in mitosis.

First, I presented direct evidence for kinetochore microtubule translocation and showed that incorporation of pre-formed kinetochore microtubule bundles into the spindle contributes to spindle morphogenesis. The capture of microtubule plus-ends by kinetochores has been well described and is widely recognized for its role in the bipolar attachment of chromosomes. My data revealed an additional mechanism that involves the minus-end translocation of pre-formed kinetochore microtubule bundles, which is dependent on the microtubule bundling protein, NuMA. These microtubule bundles were observed first in drug-treated cells, and subsequently similar dynamics of kinetochore microtubules were observed during spindle formation in control cells. These results suggest that the mechanism of capture and incorporation of pre-formed kinetochore microtubule minus-ends complements the microtubule plus-end capture mechanism and contributes to spindle formation in vertebrates.

Second, I examined the role of a non-motor MAP, TPX2, in spindle structure and function in mammalian cells. TPX2 has been implicated in the Ran-GTP pathway of chromatin-associated microtubule nucleation and spindle assembly (Gruss et al. 2002), while depletion of TPX2 by RNAi has been shown to result in multipolar spindles (Garrett et al. 2002). In order to combine live cell imaging and RNAi to study TPX2 function in spindle morphogenesis, I developed a protocol for relocating cells imaged by spinning-disk confocal microscopy to analyze by immunofluorescence and confirm knockdown. My time-lapse recordings revealed that spindle multipolarity in TPX2 knockdown cells is a result of progressive pole fragmentation. By directly observing the response of TPX2 knockdown cells to the inhibition of the microtubule motor Eg5, I also found that these multipolar spindles form monopolar spindles under conditions in which control spindles maintain inter-polar separation. In addition, I found that microtubule nucleation and growth in spindle morphogenesis are not dependent on TPX2, and that cells without TPX2 form robust kinetochore microtubule bundles. Finally, in an attempt to better understand the molecular mechanisms of TPX2, I completed a preliminary investigation of spindle morphogenesis using RNAi of Aurora-A, which suggests that Aurora-A and TPX2 produce similar effects in spindle morphogenesis. Collectively, these results shed new light on the role of TPX2 in spindle pole organization and bipolarity.

§ 5.2 Conclusion

5.2.1 Minus-end transport of kinetochore microtubules in spindle morphogenesis

Not surprisingly, the more we understand about the mitotic process the more it appears that most cell types have the capacity to build the spindle using multiple and probably redundant mechanisms (for a review, see Maiato and Sunkel 2004). For the

last twenty years, the favored model of spindle assembly was based on nucleation of microtubules at the centrosome and then capture of these microtubules by kinetochores to establish proper connections of microtubules to kinetochores (as discussed in Chapter 1, this model is called search-and-capture). In this centrosome-dependent pathway, microtubules nucleated at the centrosome (for a review, see Compton 2000), undergo dynamic instability (Mitchison and Kirschner 1984) and are captured by chromosomes through chance encounters (Mitchison and Kirschner; 1985 a and b). Experimental evidence for this mechanism in living cells has been shown in newt pneumocytes by observations of the initial interaction between a kinetochore and the forming spindle, which showed that chromosome attachment can result from an interaction between astral (centrosomal) microtubules and the kinetochore (Hayden et al. 1990).

However, microtubule assembly can be initiated by both centrosomal and chromatin-associated pathways. Chromosome-associated microtubule formation has been observed in acentrosomal Xenopus extract around chromatin-coated beads (Heald et al. 1996) and micro-manipulated bivalent chromosomes that were physically detached from the original spindle in grasshopper spermatocytes (Zhang and Nicklas 1995). Microtubule assembly at kinetochores have been observed on isolated chromosomes examined by electron microscopy (Telzer et al. 1975) as well as in endosperm in prometaphase or following recovery microtubule depolymerization (Mole-Bajer 1969), suggesting that kinetochores on isolated chromosomes can act as microtubule assembly sites.

Although microtubules had been observed to form spindles around chromosomes and that kinetochores could act as microtubule assembly sites, several questions remained about chromosome-associated kinetochore microtubules. First, it remained to be determined whether these microtubules have the same polarity as those

nucleated at the centrosome (that is, with the plus ends at the kinetochore). Second, it was unclear if chromosome-associated microtubules elongated by subunit addition at the kinetochore or at the unattached end. Finally, there was no evidence to suggest that chromosome-associated microtubules contributed to spindle morphogenesis in living cells. Since the previous studies on acentrosomal kinetochore microtubule bundles were performed on fixed cells, the significance of these findings in the context of living cells was strongly debated (see Maiato and Sunkel 2004).

Since then, Euteneuer et al. (1983) showed that the polarity of microtubules that originate from the kinetochore after recovery from microtubule depolymerization in CHO cells was the same as that observed previously in matured k-fibers, with the plus-ends at the kinetochore. This result was achieved using "hook decoration," where the cells were lysed in a detergent mixture containing bovine brain tubulin under conditions that allowed the formation of polarity-revealing hooks. They found that 95% of the decorated kinetochore microtubules had the same polarity and that, according to the hook curvature, the plus ends of the microtubules were at the kinetochores. In addition, evidence that tubulin incorporation must occur at the site of kinetochore attachment for each k-fiber has been demonstrated in several systems (Czaban and Forer 1985; Mitchison et al. 1986; Maddox et al. 2003).

In the work presented here, I have directly observed robust centrosome-independent pre-assembled k-fibers in live cells. Through my live cell imaging I have shown that these pre-assembled k-fibers can be incorporated into the spindle, and thus contribute to spindle morphogenesis in vertebrate cells. This provides the answer to the third question listed above by demonstrating that acentrosomal k-fibers contribute to spindle morphogenesis in living vertebrate cells.

My results also have important implications for how chromosomes achieve proper attachment in the spindle, especially in the context of chromosomes whose kinetochores are not oriented in a way that facilitates attachment by capture of centrosomal microtubules. Without bipolar attachment (a kinetochore microtubule bundle attaching each sister chromosome to each pole in the bipolar spindle), cells risk improper chromosome segregation, which can in turn lead to missing or extra chromosomes (known as aneuploidy) in the daughter cells following mitosis. As discussed in Chapter 1, aneuploidy can lead to birth defects if the error occurs in meiotic divisions of gametes (reviewed in Nicolaidis and Petersen 1998; Kajii et al. 2001), and in somatic cells aneuploidy is associated with cancer and tumorigenesis (reviewed in Cahill et al. 1998; Lengauer et al. 1998). In fact, a number of mitotic genes regulating chromosome segregation have been found to be mutated in human cancer cells, implicating such mutations in the induction of aneuploidy in tumors (for a review, see Sen 2000). The minus-end transport of kinetochore microtubule bundles I have observed demonstrate a mechanism by which a mono-oriented chromosome can achieve bipolar orientation in the absence of kinetochore capture by astral microtubules.

In cell division the opportunities for establishing bipolar attachments and correcting mal-oriented chromosome attachments is limited to the stages of mitosis before anaphase. After anaphase, chromosomes are irreversibly segregated and the consequences of any errors are permanent. In this regard, the minus-end transport mechanism described here contributes valuable insight into the process of how chromosomes make proper bipolar attachments during spindle morphogenesis.

5.2.2 The role of the microtubule-associated protein TPX2 in spindle morphogenesis

Proper function of the mitotic spindle is critically dependent on the interaction between chromosomes and microtubules. Although tubulin is not capable of binding to DNA *in vitro*, bipolar spindles have been shown to form around chromosomes and chromatin coated beads in the absence of centrosomes, as discussed above. In an attempt to understand the molecular mechanisms of the chromosome-microtubule interaction, it has been demonstrated that the chromatin-associated Ran in its GTP-bound form, is required for chromatin-mediated spindle assembly in vitro (Heald and Weis 00). In addition, Ran-GTP is responsible for the recruitment of several kinetochore proteins (Arnaoutov and Dasso 03). However, it is still unclear what the role of Ran-GTP is in the interaction between chromosomes and microtubules.

TPX2 has been identified as a microtubule-associated protein that is released from inhibitory interactions with nuclear import receptors in the presence of Ran-GTP (Wittmann et al. 2000; Gruss et al. 2001; Gruss et al. 2002; Schatz et al. 2003; Trieselmann et al. 2003), and based on early results of TPX2 knockdown by RNAi, it was proposed that defects in spindle morphology in the absence of TPX2 are due to a lack of TPX2-mediated microtubule formation at chromosomes (Gruss et al. 2002). Although others have since confirmed the importance of TPX2 for forming bipolar spindles in mitosis (Garrett et al. 2002; Cassimeris and Morabito 2004), the role of TPX2 in spindle morphogenesis is still unclear.

My results have clarified several aspects of the role of TPX2 in spindle morphogenesis. Most notably, I have shown that after TPX2 knockdown by RNAi, mitotic cells exhibit structural instability of the spindle (manifested in pole fragmentation and interpolar collapse in the absence of Eg5 activity), although TPX2 is <u>not</u> required for

the formation of robust kinetochore microtubule bundles or for the polymerization of spindle microtubules after nocodazole washout. One of the implications of these results is that either TPX2 (and by implication the Ran-GTP pathway) is not required for microtubule-chromosome interactions in vertebrate cells (both microtubule nucleation and kinetochore microtubule bundle formation), or that other mechanisms for assembling arrays of chromosome-associated microtubules exist in vertebrate cells to compensate after TPX2 knockdown. In addition, my observations confirm through live cell imaging what was suspected about TPX2 function in fixed cells (Garrett et al. 2002), namely that TPX2 is required for structural stability of the spindle. This role of TPX2 may be a function of the Ran-GTP pathway, or it may be related to the interaction of TPX2 with other mitotic proteins, such as the mitotic kinase Aurora-A.

While live cell imaging has provided insights into the role of TPX2 in spindle morphogenesis, it has limitations just as any other technology does, and some of these limitations became were illustrated in this investigation. First, my live-cell recordings of GFP-tubulin in HeLa cells was severely limited by the photo-toxicity introduced by the process of illuminating the sample with a light source to excite the fluorophores in the sample for fluorescence imaging. As discussed in Chapter 1, this can have a variety of effects on the cell, including heat transfer and the production of free radicals. In order to limit the photo-toxicity to allow for time-lapse imaging of the HeLa GFP-tubulin cells, I was forced to reduce the frequency of exposure of the cells to the light source, and therefore the acquisition frequency. Second, the optical limit of resolution is currently not high enough to observe the rapid dynamics of single microtubules within the spindle, and the background signal from soluble tubulin in the cells I imaged reduced the image quality and posed further obstacles for high-resolution imaging of microtubules in the spindle. In short, although recent advances in microscopy like the spinning disk confocal microscope have proved to be powerful tools for high-resolution imaging of dynamic

processes in the cell, we are still a long way away from unlimited access for observing intra-cellular processes in real time.

§ 5.3 - Future directions

5.3.1 Are pre-formed kinetochore microtubules translocated along other microtubules by dynein?

One conspicuous quality of the minus-end capture of kinetochore microtubule bundles, as I reported in chapter two, is the direct translocation of the microtubule minus-ends to the spindle poles. Although the resolution of my imaging apparatus did not allow for analysis of the rates of the translocation for looping microtubules, it appeared that microtubule translocation events progress along other microtubules. For example, the minus-ends of looping kinetochore microtubules may translocate along astral microtubules, while the non-looping kinetochore microtubules (those facing the spindle) possibly translocate along interpolar microtubules.

The mitotic MAP NuMA is associated with the minus-ends of these kinetochore microtubules and is required for their incorporation into the spindle. Since the minus-end directed motor dynein forms a complex with NuMA and dynactin that is transported to the poles in mitosis (Merdes et al. 1996; Merdes et al. 2000), dynein dependent transport is a likely candidate for the poleward translocation of minus ends of microtubules in spindle morphogenesis. To test this hypothesis, live imaging experiments could determine if the dynein/dynactin complex is also present at the minus ends of translocating kinetochore microtubules, as well as whether dynein is required for this translocation.

First, using a cell line that is stably expressing p50-GFP (p50 is a component of the dynactin complex), cells could be imaged in the presence of monastrol and examined for the presence of punctuate p50-GFP fluorescence during a looping event, which would be visible in an analysis of time-lapse experiments. If p50-GFP were observed to translocate along tracks in a similar manner to the looping microtubules that I observed in tubulin-GFP cells, this would imply that dynein is present on looping microtubules. To determine if tracks of p50-GFP in monastrol treated cells correspond to looping microtubules, cells could be fixed during a potential looping event and stained for microtubules. Alternatively, the stable p50-GFP cell line could be microinjected with fluorescently labeled tubulin or induced to express tubulin-RFP simultaneously with p50-GFP and observed with rapid two-color imaging.

Second, to determine if dynein activity is required for minus-end translocation, dynein motor activity could be inhibited during live cell imaging of tubulin-GFP cells in the presence of monastrol. If dynein is required for minus-end translocation, kinetochore microtubule bundles should be observed to accumulate in the cytoplasm, much like my collaborators Duane Compton and Mike Gordon at Dartmouth Medical School observed after the inhibition of NuMA and Eg5. One widely used method for disrupting dynein activity is the injection of cells with excessive amounts of p50 (Echeverri et al. 1996; Burkhardt et al. 1997; Howell et al. 2001). Thus, either cells could be monitored by live time-lapse microscopy after p50 microinjection, or populations of cells could be microinjected and subsequently fixed and stained. Unfortunately, small molecule inhibitors do not currently exist for dynein and RNAi is not feasible due to the vital role dynein plays in other stages of the cell life cycle, so neither technique would be appropriate for inhibiting dynein motor activity in minus-end kinetochore microtubule translocation.

5.3.2 How do kinetochore microtubules form at unattached kinetochores?

To investigate the mechanism of kinetochore microtubule elongation into the cytoplasm prior to minus-end capture, the dynamics of individual kinetochore microtubule bundles must be examined in more detail. During live-cell imaging, photo-activation of GFP-tubulin has been previously used to mark sections of microtubules within the tubulin lattice to observe microtubule translocation within the cell (Patterson and Lippincott-Schwartz 2002, 2004; Tulu et al. 2003). By following the translocation of activated fluorescent tubulin, the net flux of microtubule subunits in the microtubule lattice can be observed.

In the context of the minus-end translocation of pre-formed kinetochore microtubules described in chapter two, photo-activation of sections of microtubules at unattached kinetochores could be imaged by live cell spinning disk microscopy. In this way, it may be possible to distinguish between kinetochore microtubule elongation by tubulin subunit addition at the minus-end (in the cytoplasm) or at the plus-end (at the kinetochore).

5.3.3 What are the ultra-structural characteristics of non-centrosomal kinetochore-microtubule bundles that undergo minus-end search and capture?

Although live cell imaging provides critical information about the dynamics and the succession of morphologies that contribute to spindle morphogenesis, it cannot reveal the properties of individual microtubules, as they are smaller than the resolution of current light microscopy. In chapter 3, my collaborator Alexey Khojdakov used serial section electron microscopy to confirm that non-centrosomal kinetochore microtubules formed in monoastral spindles. However, it would be worthwhile to examine the

characteristics of pre-formed non-centrosomal kinetochore microtubule bundles that are observed to undergo translocation.

Although the data presented here has shown that non-centrosomal microtubules are embedded in the kinetochore, which suggests that these are the plus-ends of the microtubules, and as mentioned earlier, early work on the formation of non-centrosomal microtubule bundles at kinetochores have revealed by microtubule hook-decoration that the plus-ends of microtubules are embedded in the kinetochore (Euteneuer et al. 1983), this has not been repeated for non-centrosomal kinetochore microtubule bundles that undergo translocation into the spindle. By observing single cells by live microscopy, a looping event in a monopolar spindle could be fixed and prepared for hook-decoration by lysing the cells in a detergent mixture containing bovine brain tubulin under conditions that allowed the formation of polarity-revealing hooks. This cell could then be re-located and analysed by serial-section transmission electron microscopy of the whole cell to examine the polarity of the microtubules at the kinetochore.

5.3.4 What is the role of Aurora-A activity in spindle morphogenesis?

Although my preliminary results comparing the effects of TPX2 knockdown with Aurora-A knockdown on spindle morphology showed striking similarities, these results were limited to fixed samples. While this provides an interesting insight into other mitotic proteins that may be involved in the same pathway, to verify that the effect on spindle morphogenesis is analogous to that of TPX2, the effect of Aurora-A knockdown must be examined by live cell imaging.

Live imaging could be used to investigate if the multipolar spindles I observed after Aurora-A RNAi were due to pole fragmentation, as I found in TPX2 knockdown cells. In addition, live imaging of single cells by live time-lapse microscopy after Aurora-A RNAi during treatment with monastrol would reveal whether or not Aurora-A

knockdown spindles collapse to monoasters after Eg5 inhibition (the same as TPX2 knockdown spindles).

5.3.4 Can the dynamics of TPX2 be observed in mitosis with live cell imaging?

Live imaging of GFP fusion proteins has been used extensively to monitor the dynamics of localization, translocation and turnover of mitotic proteins in the spindle (for examples, see Khodjakov and Rieder 1999; Howell et al. 2000; Piel et al. 2000; Stenoien et al. 2003). To better understand the role of TPX2 in spindle morphogenesis, cells expressing GFP-TPX2 could be imaged to examine the dynamics and localization of TPX2 during normal mitosis. In addition, GFP-TPX2 localization in the cell could be monitored in response to various perturbations to elucidate the interactions of TPX2 and other mitotic proteins. For example, GFP-TPX2 cells could be imaged after injection of nuclear import receptors to examine the proposed role of importin-α in inhibition of microtubule nucleation by TPX2 (Gruss et al. 2001; Nachury et al. 2001). Although I was unable to examine the possible role of TPX2 in the minus-end transport of kinetochore microtubules at unattached chromosomes by imaging GFP-tubulin cells after TPX2 knockdown, GFP-TPX2 cells treated with monastrol and arrested with mono-astral spindles could be examined for TPX2 at distal kinetochores prior to attachment.

References

Adams, M. C., W. C. Salmon, et al. (2003). "A high-speed multispectral spinning-disk confocal microscope system for fluorescent speckle microscopy of living cells." Methods **29**(1): 29-41.

Addinall, S. G. and B. Holland (2002). "The tubulin ancestor, FtsZ, draughtsman, designer and driving force for bacterial cytokinesis." J Mol Biol **318**(2): 219-36.

Al-Bassam, J., R. S. Ozer, et al. (2002). "MAP2 and tau bind longitudinally along the outer ridges of microtubule protofilaments." J Cell Biol **157**(7): 1187-96.

Alberts, B. (2002). Molecular biology of the cell. New York, Garland Science.

Allen, C. and G. G. Borisy (1974). "Structural polarity and directional growth of microtubules of Chlamydomonas flagella." J Mol Biol **90**(2): 381-402.

Bajer, A. S. (1982). "Functional autonomy of monopolar spindle and evidence for oscillatory movement in mitosis." J Cell Biol **93**(1): 33-48.

Bayliss, R., T. Sardon, et al. (2003). "Structural basis of Aurora-A activation by TPX2 at the mitotic spindle." Mol Cell **12**(4): 851-62.

Blagden, S. P. and D. M. Glover (2003). "Polar expeditions--provisioning the centrosome for mitosis." Nat Cell Biol **5**(6): 505-11.

Blake, R. A., M. A. Broome, et al. (2000). "SU6656, a selective src family kinase inhibitor, used to probe growth factor signaling." Mol Cell Biol **20**(23): 9018-27.

Bonaccorsi, S., M. G. Giansanti, et al. (1998). "Spindle self-organization and cytokinesis during male meiosis in asterless mutants of Drosophila melanogaster." J Cell Biol **142**(3): 751-61.

Burkhardt, J. K., C. J. Echeverri, et al. (1997). "Overexpression of the dynamitin (p50) subunit of the dynactin complex disrupts dynein-dependent maintenance of membrane organelle distribution." J Cell Biol **139**(2): 469-84.

Butner, K. A. and M. W. Kirschner (1991). "Tau protein binds to microtubules through a flexible array of distributed weak sites." J Cell Biol **115**(3): 717-30.

Cahill, D. P., C. Lengauer, et al. (1998). "Mutations of mitotic checkpoint genes in human cancers." Nature **392**(6673): 300-3.

Carazo-Salas, R. E., G. Guarguaglini, et al. (1999). "Generation of GTP-bound Ran by RCC1 is required for chromatin-induced mitotic spindle formation." Nature **400**(6740): 178-81.

Cassimeris, L. and J. Morabito (2004). "TOGp, the human homolog of XMAP215/Dis1, is required for centrosome integrity, spindle pole organization, and bipolar spindle assembly." Mol Biol Cell **15**(4): 1580-90.

Cassimeris, L., C. L. Rieder, et al. (1994). "Microtubule assembly and kinetochore directional instability in vertebrate monopolar spindles: implications for the mechanism of chromosome congression." J Cell Sci **107 (Pt 1)**: 285-97.

Chi, J. T., H. Y. Chang, et al. (2003). "Genomewide view of gene silencing by small interfering RNAs." Proc Natl Acad Sci U S A **100**(11): 6343-6.

Cimini, D., B. Howell, et al. (2001). "Merotelic kinetochore orientation is a major mechanism of aneuploidy in mitotic mammalian tissue cells." J Cell Biol **153**(3): 517-27.

Cimini, D., B. Moree, et al. (2003). "Merotelic kinetochore orientation occurs frequently during early mitosis in mammalian tissue cells and error correction is achieved by two different mechanisms." J Cell Sci **116**(Pt 20): 4213-25.

Compton, D. A. (1998). "Focusing on spindle poles." J Cell Sci **111 (Pt 11)**: 1477-81.

Compton, D. A. (2000). "Spindle assembly in animal cells." Annu Rev Biochem **69**: 95-114.

Compton, D. A. and D. W. Cleveland (1994). "NuMA, a nuclear protein involved in mitosis and nuclear reformation." Curr Opin Cell Biol **6**(3): 343-6.

Compton, D. A., I. Szilak, et al. (1992). "Primary structure of NuMA, an intranuclear protein that defines a novel pathway for segregation of proteins at mitosis." J Cell Biol **116**(6): 1395-408.

Cytrynbaum, E. N., J. M. Scholey, et al. (2003). "A force balance model of early spindle pole separation in Drosophila embryos." Biophys J **84**(2 Pt 1): 757-69.

Czaban, B. B. and A. Forer (1985). "The kinetic polarities of spindle microtubules in vivo, in crane-fly spermatocytes. I. Kinetochore microtubules that re-form after treatment with colcemid." J Cell Sci **79**: 1-37.

Dammermann, A., A. Desai, et al. (2003). "The minus end in sight." Curr Biol **13**(15): R614-24.

Dasso, M. (2002). "The Ran GTPase: theme and variations." Curr Biol **12**(14): R502-8.

DeBonis, S., J. P. Simorre, et al. (2003). "Interaction of the mitotic inhibitor monastrol with human kinesin Eg5." Biochemistry **42**(2): 338-49.

Desai, A. and T. J. Mitchison (1997). "Microtubule polymerization dynamics." Annu Rev Cell Dev Biol **13**: 83-117.

Echeverri, C. J., B. M. Paschal, et al. (1996). "Molecular characterization of the 50-kD subunit of dynactin reveals function for the complex in chromosome alignment and spindle organization during mitosis." J Cell Biol **132**(4): 617-33.

Erickson, H. P. and E. T. O'Brien (1992). "Microtubule dynamic instability and GTP hydrolysis." Annu Rev Biophys Biomol Struct **21**: 145-66.

Euteneuer, U., H. Ris, et al. (1983). "Polarity of kinetochore microtubules in Chinese hamster ovary cells after recovery from a colcemid block." J Cell Biol **97**(1): 202-8.

Eyers, P. A., E. Erikson, et al. (2003). "A novel mechanism for activation of the protein kinase aurora a." Curr Biol **13**(8): 691-7.

Faruki, S., R. W. Cole, et al. (2002). "Separating centrosomes interact in the absence of associated chromosomes during mitosis in cultured vertebrate cells." Cell Motil Cytoskeleton **52**(2): 107-21.

Fry, D. W., A. J. Kraker, et al. (1994). "A specific inhibitor of the epidermal growth factor receptor tyrosine kinase." Science **265**(5175): 1093-5.

Funabiki, H. and A. W. Murray (2000). "The Xenopus chromokinesin Xkid is essential for metaphase chromosome alignment and must be degraded to allow anaphase chromosome movement." Cell **102**(4): 411-24.

Gadde, S. and R. Heald (2004). "Mechanisms and molecules of the mitotic spindle." Curr Biol **14**(18): R797-805.

Gaglio, T., M. A. Dionne, et al. (1997). "Mitotic spindle poles are organized by structural and motor proteins in addition to centrosomes." J Cell Biol **138**(5): 1055-66.

Gaglio, T., A. Saredi, et al. (1996). "Opposing motor activities are required for the organization of the mammalian mitotic spindle pole." J Cell Biol **135**(2): 399-414.

Gaglio, T., A. Saredi, et al. (1995). "NuMA is required for the organization of microtubules into aster-like mitotic arrays." J Cell Biol **131**(3): 693-708.

Garrett, S., K. Auer, et al. (2002). "hTPX2 is required for normal spindle morphology and centrosome integrity during vertebrate cell division." Curr Biol **12**(23): 2055-9.

Geuens, G., A. M. Hill, et al. (1989). "Microtubule dynamics investigated by microinjection of Paramecium axonemal tubulin: lack of nucleation but proximal assembly of microtubules at the kinetochore during prometaphase." J Cell Biol **108**(3): 939-53.

Giet, R. and C. Prigent (2000). "The Xenopus laevis aurora/Ip11p-related kinase pEg2 participates in the stability of the bipolar mitotic spindle." Exp Cell Res **258**(1): 145-51.

Glover, D. M. (2003). "Aurora A on the mitotic spindle is activated by the way it holds its partner." Mol Cell **12**(4): 797-9.

Gordon, M. B., L. Howard, et al. (2001). "Chromosome movement in mitosis requires microtubule anchorage at spindle poles." J Cell Biol **152**(3): 425-34.

Grego, S., V. Cantillana, et al. (2001). "Microtubule treadmilling in vitro investigated by fluorescence speckle and confocal microscopy." Biophys J **81**(1): 66-78.

Gruss, O. J., R. E. Carazo-Salas, et al. (2001). "Ran induces spindle assembly by reversing the inhibitory effect of importin alpha on TPX2 activity." Cell **104**(1): 83-93.

Gruss, O. J., M. Wittmann, et al. (2002). "Chromosome-induced microtubule assembly mediated by TPX2 is required for spindle formation in HeLa cells." Nat Cell Biol **4**(11): 871-9.

Hannak, E., M. Kirkham, et al. (2001). "Aurora-A kinase is required for centrosome maturation in Caenorhabditis elegans." J Cell Biol **155**(7): 1109-16.

Hannak, E., K. Oegema, et al. (2002). "The kinetically dominant assembly pathway for centrosomal asters in Caenorhabditis elegans is gamma-tubulin dependent." J Cell Biol **157**(4): 591-602.

Harborth, J., J. Wang, et al. (1999). "Self assembly of NuMA: multiarm oligomers as structural units of a nuclear lattice." Embo J **18**(6): 1689-700.

Haren, L. and A. Merdes (2002). "Direct binding of NuMA to tubulin is mediated by a novel sequence motif in the tail domain that bundles and stabilizes microtubules." J Cell Sci **115**(Pt 9): 1815-24.

Hauf, S., R. W. Cole, et al. (2003). "The small molecule Hesperadin reveals a role for Aurora B in correcting kinetochore-microtubule attachment and in maintaining the spindle assembly checkpoint." J Cell Biol **161**(2): 281-94.

Hayden, J. H., S. S. Bowser, et al. (1990). "Kinetochores capture astral microtubules during chromosome attachment to the mitotic spindle: direct visualization in live newt lung cells." J Cell Biol **111**(3): 1039-45.

Heald, R., R. Tournebize, et al. (1996). "Self-organization of microtubules into bipolar spindles around artificial chromosomes in Xenopus egg extracts." Nature **382**(6590): 420-5.

Heald, R. and K. Weis (2000). "Spindles get the ran around." Trends Cell Biol **10**(1): 1-4.

Hecht, E. (1998). Optics. Reading, Mass., Addison-Wesley.

Hotha, S., J. C. Yarrow, et al. (2003). "HR22C16: A Potent Small-Molecule Probe for the Dynamics of Cell Division." Angew Chem Int Ed Engl **42**(21): 2379-2382.

Howell, B. J., D. B. Hoffman, et al. (2000). "Visualization of Mad2 dynamics at kinetochores, along spindle fibers, and at spindle poles in living cells." J Cell Biol **150**(6): 1233-50.

Howell, B. J., B. F. McEwen, et al. (2001). "Cytoplasmic dynein/dynactin drives kinetochore protein transport to the spindle poles and has a role in mitotic spindle checkpoint inactivation." J Cell Biol **155**(7): 1159-72.

Hyman, A. and E. Karsenti (1998). "The role of nucleation in patterning microtubule networks." J Cell Sci **111 (Pt 15)**: 2077-83.

Hyman, A. A. and T. J. Mitchison (1991). "Two different microtubule-based motor activities with opposite polarities in kinetochores." Nature **351**(6323): 206-11.

Inoue, S. (1990). Foundations of Confocal Scanned Imaging in Light Microscopy. New York, Plenum Press.

Inoue, S. and T. Inoue (2002). "Direct-view high-speed confocal scanner: the CSU-10." Methods Cell Biol **70**: 87-127.

Inoue, S. and E. D. Salmon (1995). "Force generation by microtubule assembly/disassembly in mitosis and related movements." Mol Biol Cell **6**(12): 1619-40.

Jackson, A. L., S. R. Bartz, et al. (2003). "Expression profiling reveals off-target gene regulation by RNAi." Nat Biotechnol **21**(6): 635-7.

Janson, M. E., M. E. de Dood, et al. (2003). "Dynamic instability of microtubules is regulated by force." J Cell Biol **161**(6): 1029-34.

Kahana, J. A. and D. W. Cleveland (2001). "Cell cycle. Some importin news about spindle assembly." Science **291**(5509): 1718-9.

Kajii, T., T. Ikeuchi, et al. (2001). "Cancer-prone syndrome of mosaic variegated aneuploidy and total premature chromatid separation: report of five infants." Am J Med Genet **104**(1): 57-64.

Kalab, P., K. Weis, et al. (2002). "Visualization of a Ran-GTP gradient in interphase and mitotic Xenopus egg extracts." Science **295**(5564): 2452-6.

Kapoor, T. M. and D. A. Compton (2002). "Searching for the middle ground: mechanisms of chromosome alignment during mitosis." J Cell Biol **157**(4): 551-6.

Kapoor, T. M., T. U. Mayer, et al. (2000). "Probing spindle assembly mechanisms with monastrol, a small molecule inhibitor of the mitotic kinesin, Eg5." J Cell Biol **150**(5): 975-88.

Karsenti, E. and I. Vernos (2001). "The mitotic spindle: a self-made machine." Science **294**(5542): 543-7.

Kashina, A. S., R. J. Baskin, et al. (1996). "A bipolar kinesin." Nature **379**(6562): 270-2.

Khodjakov, A., R. W. Cole, et al. (1997). "Chromosome fragments possessing only one kinetochore can congress to the spindle equator." J Cell Biol **136**(2): 229-40.

Khodjakov, A., R. W. Cole, et al. (2000). "Centrosome-independent mitotic spindle formation in vertebrates." Curr Biol **10**(2): 59-67.

Khodjakov, A., L. Copenagle, et al. (2003). "Minus-end capture of preformed kinetochore fibers contributes to spindle morphogenesis." J Cell Biol **160**(5): 671-83.

Khodjakov, A. and C. L. Rieder (1999). "The sudden recruitment of gamma-tubulin to the centrosome at the onset of mitosis and its dynamic exchange throughout the cell cycle, do not require microtubules." J Cell Biol **146**(3): 585-96.

Khodjakov, A. and C. L. Rieder (2001). "Centrosomes enhance the fidelity of cytokinesis in vertebrates and are required for cell cycle progression." J Cell Biol **153**(1): 237-42.

Kirschner, M. and T. Mitchison (1986). "Beyond self-assembly: from microtubules to morphogenesis." Cell **45**(3): 329-42.

Kline-Smith, S. L. and C. E. Walczak (2002). "The microtubule-destabilizing kinesin XKCM1 regulates microtubule dynamic instability in cells." Mol Biol Cell **13**(8): 2718-31.

Kufer, T. A., H. H. Sillje, et al. (2002). "Human TPX2 is required for targeting Aurora-A kinase to the spindle." J Cell Biol **158**(4): 617-23.

Lampson, M. A., K. Renduchitala, et al. (2004). "Correcting improper chromosome-spindle attachments during cell division." Nat Cell Biol **6**(3): 232-7

Lengauer, C., K. W. Kinzler, et al. (1998). "Genetic instabilities in human cancers." Nature **396**(6712): 643-9.

Lydersen, B. K. and D. E. Pettijohn (1980). "Human-specific nuclear protein that associates with the polar region of the mitotic apparatus: distribution in a human/hamster hybrid cell." Cell **22**(2 Pt 2): 489-99.

Maccioni, R. B. and V. Cambiazo (1995). "Role of microtubule-associated proteins in the control of microtubule assembly." Physiol Rev **75**(4): 835-64.

Maddox, P., A. Desai, et al. (2002). "Poleward microtubule flux is a major component of spindle dynamics and anaphase a in mitotic Drosophila embryos." Curr Biol **12**(19): 1670-4.

Maddox, P., A. Straight, et al. (2003). "Direct observation of microtubule dynamics at kinetochores in Xenopus extract spindles: implications for spindle mechanics." J Cell Biol **162**(3): 377-82.

Maddox, P. S., B. Moree, et al. (2003). "Spinning disk confocal microscope system for rapid high-resolution, multimode, fluorescence speckle microscopy and green fluorescent protein imaging in living cells." Methods Enzymol **360**: 597-617

Maiato, H. and C. E. Sunkel (2004). "Kinetochore-microtubule interactions during cell division." Chromosome Res **12**(6): 585-97.

Mandelkow, E. and E. M. Mandelkow (1995). "Microtubules and microtubule-associated proteins." Curr Opin Cell Biol **7**(1): 72-81.

Maney, T., A. W. Hunter, et al. (1998). "Mitotic centromere-associated kinesin is important for anaphase chromosome segregation." J Cell Biol **142**(3): 787-801.

Marko, M. and A. Leith (1996). "Sterecon--three-dimensional reconstructions from stereoscopic contouring." J Struct Biol **116**(1): 93-8.

Marshall, W. F. and J. A. Kahana (2001). "Stay tuned for some importin news about spindle assembly." Trends Cell Biol **11**(4): 148.

Marumoto, T., S. Honda, et al. (2003). "Aurora-A kinase maintains the fidelity of early and late mitotic events in HeLa cells." J Biol Chem **278**(51): 51786-95.

Mastronarde, D. N., K. L. McDonald, et al. (1993). "Interpolar spindle microtubules in PTK cells." J Cell Biol **123**(6 Pt 1): 1475-89.

Matsumoto, B. (2002). Handbook of biological confocal microscopy. London, Academic Press.

Mayer, T. U., T. M. Kapoor, et al. (1999). "Small molecule inhibitor of mitotic spindle bipolarity identified in a phenotype-based screen." Science **286**(5441): 971-4.

McDonald, K. L., E. T. O'Toole, et al. (1992). "Kinetochore microtubules in PTK cells." J Cell Biol **118**(2): 369-83.

McEwen, B. F., G. K. Chan, et al. (2001). "CENP-E is essential for reliable bioriented spindle attachment, but chromosome alignment can be achieved via redundant mechanisms in mammalian cells." Mol Biol Cell **12**(9): 2776-89.

McIntosh, J. R., E. L. Grishchuk, et al. (2002). "Chromosome-microtubule interactions during mitosis." Annu Rev Cell Dev Biol **18**: 193-219.

McNally, F J. and R. D. Vale (1993). "Identification of katanin, an ATPase that severs and disassembles stable microtubules." Cell **75**(3): 419-29.

Megraw, T. L., L. R. Kao, et al. (2001). "Zygotic development without functional mitotic centrosomes." Curr Biol **11**(2): 116-20.

Meraldi, P., R. Honda, et al. (2002). "Aurora-A overexpression reveals tetraploidization as a major route to centrosome amplification in p53-/- cells." Embo J **21**(4): 483-92.

Meraldi, P. and E. A. Nigg (2002). "The centrosome cycle." FEBS Lett **521**(1-3): 9-13.

Merdes, A. and D. W. Cleveland (1997). "Pathways of spindle pole formation: different mechanisms; conserved components." J Cell Biol **138**(5): 953-6.

Merdes, A., R. Heald, et al. (2000). "Formation of spindle poles by dynein/dynactin-dependent transport of NuMA." J Cell Biol **149**(4): 851-62.

Merdes, A., K. Ramyar, et al. (1996). "A complex of NuMA and cytoplasmic dynein is essential for mitotic spindle assembly." Cell **87**(3): 447-58.

Mitchison, T., L. Evans, et al. (1986). "Sites of microtubule assembly and disassembly in the mitotic spindle." Cell **45**(4): 515-27.

Mitchison, T. and M. Kirschner (1984). "Dynamic instability of microtubule growth." Nature **312**(5991): 237-42.

Mitchison, T. and M. Kirschner (1984). "Microtubule assembly nucleated by isolated centrosomes." Nature **312**(5991): 232-7.

Mitchison, T. J. (1989). "Polewards microtubule flux in the mitotic spindle: evidence from photoactivation of fluorescence." J Cell Biol **109**(2): 637-52.

Mitchison, T. J. and M. W. Kirschner (1985). "Properties of the kinetochore in vitro. I. Microtubule nucleation and tubulin binding." J Cell Biol **101**(3): 755-65.

Mitchison, T. J. and M. W. Kirschner (1985). "Properties of the kinetochore in vitro. II. Microtubule capture and ATP-dependent translocation." J Cell Biol **101**(3): 766-77.

Mitchison, T. J. and E. D. Salmon (1992). "Poleward kinetochore fiber movement occurs during both metaphase and anaphase-A in newt lung cell mitosis." J Cell Biol **119**(3): 569-82.

Mitchison, T. J. and E. D. Salmon (2001). "Mitosis: a history of division." Nat Cell Biol **3**(1): E17-21.

Miyawaki, A., A. Sawano, et al. (2003). "Lighting up cells: labelling proteins with fluorophores." Nat Cell Biol **Suppl**: S1-7

Mole-Bajer, J. (1969). "Fine structural studies of apolar mitosis." Chromosoma **26**(4): 427-48.

Mountain, V., C. Simerly, et al. (1999). "The kinesin-related protein, HSET, opposes the activity of Eg5 and cross-links microtubules in the mammalian mitotic spindle." J Cell Biol **147**(2): 351-66.

Murphy, D. B. (2001). Fundamentals of light microscopy and electronic imaging. New York, Wiley.

Nachury, M. V., T. J. Maresca, et al. (2001). "Importin beta is a mitotic target of the small GTPase Ran in spindle assembly." Cell **104**(1): 95-106.

Nakano, A. (2002). "Spinning-disk confocal microscopy -- a cutting-edge tool for imaging of membrane traffic." Cell Struct Funct **27**(5): 349-55.

Nicklas, R. B. and G. W. Gordon (1985). "The total length of spindle microtubules depends on the number of chromosomes present." J Cell Biol **100**(1): 1-7.

Nicolaidis, P. and M. B. Petersen (1998). "Origin and mechanisms of non-disjunction in human autosomal trisomies." Hum Reprod **13**(2): 313-9.

Nishikura, K. (2001). "A short primer on RNAi: RNA-directed RNA polymerase acts as a key catalyst." Cell **107**(4): 415-8.

Noble, M., S. A. Lewis, et al. (1989). "The microtubule binding domain of microtubule-associated protein MAP1B contains a repeated sequence motif unrelated to that of MAP2 and tau." J Cell Biol **109**(6 Pt 2): 3367-76.

Nogales, E. (2000). "Structural insights into microtubule function." Annu Rev Biochem **69**: 277-302.

O'Connell, C. B. and Y. L. Wang (2000). "Mammalian spindle orientation and position respond to changes in cell shape in a dynein-dependent fashion." Mol Biol Cell **11**(5): 1765-74.

Ohba, T., M. Nakamura, et al. (1999). "Self-organization of microtubule asters induced in Xenopus egg extracts by GTP-bound Ran." Science **284**(5418): 1356-8.

Oldenbourg, R., H. Terada, et al. (1993). "Image sharpness and contrast transfer in coherent confocal microscopy." J Microsc **172 (Pt 1)**: 31-9.

Patterson, G. H. and J. Lippincott-Schwartz (2002). "A photoactivatable GFP for selective photolabeling of proteins and cells." Science **297**(5588): 1873-7.

Patterson, G. H. and J. Lippincott-Schwartz (2004). "Selective photolabeling of proteins using photoactivatable GFP." Methods **32**(4): 445-50.

Pawley, J. B. (1995). Handbook of biological confocal microscopy. New York, Plenum Press.

Pearson, C. G., P. S. Maddox, et al. (2003). "Yeast Kinetochores Do Not Stabilize Stu2p-dependent Spindle Microtubule Dynamics." Mol Biol Cell **14**(10): 4181-95.

Piel, M., P. Meyer, et al. (2000). "The respective contributions of the mother and daughter centrioles to centrosome activity and behavior in vertebrate cells." J Cell Biol **149**(2): 317-30.

Price, C. M. and D. E. Pettijohn (1986). "Redistribution of the nuclear mitotic apparatus protein (NuMA) during mitosis and nuclear assembly. Properties of purified NuMA protein." Exp Cell Res **166**(2): 295-311.

Rawlings, S. R. and J. Byatt (2002). "How microscopy produces a sharper image." Biophotonics Intl. **9**(4): 44-47.

Rieder, C. L. (1981). "The structure of the cold-stable kinetochore fiber in metaphase PtK1 cells." Chromosoma **84**(1): 145-58.

Rieder, C. L. and S. P. Alexander (1990). "Kinetochores are transported poleward along a single astral microtubule during chromosome attachment to the spindle in newt lung cells." J Cell Biol **110**(1): 81-95.

Rieder, C. L. and G. G. Borisy (1981). "The attachment of kinetochores to the pro-metaphase spindle in PtK1 cells. Recovery from low temperature treatment." Chromosoma **82**(5): 693-716.

Rieder, C. L. and G. Cassels (1999). "Correlative light and electron microscopy of mitotic cells in monolayer cultures." Methods Cell Biol **61**: 297-315.

Rieder, C. L. and R. Hard (1990). "Newt lung epithelial cells: cultivation, use, and advantages for biomedical research." Int Rev Cytol **122**: 153-220.

Rieder, C. L. and A. Khodjakov (2003). "Mitosis through the microscope: advances in seeing inside live dividing cells." Science **300**(5616): 91-6.

Rieder, C. L. and E. D. Salmon (1998). "The vertebrate cell kinetochore and its roles during mitosis." Trends Cell Biol **8**(8): 310-8.

Roos, U. P. (1976). "Light and electron microscopy of rat kangaroo cells in mitosis. III. Patterns of chromosome behavior during prometaphase." Chromosoma **54**(4): 363-85.

Rose, G. G., C. M. Pomerat, et al. (1958). "A cellophane-strip technique for culturing tissue in multipurpose culture chambers." J Biophys Biochem Cytol **4**(6): 761-4.

Rusan, N. M., C. J. Fagerstrom, et al. (2001). "Cell cycle-dependent changes in microtubule dynamics in living cells expressing green fluorescent protein-alpha tubulin." Mol Biol Cell **12**(4): 971-80.

Rusan, N. M., U. S. Tulu, et al. (2002). "Reorganization of the microtubule array in prophase/prometaphase requires cytoplasmic dynein-dependent microtubule transport." J Cell Biol **158**(6): 997-1003.

Sablin, E. P. (2000). "Kinesins and microtubules: their structures and motor mechanisms." Curr Opin Cell Biol **12**(1): 35-41.

Sakowicz, R., M. S. Berdelis, et al. (1998). "A marine natural product inhibitor of kinesin motors." Science **280**(5361): 292-5.

Salmon, E. D., R. J. Leslie, et al. (1984). "Spindle microtubule dynamics in sea urchin embryos: analysis using a fluorescein-labeled tubulin and measurements of fluorescence redistribution after laser photobleaching." J Cell Biol **99**(6): 2165-74.

Saredi, A., L. Howard, et al. (1996). "NuMA assembles into an extensive filamentous structure when expressed in the cell cytoplasm." J Cell Sci **109 (Pt 3)**: 619-30.

Saredi, A., L. Howard, et al. (1997). "Phosphorylation regulates the assembly of NuMA in a mammalian mitotic extract." J Cell Sci **110 (Pt 11)**: 1287-97.

Sawin, K. E., K. LeGuellec, et al. (1992). "Mitotic spindle organization by a plus-end-directed microtubule motor." Nature **359**(6395): 540-3.

Saxton, W. M., D. L. Stemple, et al. (1984). "Tubulin dynamics in cultured mammalian cells." J Cell Biol **99**(6): 2175-86.

Schatz, C. A., R. Santarella, et al. (2003). "Importin alpha-regulated nucleation of microtubules by TPX2." Embo J **22**(9): 2060-70.

Scholey, J. M., I. Brust-Mascher, et al. (2003). "Cell division." Nature **422**(6933): 746-52.

Semizarov, D., L. Frost, et al. (2003). "Specificity of short interfering RNA determined through gene expression signatures." Proc Natl Acad Sci U S A **100**(11): 6347-52.

Sen, S. (2000). "Aneuploidy and cancer." Curr Opin Oncol **12**(1): 82-8.

Sharp, D. J., H. M. Brown, et al. (2000). "Functional coordination of three mitotic motors in Drosophila embryos." Mol Biol Cell **11**(1): 241-53.

Sharp, D. J., G. C. Rogers, et al. (2000). "Microtubule motors in mitosis." Nature **407**(6800): 41-7.

Sharp, D. J., K. R. Yu, et al. (1999). "Antagonistic microtubule-sliding motors position mitotic centrosomes in Drosophila early embryos." Nat Cell Biol **1**(1): 51-4.

Sharp, P. A. (2001). "RNA interference--2001." Genes Dev **15**(5): 485-90.

Shimizu, T., Y. Y. Toyoshima, et al. (1995). "Comparison of the motile and enzymatic properties of two microtubule minus-end-directed motors, ncd and cytoplasmic dynein." Biochemistry **34**(5): 1575-82.

Shirasu-Hiza, M., P. Coughlin, et al. (2003). "Identification of XMAP215 as a microtubule-destabilizing factor in Xenopus egg extract by biochemical purification." J Cell Biol **161**(2): 349-58.

Smirnova, E. A. and A. S. Bajer (1992). "Spindle poles in higher plant mitosis." Cell Motil Cytoskeleton **23**(1): 1-7.

Spurck, T. P., O. G. Stonington, et al. (1990). "UV microbeam irradiations of the mitotic spindle. II. Spindle fiber dynamics and force production." J Cell Biol **111**(4): 1505-18.

Stenoien, D. L., S. Sen, et al. (2003). "Dynamic association of a tumor amplified kinase, Aurora-A, with the centrosome and mitotic spindle." Cell Motil Cytoskeleton **55**(2): 134-46.

Swedlow, J. R. (2003). "Quantitative fluorescence microscopy and image deconvolution." Methods Cell Biol **72**: 349-67.

Tassin, A. M. and M. Bornens (1999). "Centrosome structure and microtubule nucleation in animal cells." Biol Cell **91**(4-5): 343-54.

Telzer, B. R., M. J. Moses, et al. (1975). "Assembly of microtubules onto kinetochores of isolated mitotic chromosomes of HeLa cells." Proc Natl Acad Sci U S A **72**(10): 4023-7.

Terada, Y., Y. Uetake, et al. (2003). "Interaction of Aurora-A and centrosomin at the microtubule-nucleating site in Drosophila and mammalian cells." J Cell Biol **162**(5): 757-63.

Trieselmann, N., S. Armstrong, et al. (2003). "Ran modulates spindle assembly by regulating a subset of TPX2 and Kid activities including Aurora A activation." J Cell Sci **116**(Pt 23): 4791-8.

Tsai, M. Y., C. Wiese, et al. (2003). "A Ran signalling pathway mediated by the mitotic kinase Aurora A in spindle assembly." Nat Cell Biol **5**(3): 242-8.

Tulu, U. S., N. M. Rusan, et al. (2003). "Peripheral, non-centrosome-associated microtubules contribute to spindle formation in centrosome-containing cells." Curr Biol **13**(21): 1894-9.

van Breugel, M., D. Drechsel, et al. (2003). "Stu2p, the budding yeast member of the conserved Dis1/XMAP215 family of microtubule-associated proteins is a plus end-binding microtubule destabilizer." J Cell Biol **161**(2): 359-69.

Wadsworth, P. (1999). "Microinjection of mitotic cells." Methods Cell Biol **61**: 219-31.

Walczak, C. E., I. Vernos, et al. (1998). "A model for the proposed roles of different microtubule-based motor proteins in establishing spindle bipolarity." Curr Biol **8**(16): 903-13.

Walker, R. A., E. T. O'Brien, et al. (1988). "Dynamic instability of individual microtubules analyzed by video light microscopy: rate constants and transition frequencies." J Cell Biol **107**(4): 1437-48.

Waterman-Storer, C. M., A. Desai, et al. (1998). "Fluorescent speckle microscopy, a method to visualize the dynamics of protein assemblies in living cells." Curr Biol **8**(22): 1227-30.

Waters, J. C., T. J. Mitchison, et al. (1996). "The kinetochore microtubule minus-end disassembly associated with poleward flux produces a force that can do work." Mol Biol Cell **7**(10): 1547-58.

Wiese, C., A. Wilde, et al. (2001). "Role of importin-beta in coupling Ran to downstream targets in microtubule assembly." Science **291**(5504): 653-6.

Witt, P. L., H. Ris, et al. (1980). "Origin of kinetochore microtubules in Chinese hamster ovary cells." Chromosoma **81**(3): 483-505.

Wittmann, T., H. Boleti, et al. (1998). "Localization of the kinesin-like protein Xklp2 to spindle poles requires a leucine zipper, a microtubule-associated protein, and dynein." J Cell Biol **143**(3): 673-85.

Wittmann, T., M. Wilm, et al. (2000). "TPX2, A novel xenopus MAP involved in spindle pole organization." J Cell Biol **149**(7): 1405-18.

Zhai, Y., P. J. Kronebusch, et al. (1996). "Microtubule dynamics at the G2/M transition: abrupt breakdown of cytoplasmic microtubules at nuclear envelope breakdown and implications for spindle morphogenesis." J Cell Biol **135**(1): 201-14.

Zhang, C., M. Hughes, et al. (1999). "Ran-GTP stabilises microtubule asters and inhibits nuclear assembly in Xenopus egg extracts." J Cell Sci **112 (Pt 14)**: 2453-61.

Zhang, D. and R. B. Nicklas (1995). "Chromosomes initiate spindle assembly upon experimental dissolution of the nuclear envelope in grasshopper spermatocytes." J Cell Biol **131**(5): 1125-31.